AD-A049 030 ARMY ELECTRONICS COMMAND FORT MONMOUTH N J F/G 4/1
STRATOSPHERIC COMPOSITION BALLOON-BORNE EXPERIMENT 23-26 SEPTEM--ETC(U)
OCT 77 H N BALLARD, F P HUDSON
UNCLASSIFIED ECOM-5830 NL

1 of 2
ADA049 030

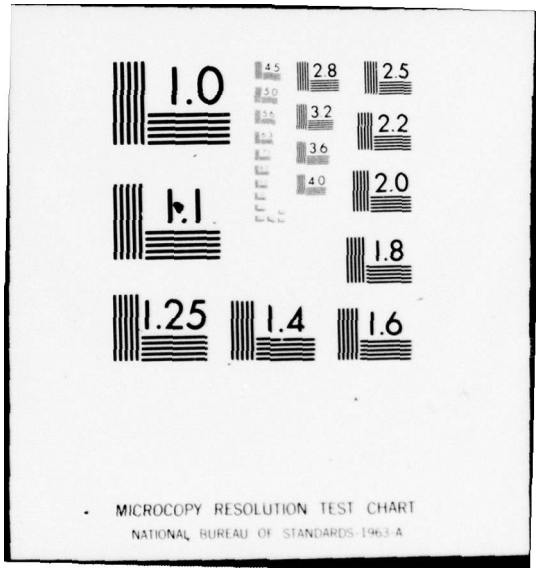
1.0
1.1
1.25
1.4
1.6
1.8
2.0
2.2
2.5
2.8
3.2
3.6
4.0
4.5
5.0
MICROCOPY RESOLUTION TEST CHART
NATIONAL BUREAU OF STANDARDS-1963-A

RESEARCH AND DEVELOPMENT TECHNICAL REPORT
ECOM-5830

STRATOSPHERIC COMPOSITION BALLOON - BORNE EXPERIMENT 23 - 26 SEPTEMBER 1975

Compiled by
Harold N. Ballard
Frank P. Hudson

A cooperative experiment among

Atmospheric Sciences Laboratory
Sandia Laboratories, Albuquerque
Air Force Geophysics Laboratory
National Center for Atmospheric Research
University of Denver
New Mexico State University

with contract support from

University of Texas at El Paso
Pennsylvania State University
Panametrics, Inc.
Winzen Research Inc.

October 1977

ECOM
UNITED STATES ARMY ELECTRONICS COMMAND - FORT MONMOUTH, NEW JERSEY 07703

NOTICES

Disclaimers

The findings in this report are not to be construed as an official Department of the Army position, unless so designated by other authorized documents.

The citation of trade names and names of manufacturers in this report is not to be construed as official Government indorsement or approval of commercial products or services referenced herein.

Disposition

Destroy this report when it is no longer needed. Do not return it to the originator.

SECURITY CLASSIFICATION OF THIS PAGE *(When Data Entered)*

REPORT DOCUMENTATION PAGE

READ INSTRUCTIONS BEFORE COMPLETING FORM

1. REPORT NUMBER: ECOM-5830	2. GOVT ACCESSION NO.
3. RECIPIENT'S CATALOG NUMBER: Research and development	
4. TITLE *(and Subtitle)*: STRATOSPHERIC COMPOSITION BALLOON-BORNE EXPERIMENT 23-26 SEPTEMBER 1975	5. TYPE OF REPORT & PERIOD COVERED: R&D Technical Report
	6. PERFORMING ORG. REPORT NUMBER
7. AUTHOR(s): Harold N. Ballard, Frank P. Hudson	8. CONTRACT OR GRANT NUMBER(s)
9. PERFORMING ORGANIZATION NAME AND ADDRESS: Atmospheric Sciences Laboratory, White Sands Missile Range, New Mexico 88002	10. PROGRAM ELEMENT, PROJECT, TASK AREA & WORK UNIT NUMBERS: DA Task No. 1L161102B53A5A2
11. CONTROLLING OFFICE NAME AND ADDRESS: US Army Electronics Command, Fort Monmouth, New Jersey 07703	12. REPORT DATE: October 1977
	13. NUMBER OF PAGES: 127
14. MONITORING AGENCY NAME & ADDRESS *(if different from Controlling Office)*: 123p.	15. SECURITY CLASS. *(of this report)*: UNCLASSIFIED
	15a. DECLASSIFICATION/DOWNGRADING SCHEDULE

16. DISTRIBUTION STATEMENT *(of this Report)*

Approved for public release; distribution unlimited.

17. DISTRIBUTION STATEMENT *(of the abstract entered in Block 20, if different from Report)*

18. SUPPLEMENTARY NOTES

19. KEY WORDS *(Continue on reverse side if necessary and identify by block number)*

Solar uv flux	Stratosphere
Atmospheric composition	Balloon-borne platforms
Thermodynamic structure	Multiple related measurements

20. ABSTRACT *(Continue on reverse side if necessary and identify by block number)*

Within the period September 1968 to September 1975, six balloon-borne experiments were conducted under the title of "STRATospheric COMPosition (STRATCOM) Experiments." The initial experiments (September 1968 and September 1969) were designed to measure the temperature variation near an altitude of 50 km that were to be associated with the diurnal stratospheric tide. Requirements by the Department of Defense for information concerning stratospheric composition, as well as measurements of national interest to the possible pollution of the ozone

DD FORM 1 JAN 73 1473 EDITION OF 1 NOV 65 IS OBSOLETE

SECURITY CLASSIFICATION OF THIS PAGE *(When Data Entered)*

037620

stratosphere by the Super Sonic Transport and by chlorofluorocarbons, gradually increased the number, types, and complexity of measurements conducted during each successive experiment.

This composite report presents, in one publication, the related results obtained from the various experiments comprising the STRATCOM VI-A and VI-B payloads as determined by the various experimenters. The results, coupled with the ECOM Report "Correlation of Selected Atmospheric Composition Parameters for the Mid-Latitude September Stratosphere," are representative of the correlated multi-instrument approach of the STRATCOM Program to the experimental study of the stratosphere, backed by chemical kenetic theory and atmospheric modeling.

CONTENTS

CHAPTER 1

EXPERIMENT BACKGROUND AND DESCRIPTION

HAROLD N. BALLARD
Atmospheric Sciences Laboratory, WSMR, NM

FRANK P. HUDSON
Physics and Technology Programs
Energy Resources Dev Admin, Washington, DC

Art Korn
Air Force Geophysics Lab, Harrison AFB, MA

BACKGROUND

Within the period September 1968 to September 1975, six balloon-borne experiments were conducted under the title of "STRATospheric COMposition (STRATCOM) Experiments." The initial experiments were designed to measure the temperature variations near an altitude of 50 km that were to be associated with the diurnal stratospheric tide [1,2,3].

Requirements by the Department of Defense for information concerning stratospheric composition, as well as measurements of national interest to the possible pollution of the stratosphere by the Super Sonic Transport and by chlorofluorocarbons, gradually increased the number, types, and complexity of measurements conducted during each successive flight.

The STRATCOM III balloon-borne experiment of September 1972 [4] carried 17 instruments to an altitude of 48 km to measure solar uv radiation, atmospheric composition and thermodynamic structure. Mass spectrometry and uv spectroscopy measurement techniques were added to the techniques utilized during the STRATCOM II and III experiments of September 1968 and September 1969, respectively.

STRATCOM IV and V, launched October 1973 and May 1974, were primarily dedicated to the measurement of the oxides of nitrogen, water vapor, and ozone by a laser opto-acoustic technique developed by Bell Laboratories and fielded through their relationship with Sandia Laboratories of Albuquerque, NM. Measurements made by other instruments aboard the two balloon-borne platforms in the 19-28 km altitude interval indicate that these flights provided little new information concerning the unperturbed composition and thermal structure of the stratosphere [5].

The next experiment in the series, termed STRATCOM VI, was a two-balloon experiment conducted 23-26 September 1975. It was directly or indirectly supported by six federal agencies, with experiment participation by ten federal, university, and private laboratories [6].

The STRATCOM VI-A payload of 29 instruments was borne aloft on 23 September by a 15.6 million ft^3 balloon to measure, in more detail, the related solar uv flux, atmospheric composition, and thermodynamic structure of the stratosphere. A proper combination of balloon characteristics, payload weight, adequate ballast, and favorable winds permitted a flight of 33 hours within the 27-40 km altitude interval.

The STRATCOM VI-B payload, lifted by a 2.9 million ft^3 balloon to an altitude of 30 km on 26 September 1975, was devoted to making specific measurements related to the possible contamination of the stratosphere by the chlorofluorocarbons.

Both the STRATCOM VI-A and VII-B balloons were designed and launched by the Aerospace Instrumentation Division and Balloon Branch, respectively, of Air Force Geophysics Laboratory. The balloons were fabricated by Winzen Research, Inc. They were launched from Holloman Air Force Base (HAFB), NM (32° N latitude). Experimental support in terms of radars, rockets, and meteorological data was supplied by White Sands Missile Range (WSMR), NM.

This composite report presents, in one publication, the related results obtained from the various experiments comprising the STRATCOM VI-A and VI-B payloads as determined by the individual investigators. The results, coupled with ECOM Report 5818 [7], "Calculation of Selected Atmospheric Composition Parameters for the Mid-Latitude September Stratosphere," are representative of the correlated multi-instrument approach of the STRATCOM Program to the experimental study of the stratosphere, backed by chemical kinetic theory and atmosphere modeling.

EXPERIMENT DESCRIPTION

The STRATCOM VI-A balloon supported an atmospheric sensing payload weight of 1180 pounds consisting of 29 instruments to make simultaneous measurements of solar uv flux, atmospheric composition, and thermodynamic structure in the 27-40 km altitude interval. The 15.6 million ft^3 balloon (diameter 347 feet) was launched at 2257 MST, 23 September 1975, from HAFB, NM (32° N). It reached its initial float altitude of 38.5 km at 0300 MST on 24 September. The various instruments were activated intermittently during ascent and then continuously for a period extending from 1 hour before to 1 hour after sunrise at 38.5 km (0529 MST). Periodic measurements were made near 38.5 km and during a slow descent which was initiated at 1100 MST. A 2-hour period of continuous measurements was conducted near 27 km through the time of sunset (1828 MST). Sufficient ballast was then released to effect a slow ascent with the balloon reaching an altitude of 36 km at 0200 MST, 25 September. The balloon floated at 36 km until the time of sunrise (0542 MST). The balloon and payloads then rose abruptly to 39.7 km, reaching this altitude at 0812 MST. All instruments were activated before sunrise and made continuous measurements between the altitudes of 36.0 and 39.7 km. These measurements were continued at 39.7 km until 0900 MST when the principal payload

was separated from the balloon and floated downward on a radar-reflective parachute, reaching the earth's surface at 0935 MST. Thus, 33 hours and 38 minutes of atmospheric data were obtained between the altitudes of 2.0 and 39.7 km during the STRATCOM VI-A experiment.

Figure 1 shows the principal payload just before the balloon was launched. The payload was reeled downward to 650 feet beneath the balloon shortly after the time of balloon launching.

A secondary payload was attached to the apex plate of the balloon as shown in Figure 2. Spherical bead thermistors attached to the balloon skin measured this temperature during the flight. Figure 3 shows the horizontal trajectory of the balloon, and Figure 4 shows the balloon altitude versus time, corresponding to the horizontal trajectory of Figure 3.

Figure 5 is a photograph of the principal payload after its parachute descent to the earth's surface at the location indicated in Figure 3. The parachute descent and subsequent landing were such that the payload was recovered intact.

The STRATCOM VI-B payload was launched aboard a 2.9 million ft^3 balloon at 1448 MST, 26 September 1975, from HAFB. The payload is shown in Figure 6.

The average ascent rate of the balloon and payload was approximately 750 feet per minute with a float altitude of 30 km being reached at approximately 1720 MST. Sunset on the balloon occurred at 1830 MST. The altitude of the balloon was stabilized at 30 km through appropriate ballasting. The projection of the balloon trajectory onto a horizontal plane shows that the balloon moved first eastward a distance of 20 miles after launching and during the ascent phase of the flight. After reaching its float altitude near 30 km, the balloon then drifted slowly westward. The flight was terminated near Deming, NM, at a distance of 100 miles west of the launching site. The payload was recovered in good condition.

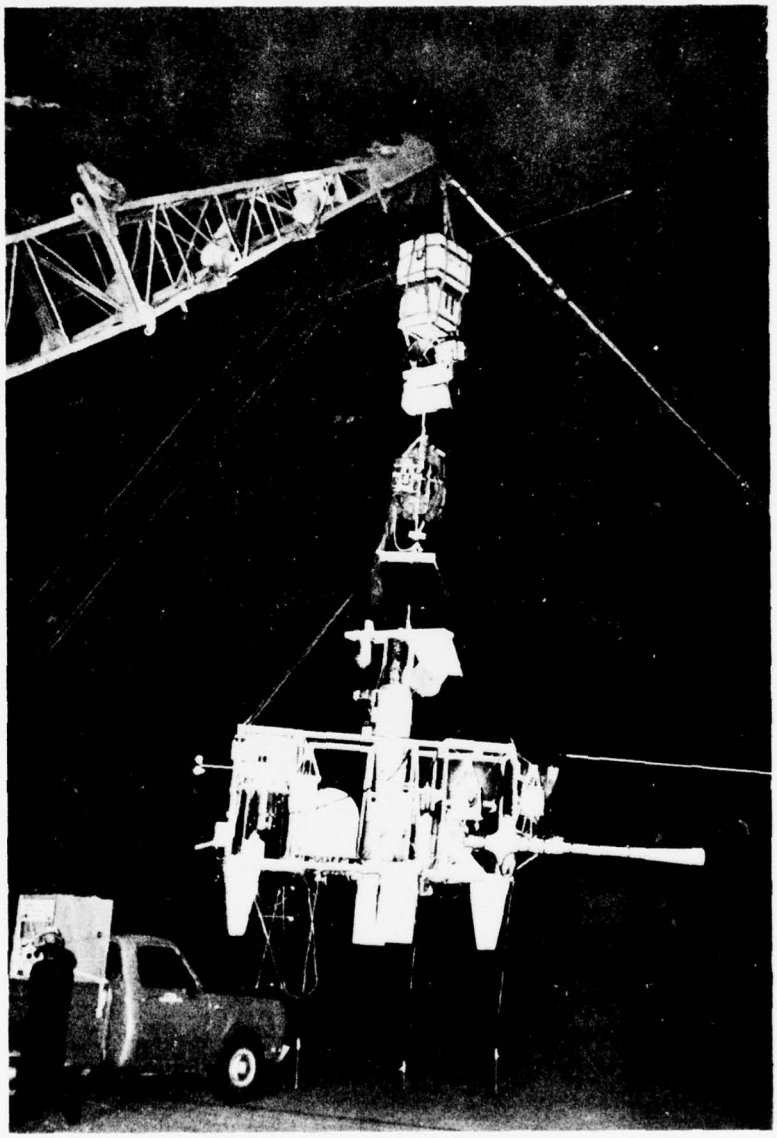

Figure 1. STRATCOM VI-A payload - September 1975.

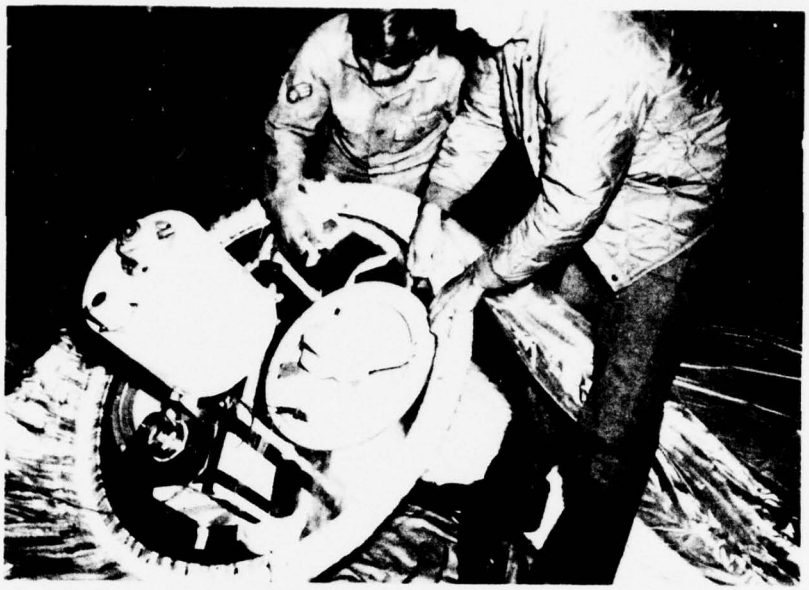

Figure 2. STRATCOM VI apex plate, mounted instrument package - September 1975.

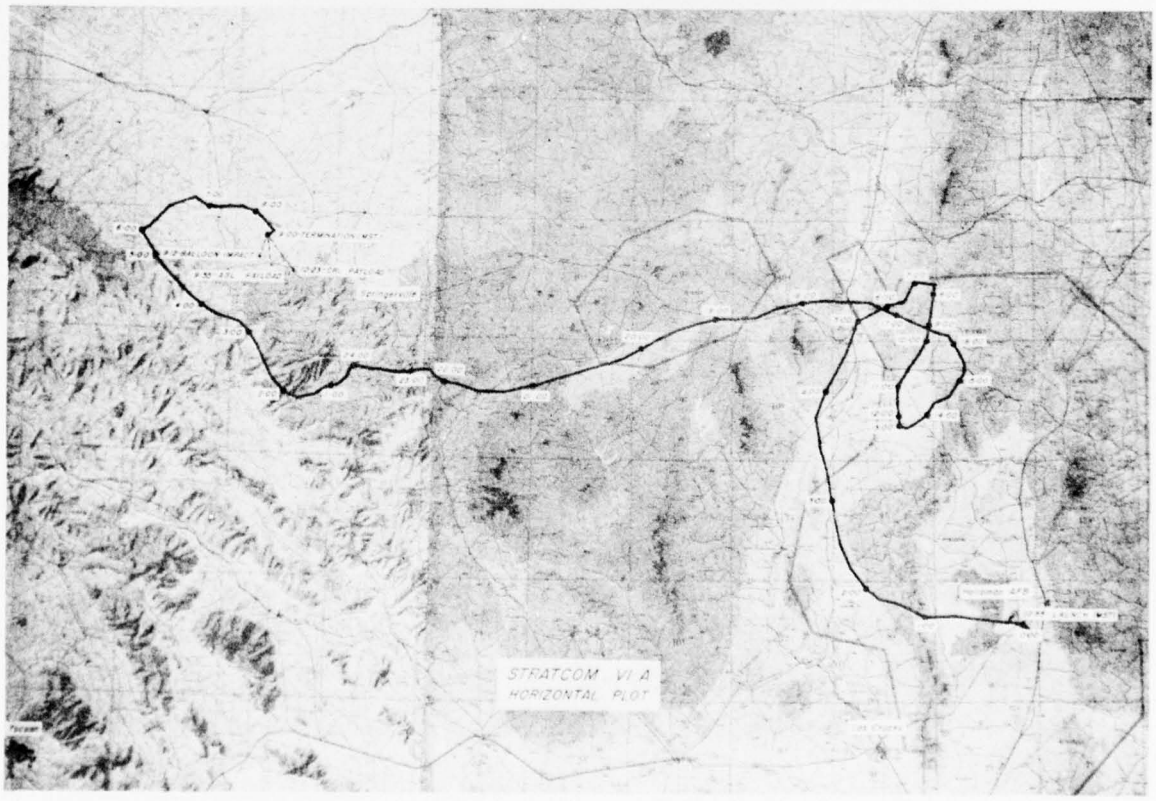

Figure 3. STRATCOM VI-a horizontal trajectory - September 1975.

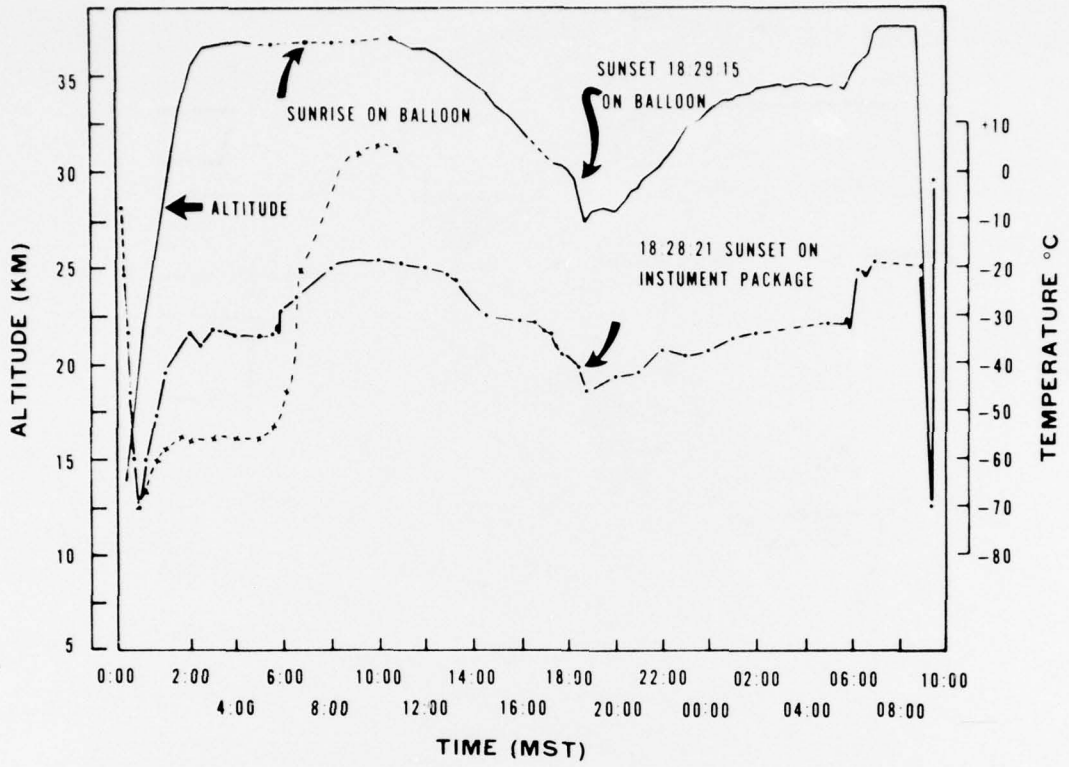

Figure 4. STRATCOM VI balloon altitude as a function of time - September 1975.

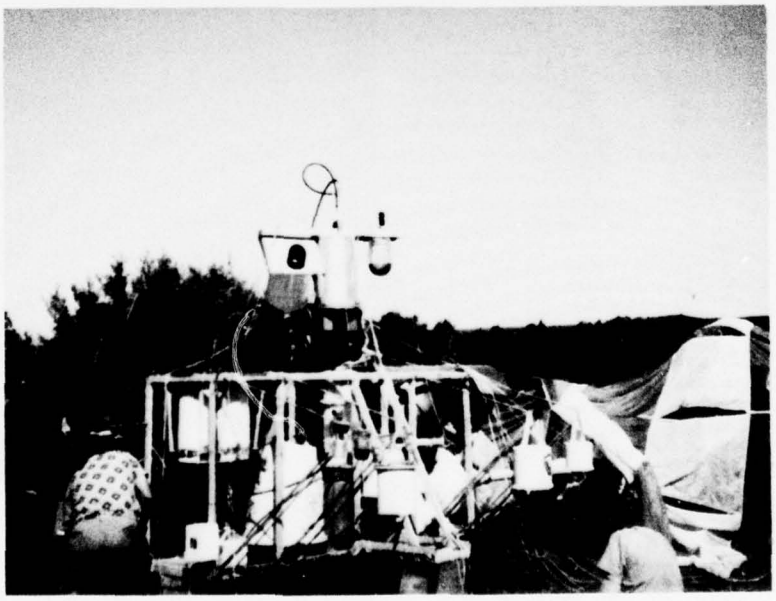

Figure 5. STRATCOM VI-A payload at the recovery site.

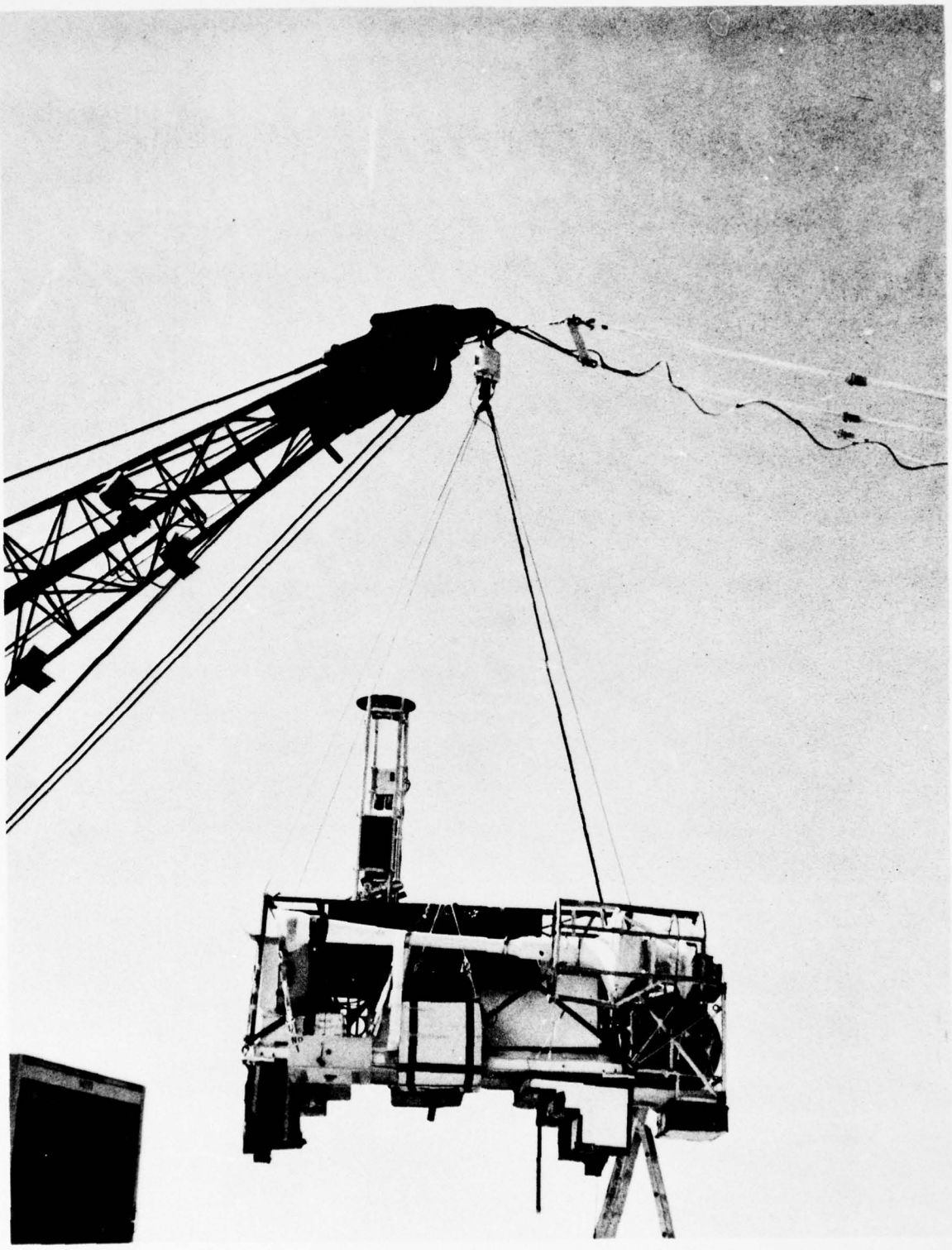

Figure 6. STRATCOM VI-B payload - September 1975.

REFERENCES

1. Ballard, Harold N., N. J. Beyers, M. Izquierdo, and J. Whitacre, 1970, "A Constant Altitude Balloon Experiment at 48 Kilometers," J. Geophys. Res., 75(18):3501-3512.

2. Beyers, N. J., and B. T. Meyers, 1970, "Measurement from a Zero-Pressure Balloon in the Stratopause (48 km)," J. Geophys. Res., 75:3513-3522.

3. Ballard, Harold N., N. J. Beyers, and B. T. Miers, 1972, "Atmospheric Tidal Measurements at 50 km from a Constant-Altitude Balloon," J. Appl. Meteorol., 11(7):1138-1149.

4. Ballard, Harold N., and Frank P. Hudson, 1975, "Stratospheric Composition Balloon-Borne Experiment - 18 September 1972," R&D Report, ECOM-5554, Atmospheric Sciences Laboratory, US Army Electronics Command, WSMR, NM.

5. Ballard, Harold N., M. Izquierdo, Carlos McDonald, and John Whitacre, 1976, "Temperature Measurements in the Stratosphere from Balloon-Borne Instrument Platforms, 1968-1975," R&D Report, ECOM-5808, Atmospheric Sciences Laboratory, US Army Electronics Command, WSMR, NM.

6. Hudson, Frank P., 25 February and 1 March 1976, "Stratospheric Ozone Research and Effects," Hearings before the Subcommittee on the Upper Atmosphere of the Committee on Aeronautical and Space Sciences, United States Senate, Ninety-Fourth Congress, Second Session, pp 146-258.

7. Ballard, Harold N., J. M. Serna, and F. P. Hudson, 1977, "Calculation of Selected Atmospheric Composition Parameters for the Mid-Latitude September Stratosphere," R&D Report, ECOM-5818, Atmospheric Sciences Laboratory, US Army Electronics Command, WSMR, NM.

CHAPTER 2

SUMMARY OF SYSTEM STATE-OF-HEALTH MEASUREMENTS STRATCOM VI-A BALLOON EXPERIMENT

P. B. Herrington
Sandia Laboratories, Albuquerque, NM

ABSTRACT

Various measurements were made to determine the temperature and attitude of the gondola and the status of primary power source and associated power converters. Platinum rod and bead thermistors were used to measure temperatures at selected points throughout the gondola. A two-axis magnetometer and a two-axis pendulum were used to measure principal payload attitude. Voltage and current measurements indicated the status of the primary power sources and associated power converters.

TEMPERATURE MEASUREMENTS

Five temperature measurements were made in order to monitor system status.

The locations of the measurements and type were as follows:

Sensor No.	Location	Type	Temp Range(°C)
1	TM can (top)	Platinum rod	-30 to +70
2	TM can (near bottom)	Bead thermistor	-50 to +50
3	TM can (outside bottom)	Bead thermistor	-50 to +50
4	Battery 1 container	Bead thermistor	-50 to +50
5	Frame (azimuth drive)	Platinum rod	-45 to +55

Sensors 1 and 2 were located inside the main electronics housing (TM can) which was located on the principal payload. The top and sides of the TM can (which was pressurized to 15 psia) were aluminum painted on the outside surfaces with EPO-LUX No. 100 white epoxy paint. Approximately 1-1/2 in. of styrofoam insulation was used around the inside of the top and sides of the can. The bottom of the TM can was alodyne (conductive chromate) aluminum which was approximately half covered with 1-in. styrofoam. The power dissipated within the housing was 6 W on standby and between 50 and 120 W while the system was on. During the STRATCOM VI-A experiment, the power dissipated inside the TM can averaged 70 W while the system was on.

Sensor 3 was mounted to the outside of the bottom of the TM can.

Sensor 4 was mounted inside the battery 1 container which was mounted on the gondola. This container housed 18 Yardney LR-100 cells which were insulated from the walls of the container by 2-1/2 in. of styrofoam. All surfaces of the container were alodyne aluminum. Prior to launch, the battery 1 container was heated (with heating tapes wrapped around the exterior) to a sensor reading of 28°C. Very little power (700 mW peak) was dissipated inside the battery container during the flight.

Sensor 5 was mounted to the azimuth drive section of the sun tracker system. Since very little power (less than 1 W) was dissipated within the azimuth drive section, sensor 5 essentially measured the frame temperature.

Figure 1 shows variation in temperature as measured by sensors 1 through 5.

ATTITUDE MEASUREMENTS

Pendulum

A two-axis potentiometric pendulum was used to determine the levelness of the instrument frame. The reference directions for the "X" and "Y" pendulums are shown in Fig. 2. The full-scale measurement range in both the x and y directions was ±5 deg with a sensitivity of 0.5 V/deg.

The X pendulum readings showed a nearly linear variation of levelness from 0.5 deg at launch to 1.25 deg at sunset. The readings remained constant from sunset until immediately prior to cutdown.

The Y pendulum readings showed a constant offset of -0.5 deg throughout the experiment.

The variations in the X pendulum readings were probably caused by the evaporation of the cryogens used by various experiments on the gondola.

The pendulum data reflected only the levelness of the instrument frame. Any pendulum motion of the payload on the support between the payload and the balloon could not be detected.

Magnetometer

Two Heliflux RAM-5C magnetometers were used to measure the magnetic direction of the x-axis of the principal instrument frame. Figure 2 shows the payload instrument layout and magnetometer reference direction. The top payload on which was mounted the sun tracker, heterodyne radiometer, uv photometer, and uv spectrometer, was not hard mounted to the bottom instrument frame. Therefore, its pointing direction was unknown except during most of the daylight hours when it was pointing at the sun.

Figures 3A through G show the magnetic direction in the x-axis during the sunrise and sunset periods. Analysis of these plots shows that the payload is much more likely to oscillate through an angle less than 360 deg than it is to spin in the same direction for a 360-deg rotation.

A comparison of the magnetometer data from STRATCOM VI-A with that of STRATCOM III* reveals that it would be a difficult task to predict a "typical" spin rate of a balloon-borne instrument package.

POWER SUPPLY MONITORS

Primary power for the experiments was supplied by three battery packages. Battery 1 was made up of 18 Yardney LR-100 silver-zinc cells, and batteries 2 and 3 were made up of 18 Yardney LR-20 silver-zinc cells. Each LR-100 cell has an average voltage of 1.5 and a capacity of 100 ampere-hours. Each LR-20 cell has an average voltage of 1.5 and a capacity of 20 ampere-hours.

Battery 1 was used from launch until 0400 MDT 25 September. The voltage monitor indicated a launch voltage of 29 and a final (0400 MDT 25 September) voltage of 25. Battery 2 was used from 0400 MDT through 0900 MDT 25 September. The voltage monitor indicated an initial voltage of 27.5 and a final voltage of 26.5. Battery 3 was used from 0900 MDT, 25 September through termination. The voltage monitor indicated no change in the initial reading of 28 V.

Twelve dc-dc power converters were employed to supply various voltages to the experiments. The voltage monitors indicated that all 12 converters maintained voltage outputs within ±2.5 percent of the prelaunch voltage values.

---

*H. N. Ballard and F. P. Hudson, "Stratospheric Composition Balloon-Borne Experiment," ECOM-5554, Atmospheric Sciences Laboratory, US Army Electronics Command, WSMR, NM, Sep 72.

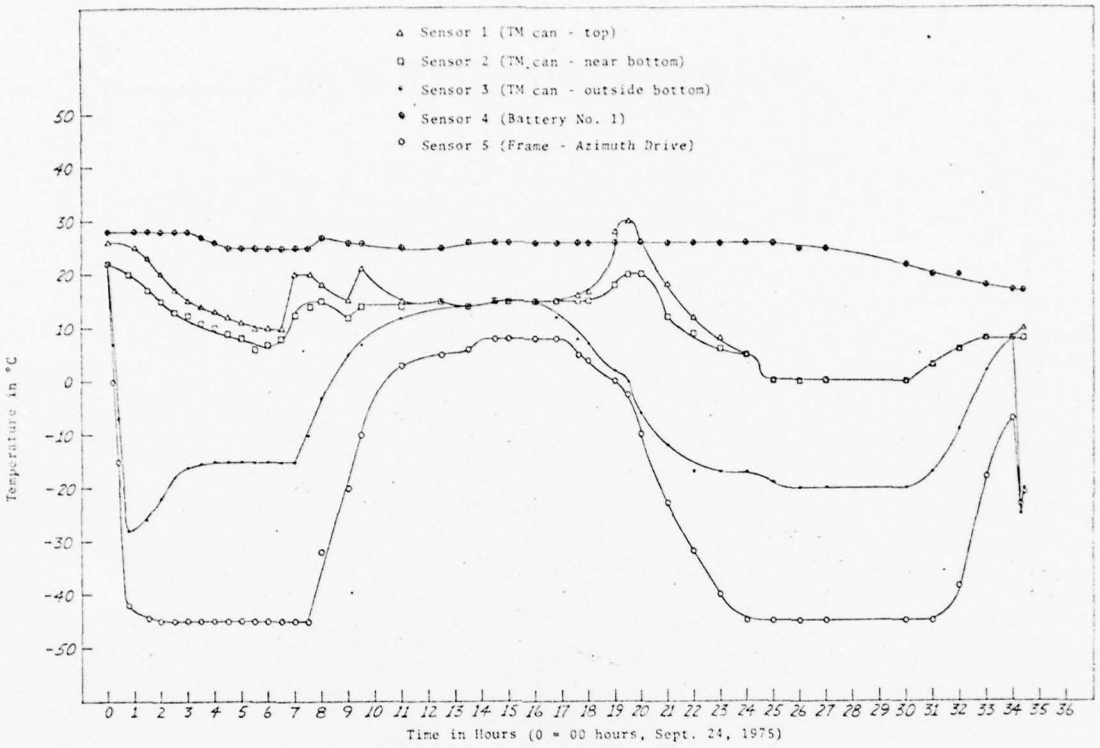

Figure 1. STRATCOM VI-A system temperature monitors.

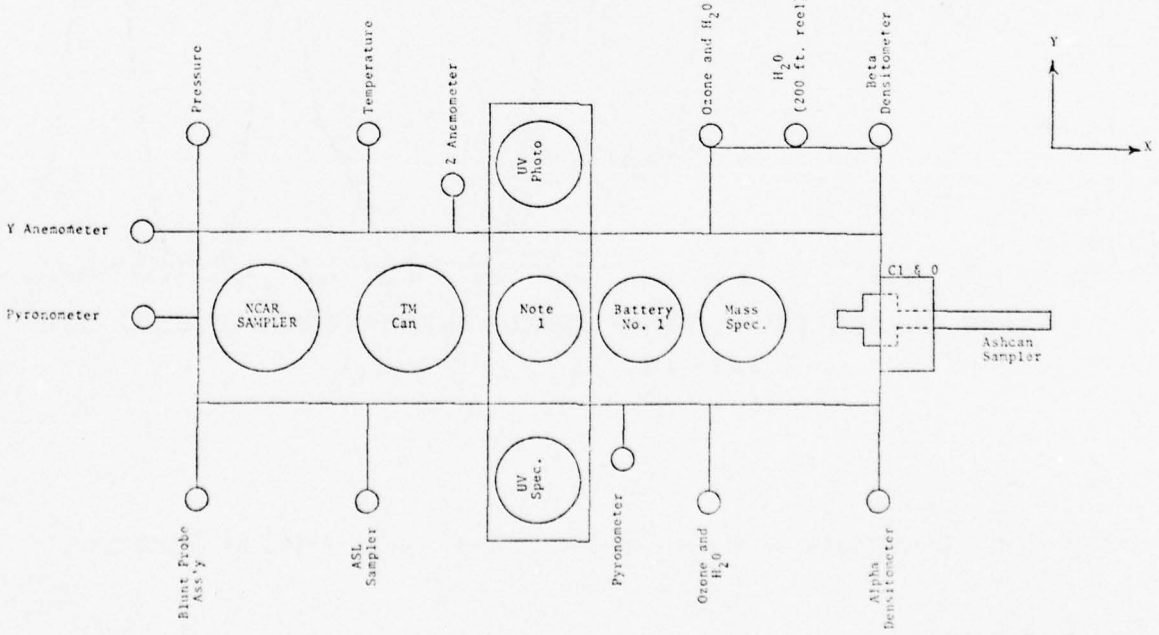

Figure 2. STRATCOM VI-A instrument frame with X and Y reference directions.

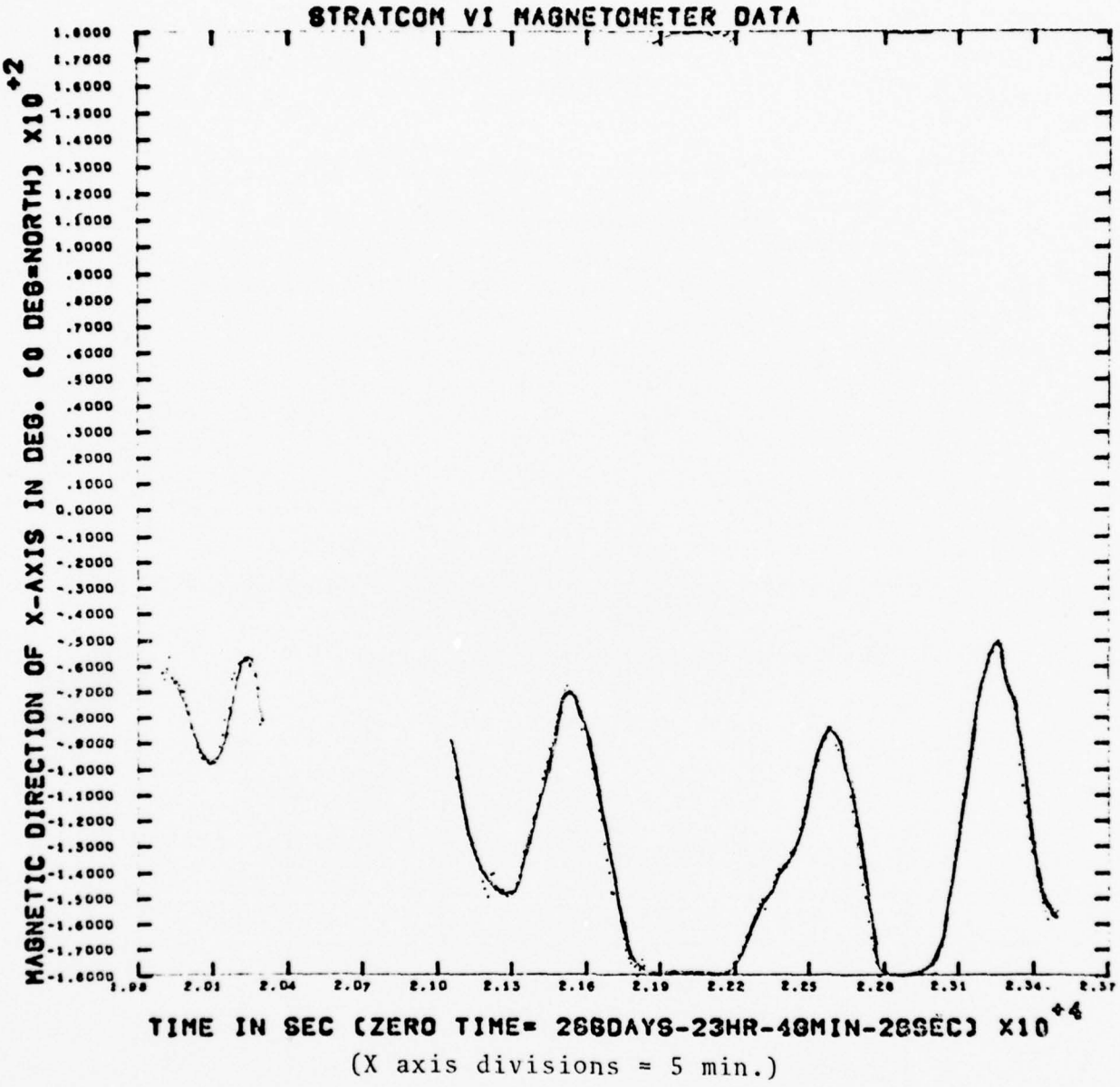

(X axis divisions = 5 min.)

Figure 3a. Directions of X axis during sunrise data period 24 September.

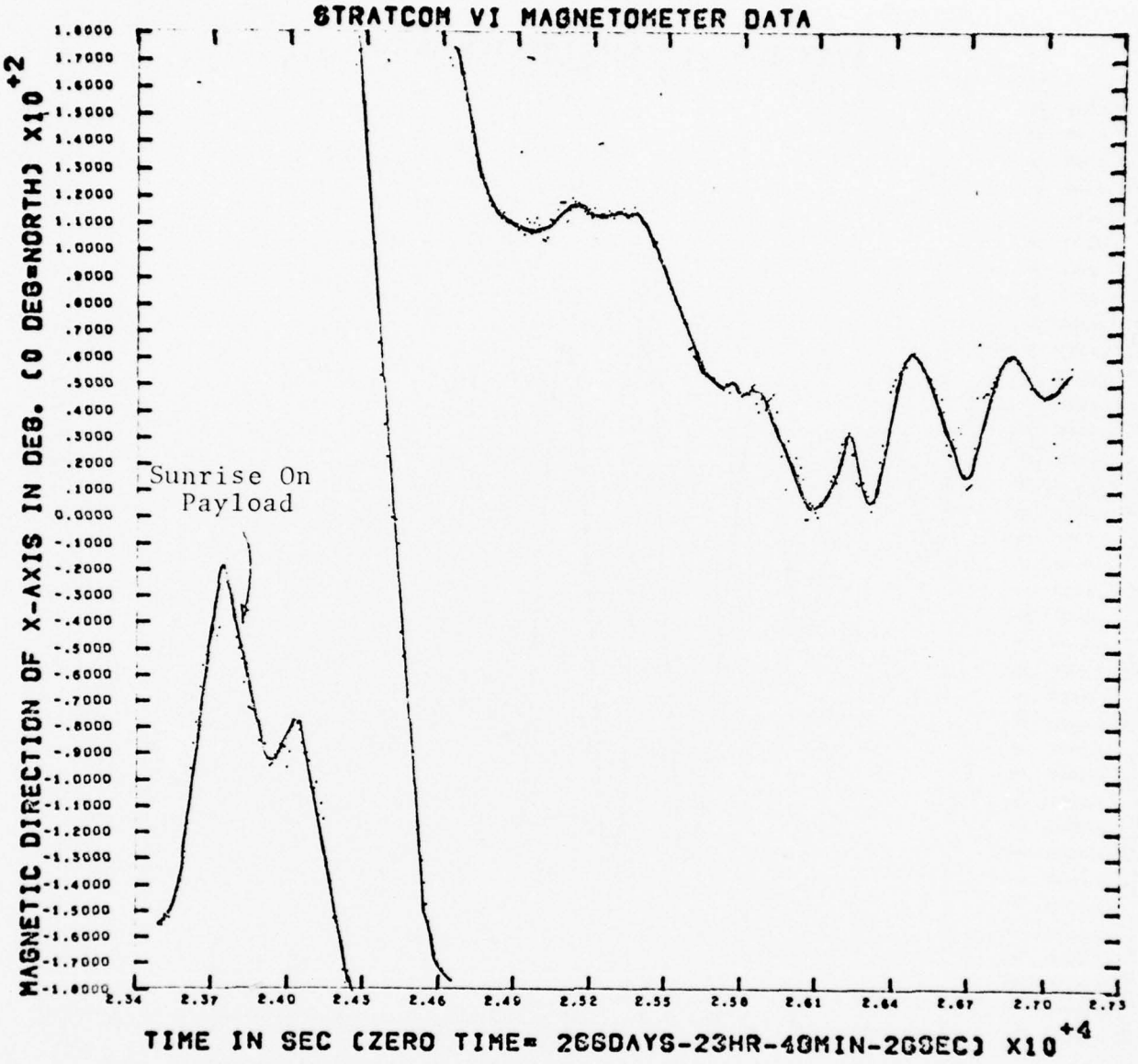

(X axis divisions = 5 min.)

Figure 3b. Direction of X axis during sunrise data period 24 September.

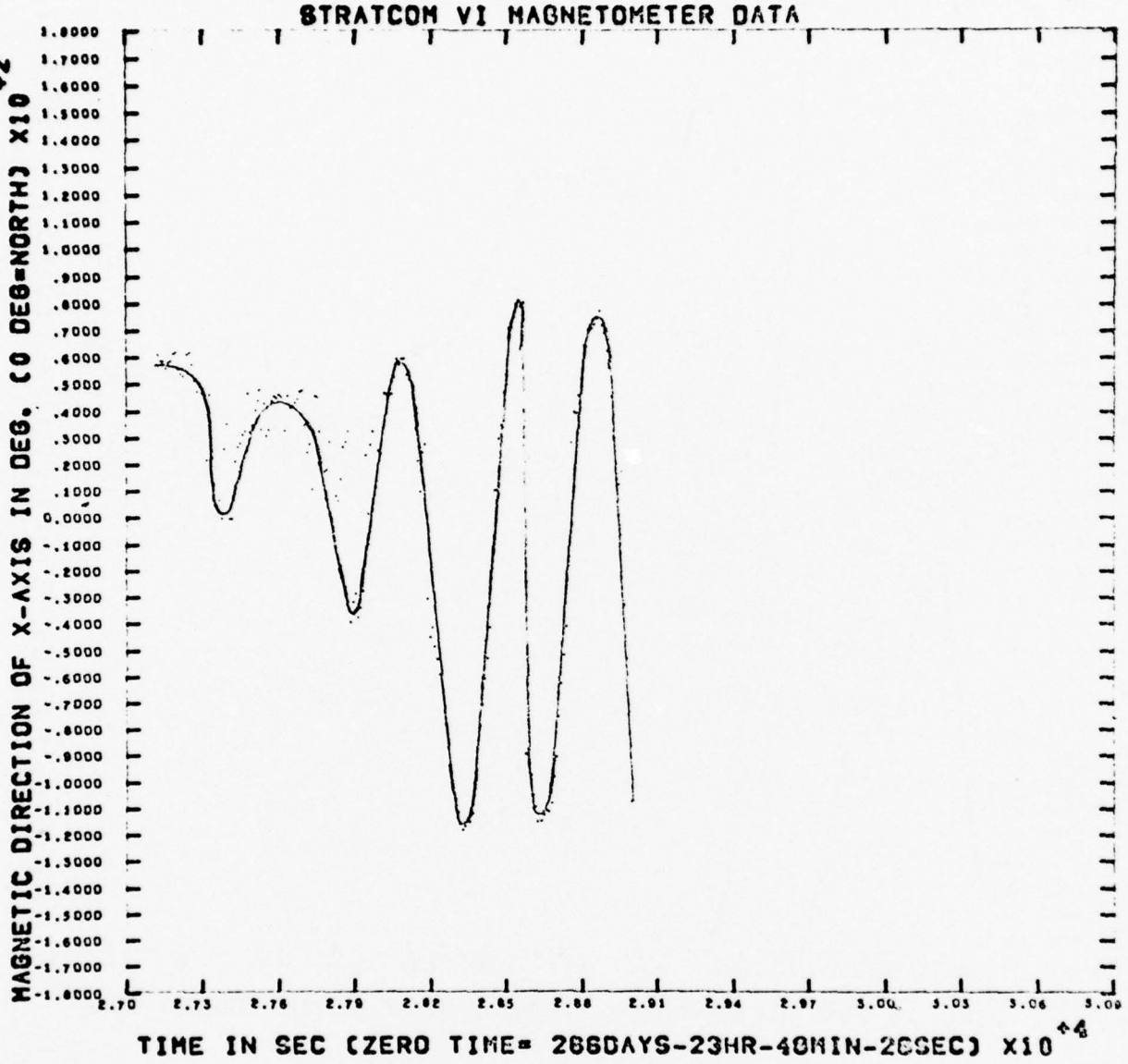

(X axis divisions = 5 min.)

Figure 3c. Direction of X axis during sunrise data period 24 September.

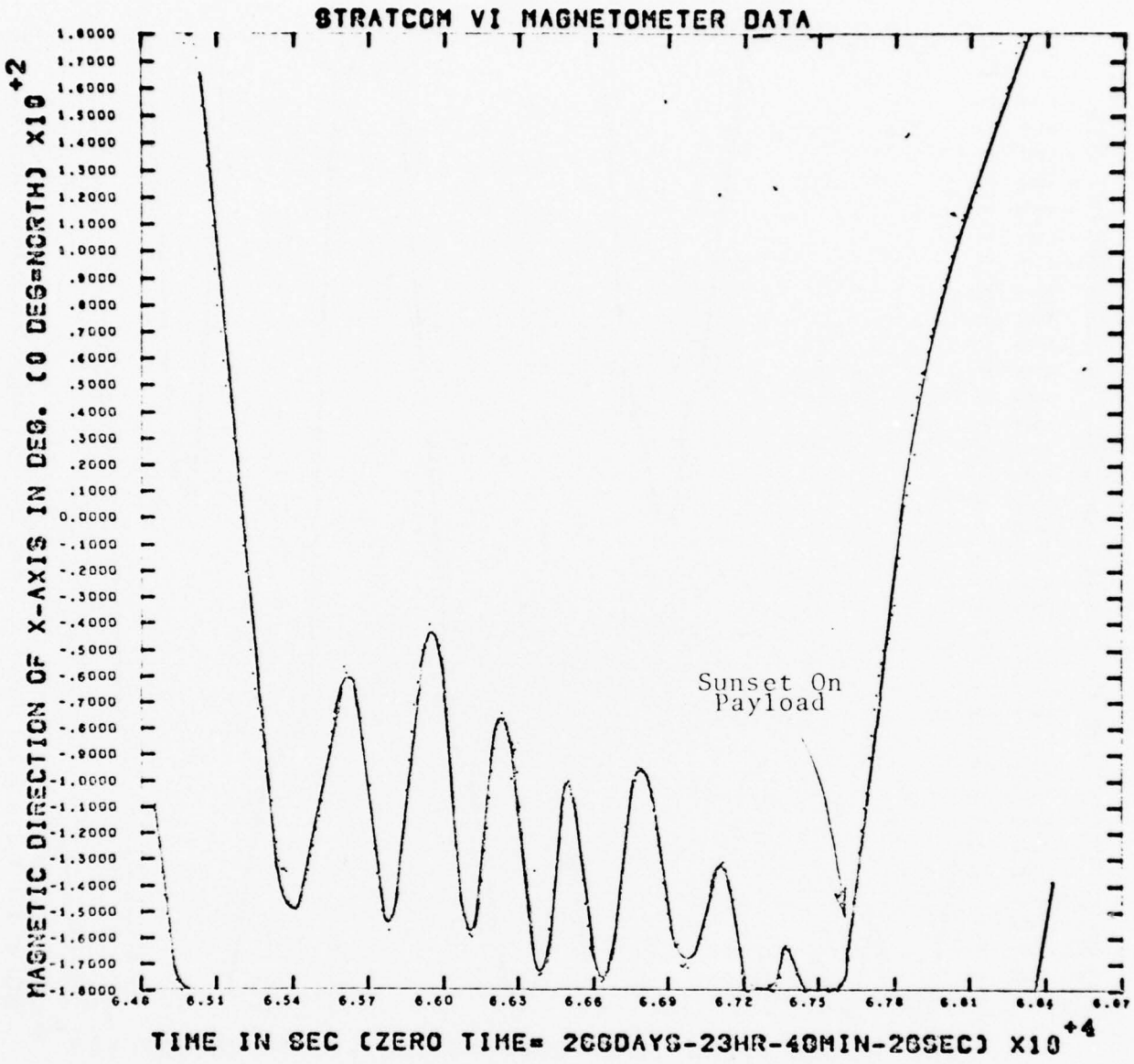

(X axis divisions = 5 min.)

Figure 3d. Direction of X axis during sunset data period 24 September.

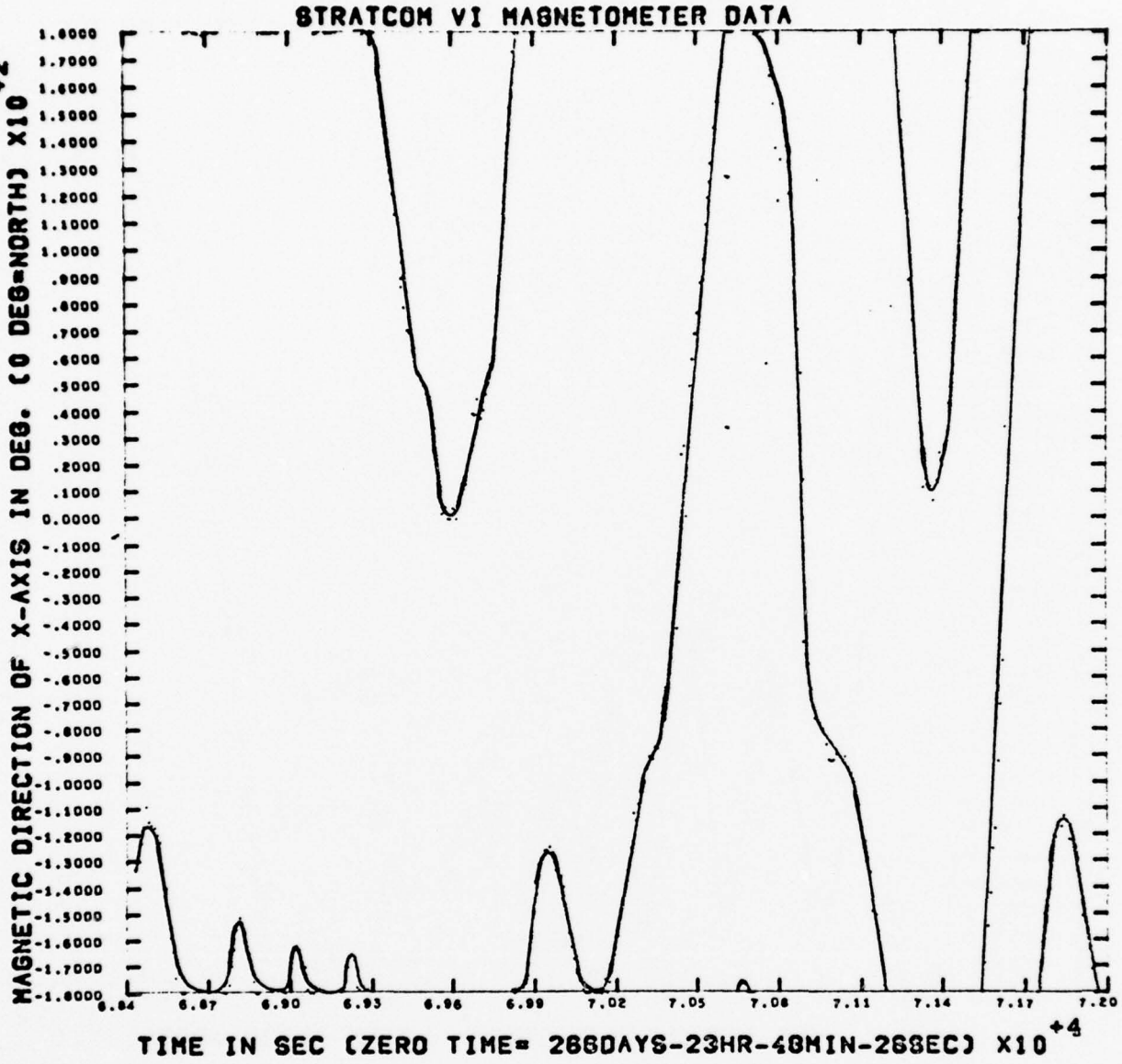

(X axis divisions = 5 min.)

Figure 3e. Direction of X axis during sunset data period 24 September.

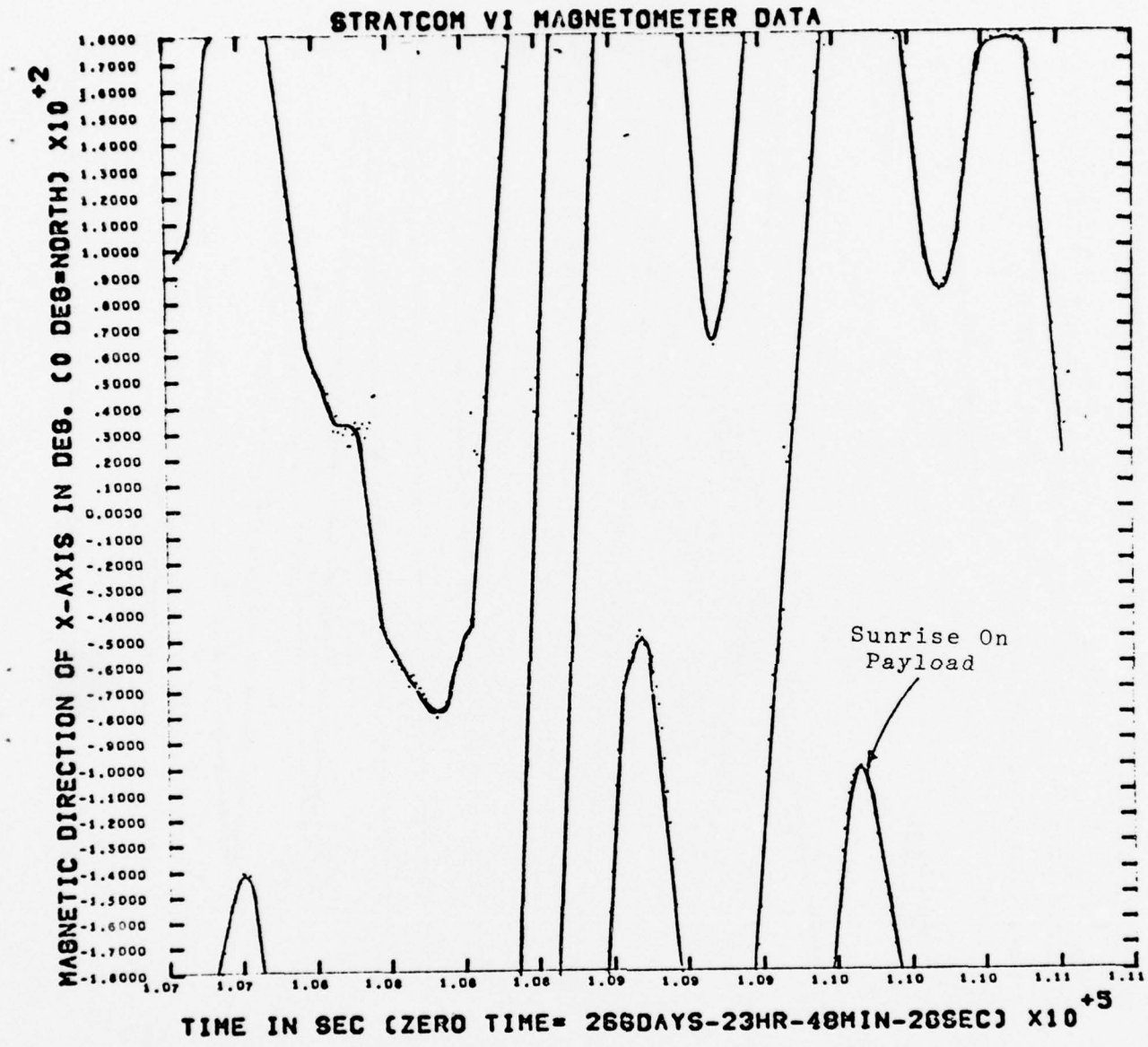

(X Axis divisions = 5 min.)

Figure 3f. Direction of X axis during sunrise data period 25 September.

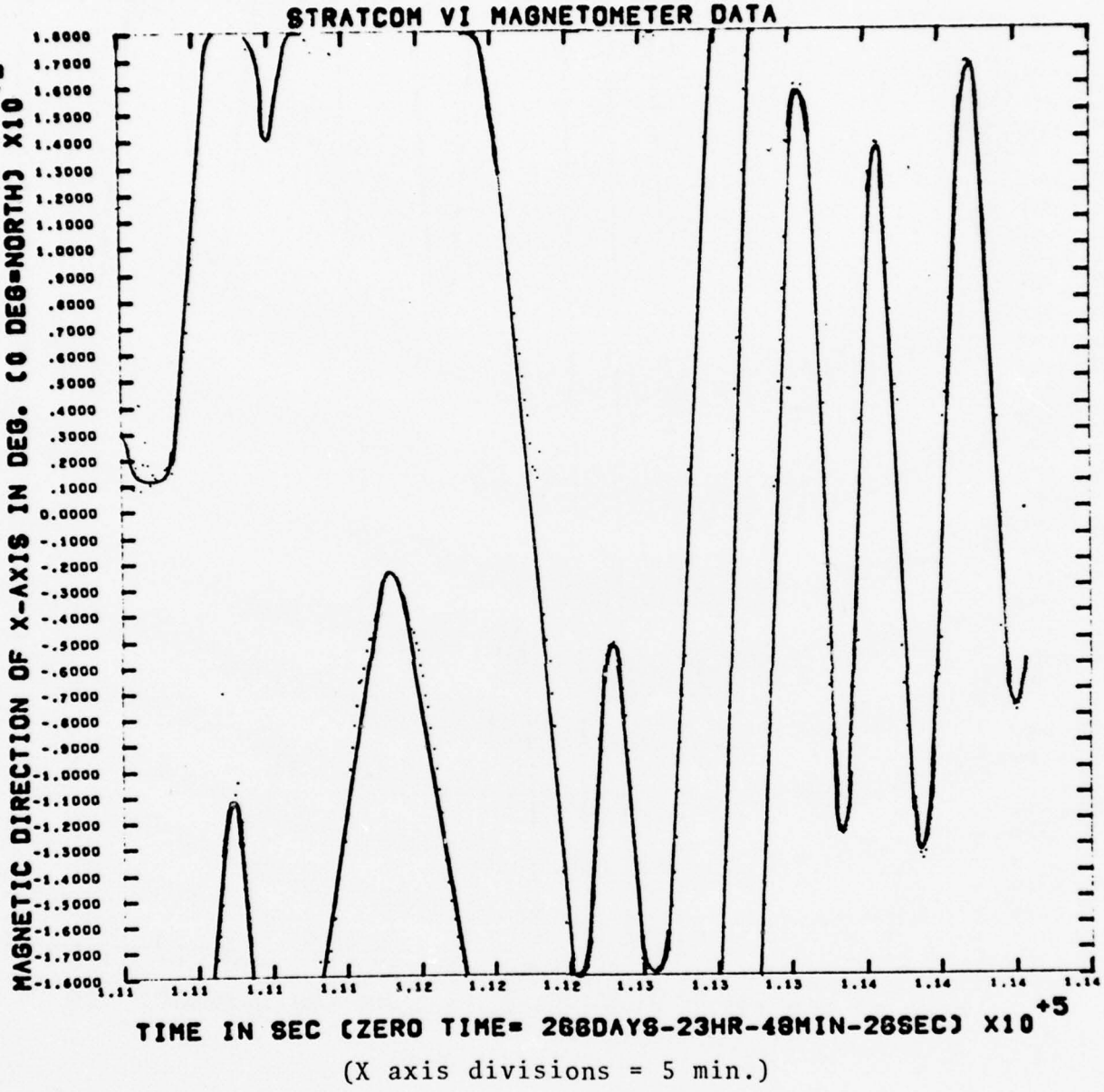

(X axis divisions = 5 min.)

Figure 3g. Direction of X axis during sunrise data period 25 September.

CHAPTER 3

TEMPERATURE MEASUREMENTS IN THE 27-40 KM ALTITUDE INTERVAL, STRATCOM VI-A BALLOON-BORNE EXPERIMENT

Harold N. Ballard
Atmospheric Sciences Laboratory, WSMR, NM

Miguel Izquierdo
Carlos McDonald
John Whitacre
University of Texas at El Paso, El Paso, TX

ABSTRACT

By mounting film-mounted thermistors in the configuration described in this report and by separating the payload-mounted sensors as far as practical from the balloon surface (2 to 3 balloon diameters), accurate (±1°C) measurements of atmospheric temperature can be made directly from balloon-borne platforms without recourse to theoretical corrections to the observed temperatures. Temperature measurements made with these sensors during a period of approximately 33 hours as the balloon traversed the 27-40 km atmospheric altitude interval, when supplemented by temperature measurements from previous STRATCOM balloon-borne experiments in the 40-50 km interval, indicated that the range of temperature variations to be associated with the atmospheric diurnal tide within the 30-50 km altitude interval lies between 7° and 12°C and is highly variable on a day-to-day basis.

INTRODUCTION

Based upon information obtained and experience gained in the measurement of temperatures in the stratosphere with sensors mounted on the balloon-borne platforms of STRATCOM I through STRATCOM V [1], a coupled pair of film-mounted spherical bead thermistors again served as atmospheric temperature sensors aboard the principal payload beneath the STRATCOM VI-A balloon. The solar radiation correction to the measured temperatures can be experimentally determined through the known geometric orientation of the two film-mounted sensors relative to the known direction of incident solar radiation and determination of instrument platform rotation rate from magnetometer data [2]. Figure 1 shows the film-mounted thermistor configuration. Figure 1 of Chapter 1 shows the location of the two temperature sensors on the STRATCOM VI-A payload with the temperature sensors extending below the left end of the instrument-bearing frame.

It was also established during these balloon-borne experiments that the temperature sensors were greatly influenced by the presence of the large balloon as the balloon floated upward with the sensors following in the balloon wake; however, if the instrument platform beneath the balloon was separated from the balloon by a distance of as much as two balloon diameters, the temperature recorded by the sensors on the platform was not influenced by the presence of the balloon when the balloon was stably floating or slowly descending [2].

Therefore, shortly after the time of balloon launching, the principal payload of STRATCOM VI-A was reeled downward a distance of approximately 650 ft (balloon diameter 347 ft), the maximum allowable distance based upon weight restrictions for the reel-down mechanism as related to total system weight and the planned vertical trajectory of the balloon and payload.

The previous STRATCOM flights had also demonstrated that it was extremely informative, as related to the problem of the thermal contamination of the atmosphere as caused by the presence of the relatively large balloon, to measure the temperature of the balloon surface. Therefore, spherical bead thermistor temperature sensors were attached to the balloon surface of the STRATCOM VI-A balloon as shown in Fig. 2. The output of these sensors was then coupled to the instrument package mounted on the balloon apex plate (Fig. 2, Ch 1).

TEMPERATURE MEASUREMENTS

The balloon altitude corresponding to the horizontal trajectory of Fig. 3, Ch 1, as well as the temperatures measured by the thermistors mounted on the principal payload and the balloon skin are presented as functions of time in Fig. 3 of this chapter. The balloon-skin temperature measurement, after 1100 MST, was not transmitted to the ground-based receiver due to depletion of battery power by the instrument on the apex plate. Excessive use of heater power at the low temperature of -35°C, in the period 0100 to 0600, 25 September (Fig. 3), produced this instrument failure.

With the payload separated from the base of the balloon by a distance of 650 ft, many of the characteristics of the temperature records which were obtained in the 5-38 km interval (0000-0600 MST, 24 September, Fig. 3) are similar to the temperature-versus-time record for the STRATCOM III experiment of September 1972 [3]. As the balloon ascended during the night, the atmospheric and balloon-skin temperatures approached the tropopause temperature of -72°C (17.5 km). After the balloon passed through the tropopause, the balloon-skin temperature came to -54°C and remained near this temperature until the time of visible sunrise at the balloon altitude.

With the balloon floating at 38.5 km, the atmospheric temperature recorded by the sensors on the principal payload beneath the balloon registered -34°C at 0400 MST. After the time of sunrise, with the balloon remaining at an altitude of 38.5 km, the atmospheric temperature increased rapidly

until 1100 when the sensors registered -22°C, a temperature increase of 12°C in the period 0400-1100 MST. In the same time interval, the balloon-skin temperature increased from -54° to +5°C, becoming 24°C warmer than the surrounding atmospheric temperature.

The temperature between 1100 MST on 24 September and 0400 on 25 September, corresponding to the indicated altitude profiles of the balloon, is as represented in Fig. 3.

At 0400 on 25 September, the balloon was floating at 36.0 km with the sensors registering an atmospheric temperature of -33°C. At 0900, with the balloon now floating at 39.7 km, the recorded air temperature had increased to -24°C. From the 1962 Standard Atmosphere, the temperature gradient in the 36-40 km interval is +3°C/km. The change in altitude of approximately 4 km thus precludes any conclusion concerning the temperature change at 36 km in the time interval 0400-0900 on 25 September; however, when the payload was descending on its parachute after separation from the balloon at 0900, the temperature recorded at 36 km by the film-mounted thermistor atmospheric temperature sensors suspended below the payload was -31°C. The descent rate of the parachute and payload at 36 km was 62 m/s. The aerodynamic heating term and dissipation factor in the heat transfer equation for the film-mounted spherical bead thermistors [4] are of such values so as to give an aerodynamic heating correction to the observed temperature at 36 km of -1.5°C while the parachute is descending at the indicated speed.

Thus, the temperature change at 36 km registered on 25 September by the temperature sensor, first floating on the balloon at 0400 and then descending on the parachute at 0900 + 1 minute, is essentially zero.

A comparison of results obtained on 24 September at 38.5 km (the change in temperature equal to +12°C in the period 0400-1100) with the results obtained at 36 km on 25 September (the change in temperature being essentially zero in the period 0400-0900) indicates that the results are not systematically repetitive on two successive days.

SUMMARY AND CONCLUSIONS

When launched so as to reach its float altitude in the stratosphere during the night, the balloon remains much colder than the atmosphere after it passes through the tropopause. After the time of sunrise, the balloon is heated by incident solar radiation, finally reaching temperatures warmer than the surrounding atmosphere.

The argument has been proposed, based upon evidence presented [1], that infrared energy radiated from the balloon surface is absorbed by an envelope of water vapor surrounding the balloon. The degree of absorption is related to the concentration of water vapor in the envelope. As the radiation is absorbed by the water vapor, converted to thermal energy and trapped in the water vapor envelope, the maximum temperature measured on

the balloon surface is then directly related to the water vapor concentration surrounding the balloon and the rate of deposition of solar energy.

By mounting the film-mounted thermistors in the configuration described in this and referenced previous reports, and by separating the payload mounted sensors as far as experimentally practical from the balloon surface (2 to 3 balloon diameters), accurate (±1°C) measurements of atmospheric temperature can be made directly, without recourse to theoretical corrections to the observed temperatures.

The attempts to establish the amplitude of the temperature variations to be associated with the stratospheric diurnal tide, as determined by balloon-borne temperature sensors floating generally with a specific parcel of air, are not entirely conclusive; however, the results obtained previously from the STRATCOM II and III experiments [1] and now from this balloon-borne experiment indicate that the range of the variations to be associated with this tide within the 40-50 km altitude interval lies between 7° and 12°C and is highly variable on a day-to-day basis.

It is advocated that temperature measurements be made aboard balloon-borne experiments related to the composition and charged particle structure of the stratosphere. In addition to giving background data for temperature-dependent experiments, a close examination of the records of the temperature sensor serves as a useful tool for obtaining detailed information concerning the balloon and payload behavior.

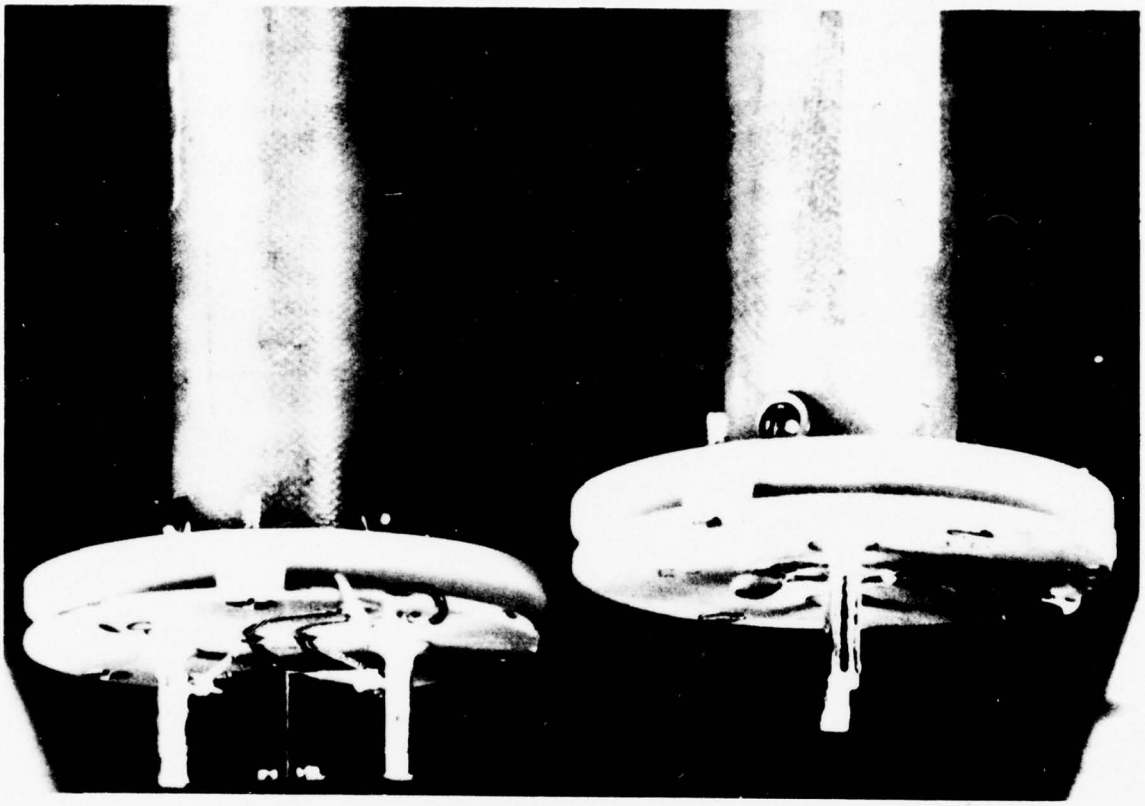

Figure 1. STRATCOM VI-A film-mounted spherical bead thermistor configuration - September 1975.

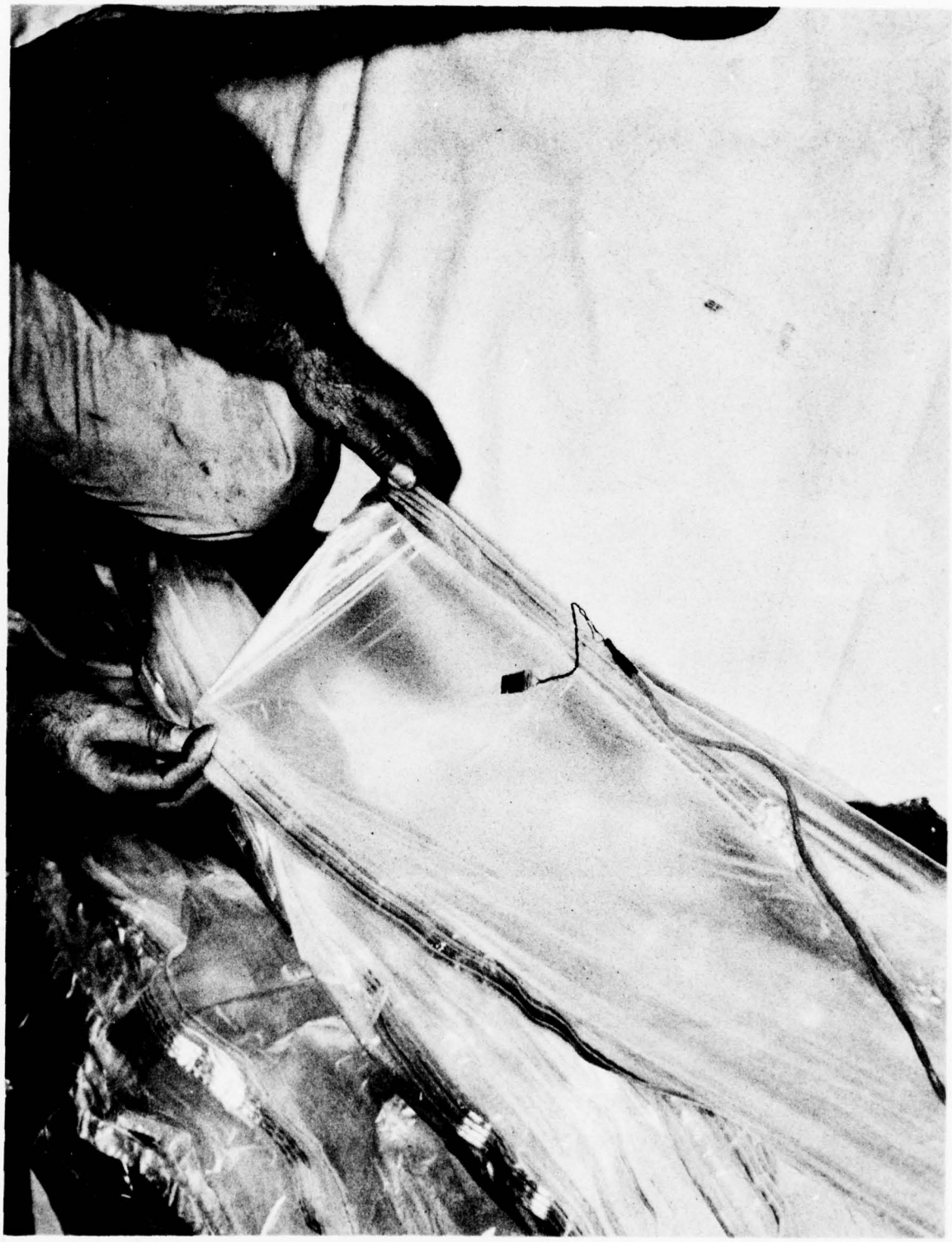

Figure 2. Balloon-skin temperature sensors STRATCOM-VI-A - September 1975.

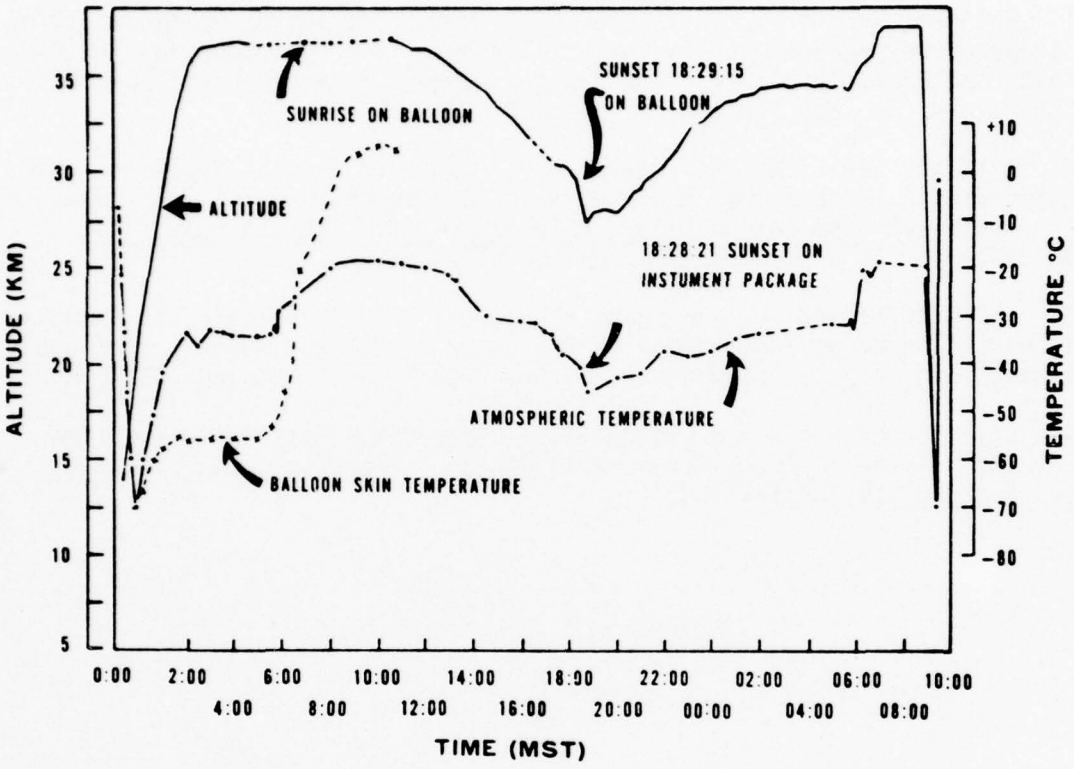

Figure 3. STRATCOM VI-A balloon altitude, atmospheric and balloon-skin temperatures as functions of time - September 1975.

REFERENCES

1. Ballard, Harold N., M. Izquierdo, C. McDonald, and J. Whitacre, 1976, "Temperature Measurements in the Stratosphere from Balloon-Borne Instrument Platforms, 1968-1975," R&D Report, ECOM-5808, Atmospheric Sciences Laboratory, US Army Electronics Command, WSMR, NM.

2. Ballard, Harold N., M. Izquierdo, C. McDonald, and J. Whitacre, 1974, "Atmospheric Temperatures Measured Near 48 Kilometers by Balloon-Borne Thermistors," Proceedings Eighth AFCRL Scientific Balloon Symposium, 30 September to 3 October 1974, pp 401-415.

3. Ballard, Harold N., and Frank P. Hudson, 1975, "Stratospheric Composition Balloon-Borne Experiment, 18 September 1972," R&D Report, ECOM-5554, Atmospheric Sciences Laboratory, US Army Electronics Command, WSMR, NM.

4. Ballard, H. N., and B. Rofe, 1969, "Thermistor Measurements of Temperature in the 30-65 km Atmospheric Region," Progress in Astronautics and Aeronautics, 22:141-166.

CHAPTER 4

ION ANEMOMETRY AS A MEANS OF DETERMINING RELATIVE WINDS DURING A STRATOSPHERIC BALLOON EXPERIMENT

R. O. Woods
D. S. Miyoshi
Sandia Laboratories, Albuquerque, NM

ABSTRACT

Developmental models of a flight instrument have been flown on two occasions. During STRATCOM V, operation was intermittent but adequate to demonstrate feasibility of concept. Further refinement produced the STRATCOM VI instrument described here. Operation was achieved during virtually the entire flight, although the windspeed was below the range of the instrument during most of the flight. This is not a fundamental limitation; instruments can be configured for a lower threshold airspeed.

ACKNOWLEDGMENT

This program involved a cooperative effort among a number of persons besides the authors of this paper. The authors would like to record here their gratitude to R. D. Myers and L. L. Sandlin for the initial circuit design and layout, to R. W. Willey for additional circuit development, and to R. L. Schellenbaum for his assistance in preparing the system for its second flight.

INTRODUCTION

The objective of this program has been to develop an instrument which can be installed on any stratospheric balloon when data are required concerning relative winds. The need for such data is becoming increasingly urgent because of the trend toward in situ analysis of atmospheric composition and properties. Experiments wherein air is sampled in the immediate vicinity of the payload rather than analyzed remotely (viz., by absorption spectroscopy) require at the very least an estimate of the extent to which the sample has been perturbed by contact with payload surfaces. Ideally, a clean sample could be obtained if a finite airflow were known to exist and sampling were performed on the upwind side. No means exists at present for making the necessary airflow measurements.

Beyond aiding with the strictly technical problem of sampling, data regarding wind shears and small-scale turbulence [1] would be of considerable theoretical interest in obtaining an understanding of the transport properties of the stratosphere and hence of its interactions with pollutants.

PRIOR ART

Conventional mechanical sensors such as rotating-vane anemometers or Pitot-static probes are excluded for the present application because of the extremely low dynamic pressures involved. Velocity may range down to a few centimeters per second and density to a small fraction of 1 percent of its sea level value. Thus, an alternate approach was chosen in which a parcel of air is tagged and its transit time measured over a known distance. This is most easily accomplished by using an electrical discharge to produce ions and then sensing the arrival of a current pulse at another point by using an electrometer.

Ion anemometry is not a new technique and has, in fact, been applied to a balloon experiment in the past [2]. That instrument, however, was used to measure flow speeds in a sampling duct, whereas this one is to measure the free-stream air velocity. This instrument differs also in that it is intended to measure speeds approximately an order of magnitude lower than those measured by earlier instruments.

Other anemometer concepts are described in [3] through [5]. These instruments are for the most part still in the developmental stage, and all are intended for use at one atmosphere. They should, however, be regarded as possible alternative approaches to the problem.

DESCRIPTION OF APPARATUS

Figure 1 shows mechanical details of the anemometer. Three such assemblies mounted along mutually perpendicular axes comprise an omnidirectional system. An open-ended tube is equipped with grids at each end and a pair of electrodes at the center. An intermittent electrical discharge is produced at "A." The resulting ions drift through the tube and are collected at grid "C." The current pulse is carried by the signal lead "D" to a remotely located electrometer and telemetering circuitry. Grid "B" is grounded to the shell of the tube and serves to reduce capacitive coupling between the high-voltage electrode and the signal grid. Three such assemblies have a mass of 1.2 kg.

Because the signal grids on opposite ends of the tube are connected to a common lead, the instrument is capable of determining flow speed but not direction. The ambiguity could be removed at the expense of additional circuitry. This would involve connecting each grid to a separate detector. Such a complication was regarded as unnecessary on a prototype flight, especially since the primary interest was in determining net movement of the air past the payload, the direction being a matter of relatively little concern.

The outputs of the three single-axis anemometers were multiplexed upon a single telemetering channel. The system which accomplished this is shown in Fig. 2. On the left are three high-voltage supplies which continually transmitted 3000 V pulses of approximately 1-ms duration at intervals of 0.2 s to each of three electrode assemblies. On the right are shown the electrometer and sampling circuitry in which the outputs of the three instruments are sampled in sequence and transmitted to the telemetry system. The three anemometers are sampled for periods of 15 s each with the remaining 15 s being an "off" condition for time reference.

Figure 3 shows all the circuitry required by the three instruments. The circuit board is 10 by 12.5 cm. The two metal boxes contain power supplies. The mass of the entire assembly including cables is 0.623 kg, and no particular effort has been made to miniaturize the circuitry. Three leads extending to the left carry signals, and the leads which extend downward are for high voltages. The multipin connector brings in battery power and carries the connections to the telemetering system.

Figure 4 is a schematic of the electronic circuitry. The 5 Hz clock generates timing pulses which fire the SCR 2N3004. Capacitor C stores the energy to be delivered to the high-turns-ratio pulse transformer which then generates the high-voltage pulse for the electrodes. The value of C can be chosen to optimize operation at a given altitude. A single TEC 150 V at 1 W power supply serves all three high-voltage driver sections. The 5 Hz clock output is superimposed on the input to the VCO channel to provide a time-mark indicating initiation of the discharge. The amplifier section has a field-effect-transistor input followed by a logarithmic amplifier. A data multiplexer samples the three anemometers and provides an "open" position as determined by a 15-s clock and counter combination.

For STRATCOM VI the three anemometers were oriented as given by Table 1.

TABLE 1

ANEMOMETER ORIENTATION, STRATCOM VI

Anemometer	Orientation	Capacitor, C	Optimum Altitude Range
X	Horizontal	.022μF	20-40 km
Y	Vertical	.022μF	20-40 km
Z	Vertical	.047μF	5-30 km

This arrangement was chosen to maximize the probability of obtaining data from the flight, for cross-checking air velocity readings, and for testing the effect of varying the value of C. Greater emphasis was placed upon

sensing vertical winds because of interest in the "bobbing" motion of the balloon about its nominal float altitude and because data gathered during ascent and descent could be compared to radar data.

PERFORMANCE

Anemometer data were gathered at intervals during the 34-hour flight of STRATCOM VI on 24-25 September 1975 with approximately 9 hours of data accumulated. The anemometers were continuously operated whenever the instrument payload was turned on. Performance of the system was excellent, with only isolated, temporary instances of anemometer malfunction. These occurred primarily at low altitudes and during the rapid descent following payload cutdown. At low altitudes the air pressure was too great to reliably sustain an electrical discharge at the ion-generating electrodes, and at high-air velocities misfires also occurred.

The range of velocities that could be measured by the anemometers was determined in the laboratory to be approximately 0.6 to 8.0 m/s. The anemometers were uncalibrated; the results should therefore be only used as a qualitative indication of air movement. The lower velocity detection limit was a consequence of the diffusion of the ion cloud during transit from the source to the receiving grid; the longer the transit time the poorer the quality of the signal received. At high velocities, misfires occurred, as well as saturation of the electronics when a discharge did take place. During most of the flight, air velocities were below the lower limit of the anemometers, but there were sufficient instances of definite air movement to be assured that the anemometers were functioning properly. Reasonably good agreement was obtained between the vertical anemometer data and the time variation in radar altitude data for the ascent portion of the flight. At cutdown, all anemometers indicated air motion which soon exceeded their upper limits.

Figure 5 shows a sketch of the data format. The repetition rate was approximately five per second. The spike is a mark that indicates the time of the ion-generating electrical discharge, and the current waveform follows. From the circuit schematic (Fig. 4), note that ac coupling was used; consequently, the trigger pulse caused an undershoot and subsequent return to zero upon which the ion signal was superimposed. Arrival of the ion cloud at the receiving grid was determined by visual analysis of the anemometer output on an oscilloscope. For short transit times (high velocities) the arrival time of the center of the ion cloud is easily recognized. For transit times greater than about 100 ms, judgement is required on the part of the observer. The air velocities shown in the figures were determined by taking the ratio of the anemometer pathlength (0.1 m) to the transit time of the ion cloud generated by the electrical discharge. As mentioned above, such velocities must be regarded as uncalibrated pending wind tunnel tests to relate airflow through the tubes to true airspeed at varying angles of attack.

DATA PRESENTATION

The data gathered during STRATCOM VI are shown in Fig. 6-a through 6-i and are expressed in air velocity (m/s) as a function of MDT. Each anemometer output was sampled on a 15-s/min basis by a data multiplexer, with one 15-s period being an "off" condition. Therefore only 25 percent of the total data were transmitted to the ground. The data presented in the figures are of potential value to other experimenters on STRATCOM VI as a means of indicating the presence of horizontal or vertical winds. Since the time-of-day which happens to be of interest and the time resolution required in the data will vary from experiment to experiment, all data received on the ground are included in the figures. The data are represented by the following symbols:

⊙ Horizontal anemometer

⊡ Vertical anemometer - optimized for 20-40 km

◈ Vertical anemometer - optimized for 5-30 km

Each data symbol is a summary of the 15-s sampling interval and represents about 75 data points. The error bars shown in the figures indicate the range of velocities recorded during the interval. A time history of the 75 data points within a sampling interval is available upon request.

The lower and upper limits of the anemometers are approximately 0.6 and 8.0 m/s. Most of the data gathered during the flight were less than the lower velocity limit and are represented by a symbol at 0.6 m/s with an error bar extending to zero velocity; i.e., the actual air velocity was between zero and 0.6 m/s. A horizontal line is drawn at 0.6 m/s to facilitate identification of these lower limit measurements.

Occasional data points are missing due to a variety of conditions:

Noise in the payload-to-ground communications link.

Inoperative payload-to-ground communications link.

Noise in the anemometer circuitry.

Suppression of the electrical discharge due to low altitude or high air velocity.

CONCLUSION

Three prototype anemometers were flown as part of the instrument payload on STRATCOM VI. Data gathered during the flight are presented. Results indicate net air velocities of less than 0.6 m/s throughout most of the flight, although horizontal components between 1 m/s and 2 m/s due to wind shear were occasionally noted. Significant horizontal wind probably existed for greater portions of the flight than are indicated by our data

since flow parallel to only a single axis in the horizontal plane was sensed. Since the instruments were not calibrated these results should be regarded as order-of-magnitude only.

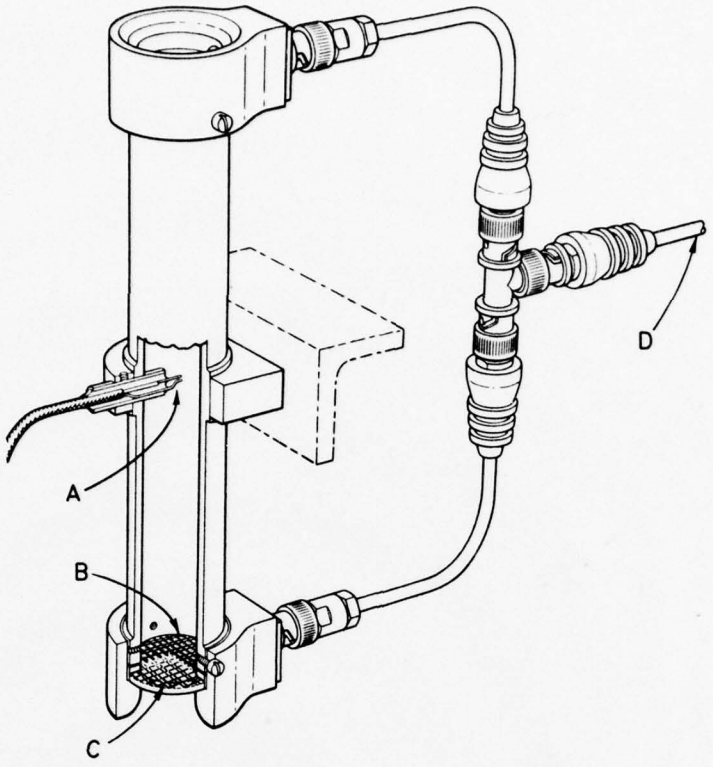

Figure 1. Anemometer geometry.

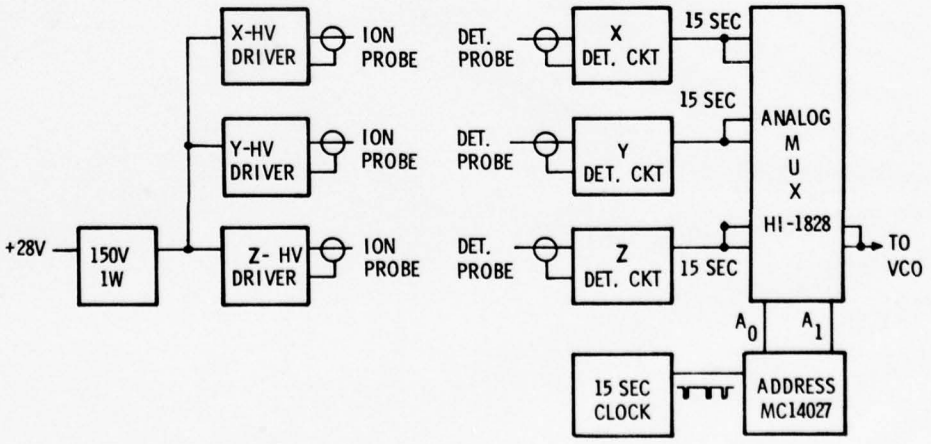

Figure 2. Block diagram of system.

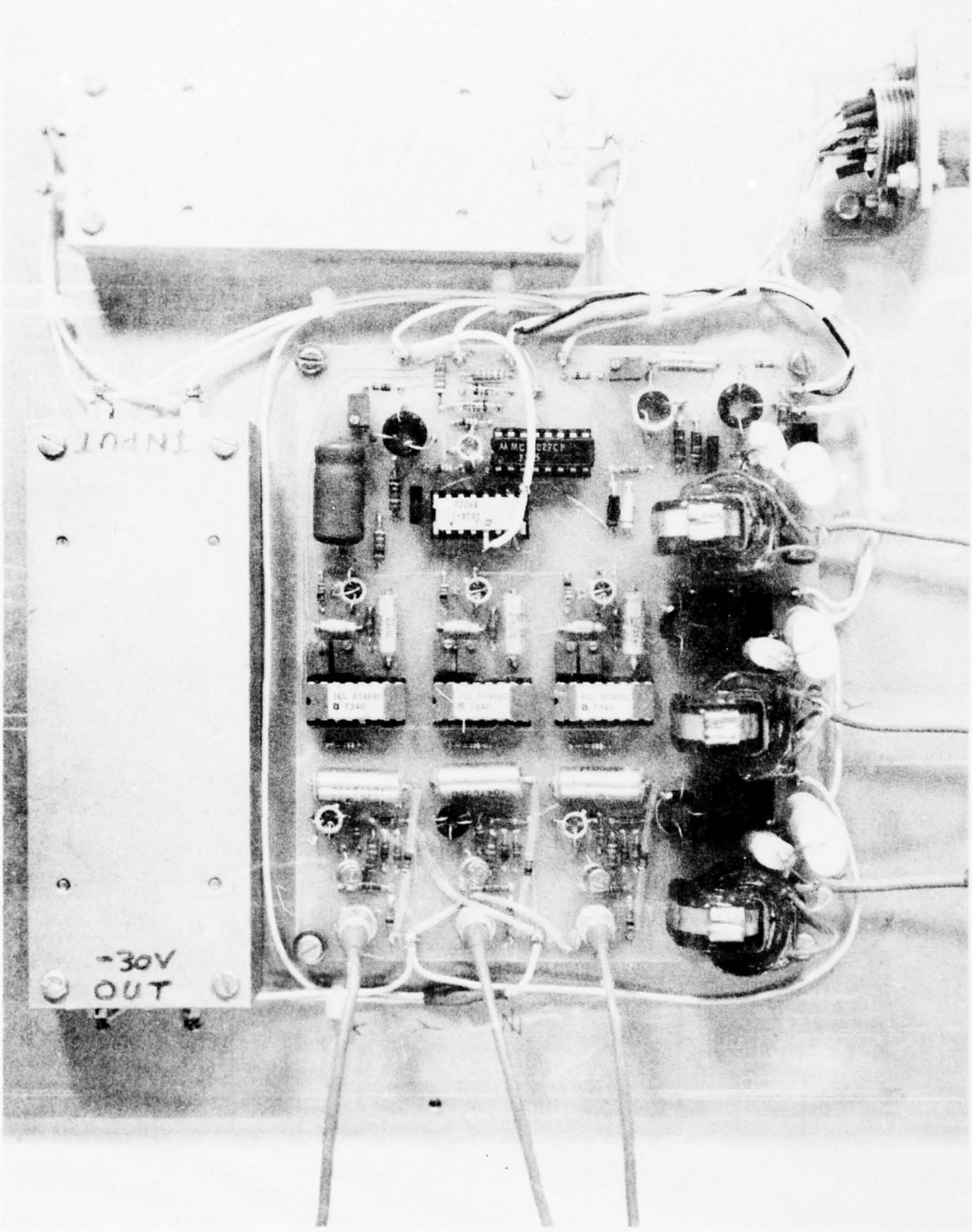

Figure 3. Photograph of circuitry required by the three anemometers.

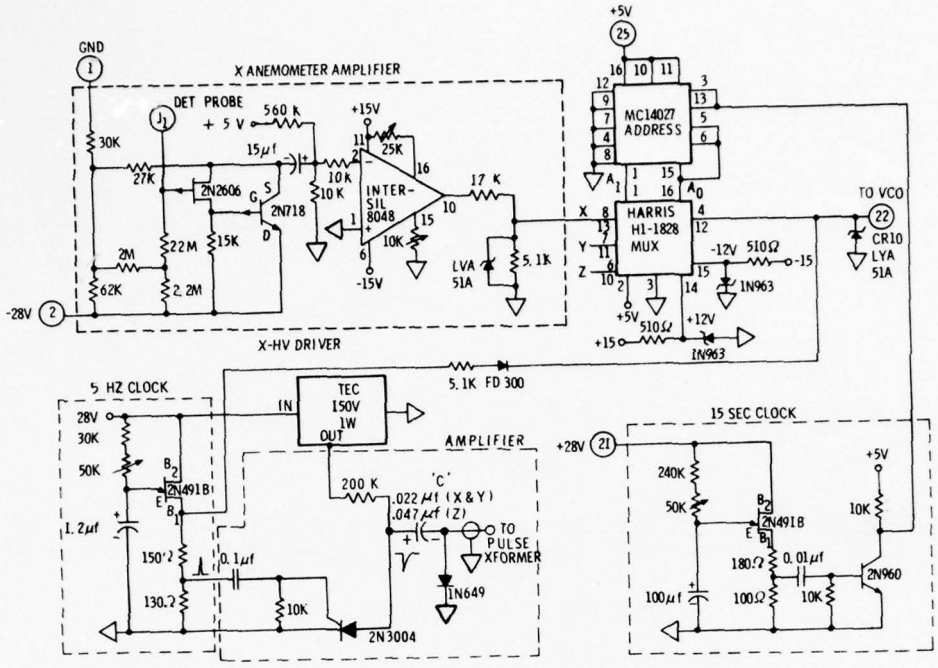

NOTE: REPEAT ANEMOMETER AMPLIFIER FOR Y AND Z AZIS.
REPEAT AMPLIFIER SECTION OF H. V. DRIVER FOR Y & Z AXIS.

Figure 4. Circuit diagram of anemometer electronic circuitry.

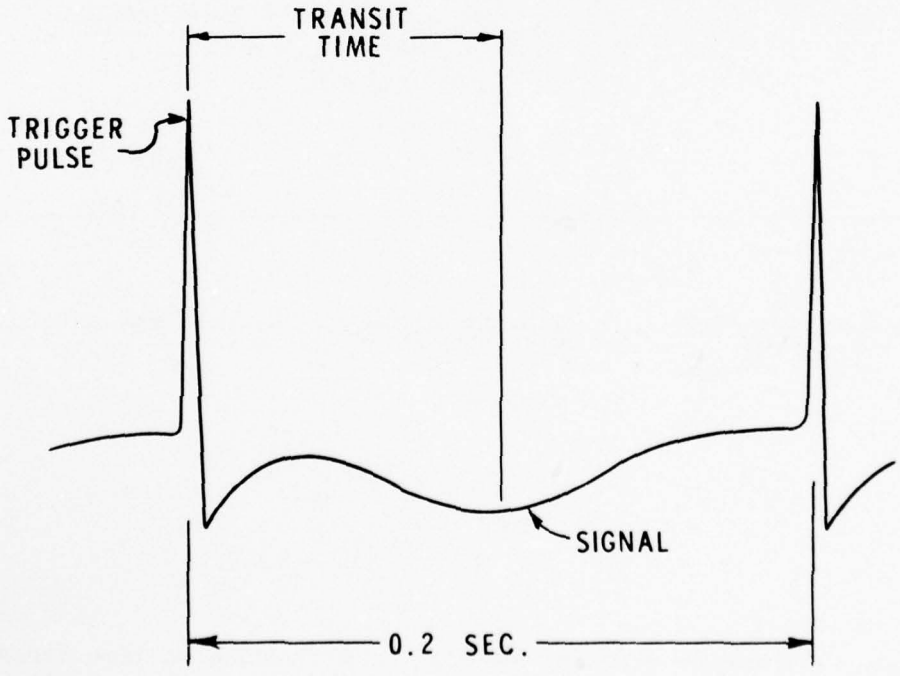

Figure 5. Data format.

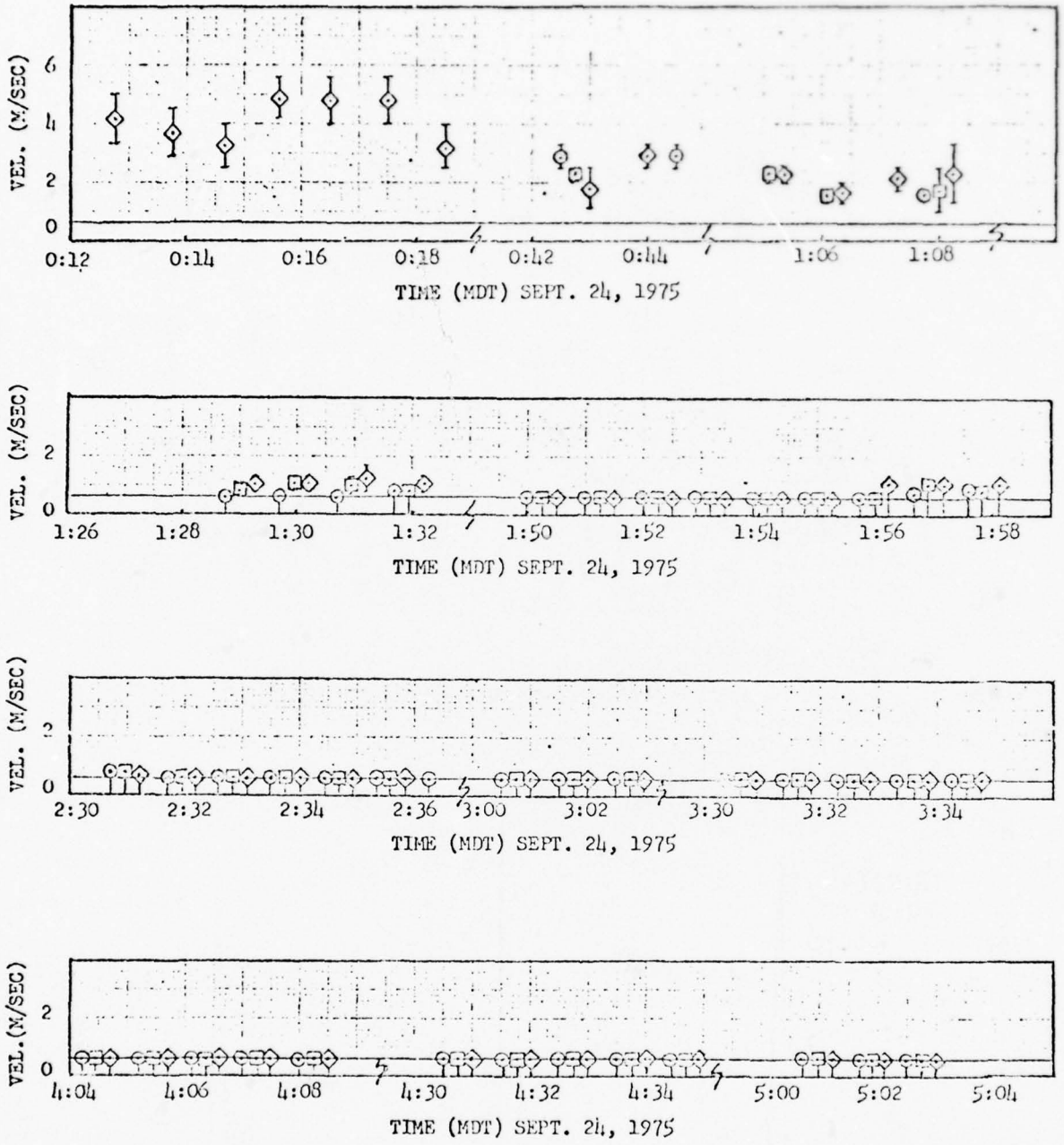

Figure 6-a. Anemometer velocity readings as a function of time (mountain daylight time). Data shown are range of readings during 15-second sampling intervals. The horizontal line at 0.6 m/sec. is the lower limit of the anemometer. ⊙ = Unit "X" (Horizontal), ⊡ = Unit "Y" (Vertical) ◇ = Unit "Z" (Vertical). See text.

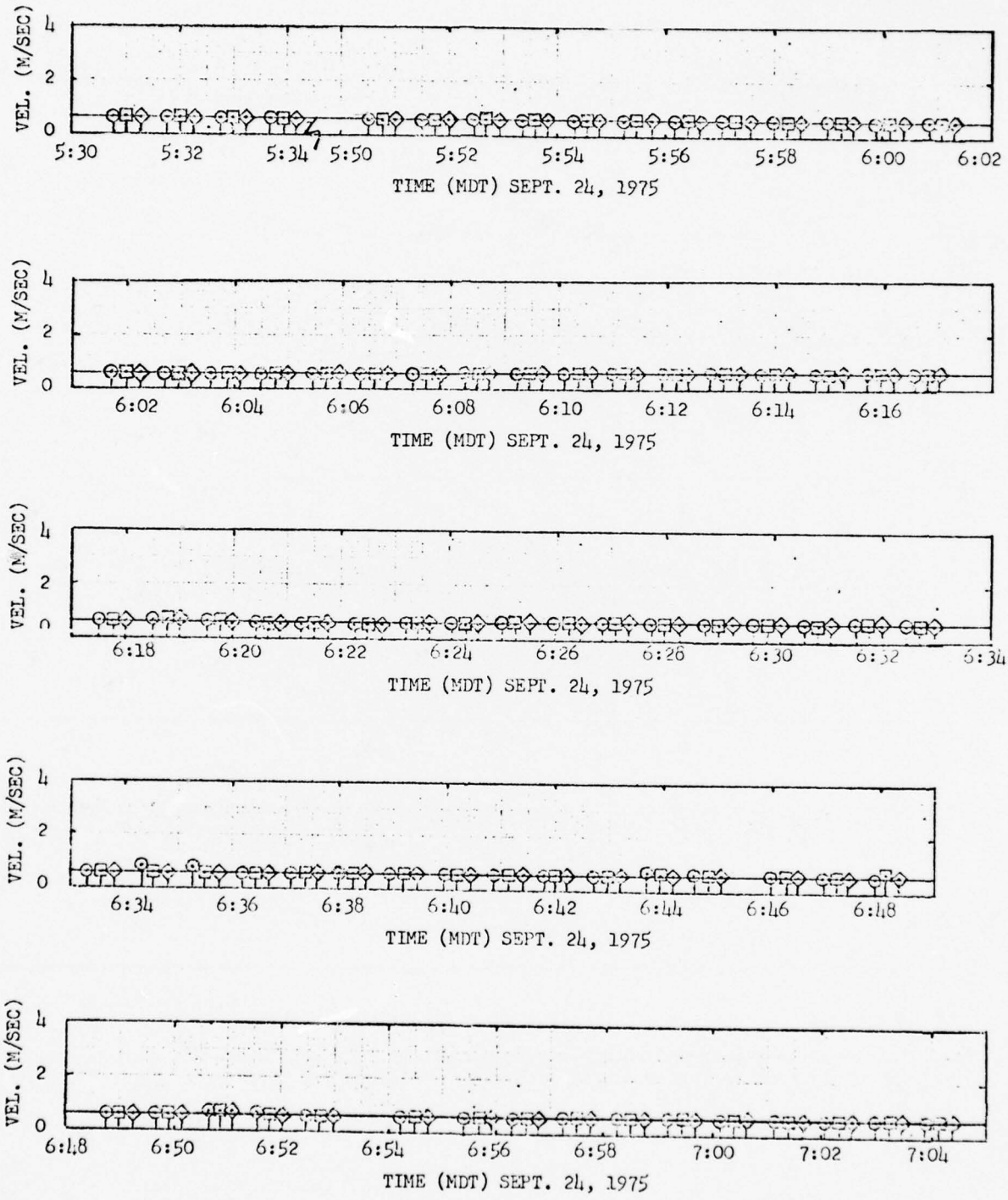

Figure 6-b. Anemometer velocity readings as a function of time (MDT).

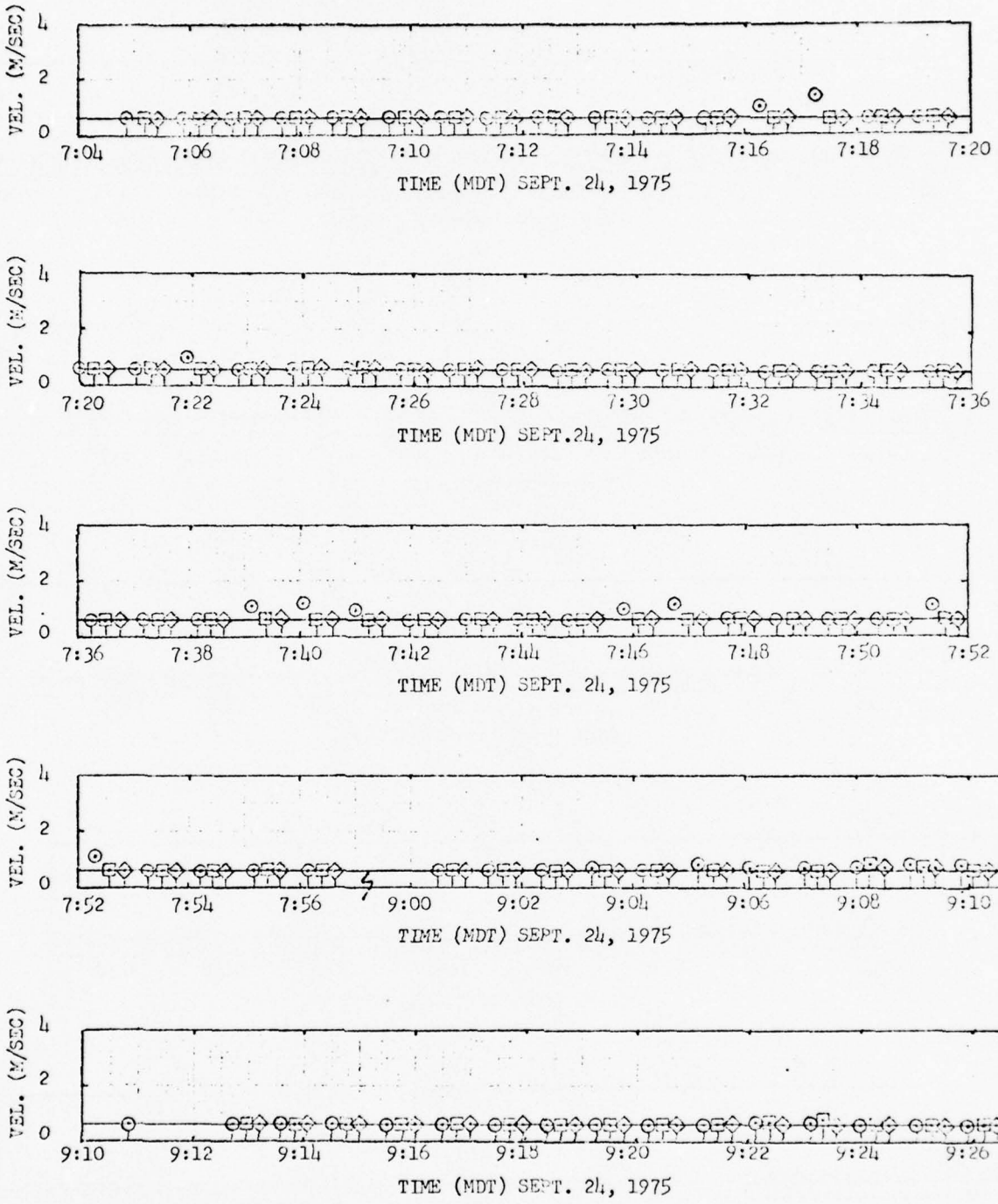

Figure 6-c. Anemometer velocity readings as a function of time (MDT).

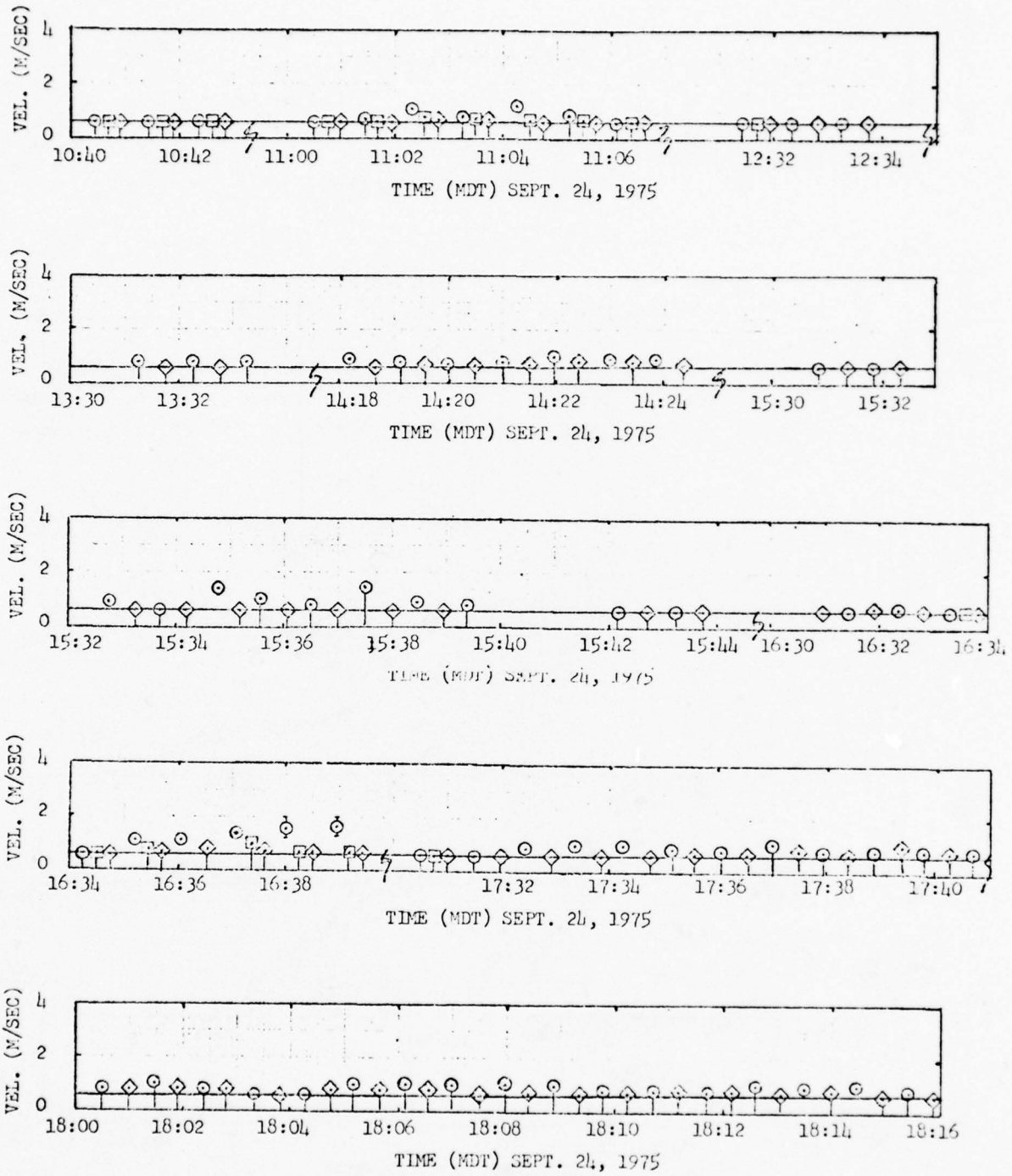

Figure 6-d. Anemometer velocity readings as a function of time (MDT).

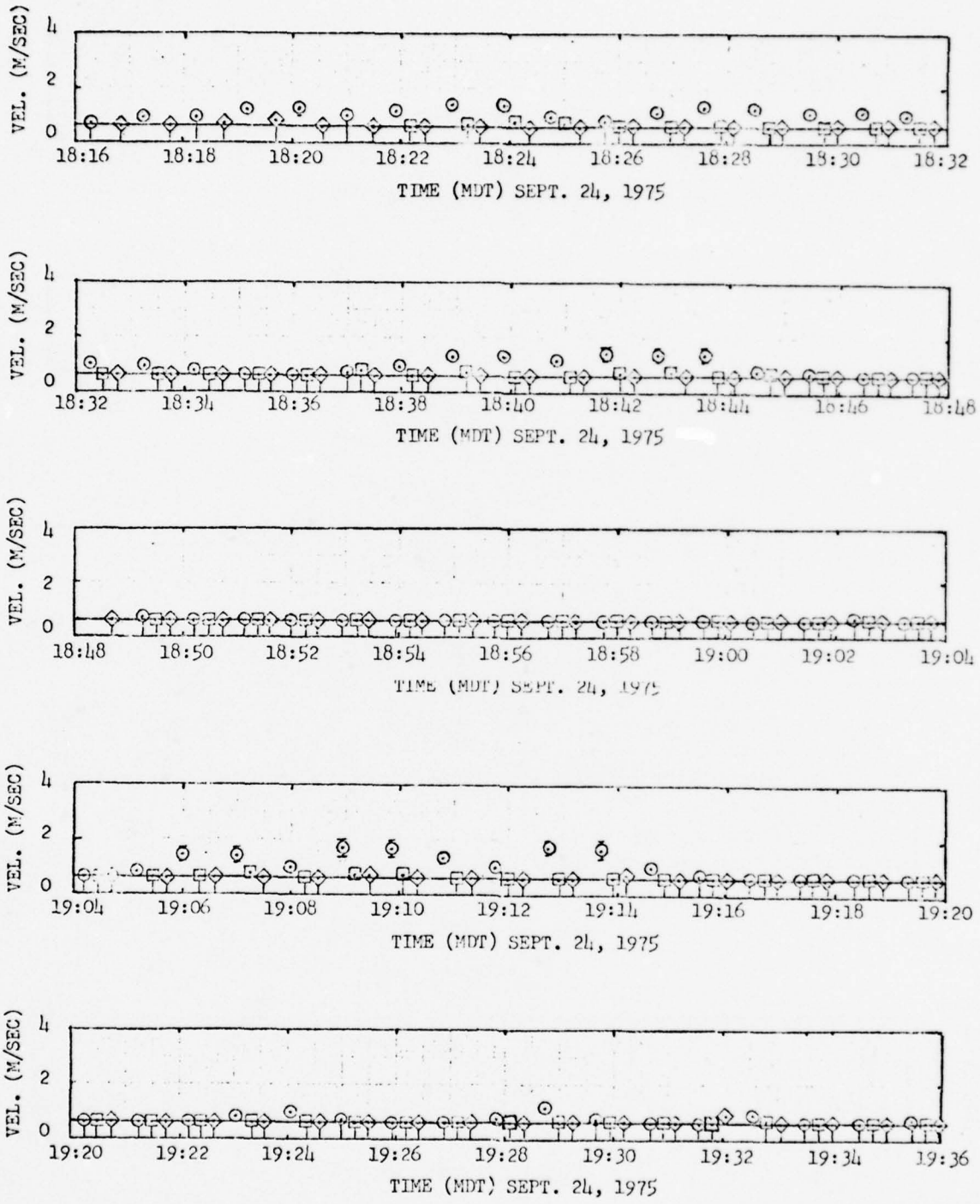

Figure 6-e. Anemometer velocity readings as a function of time (MDT).

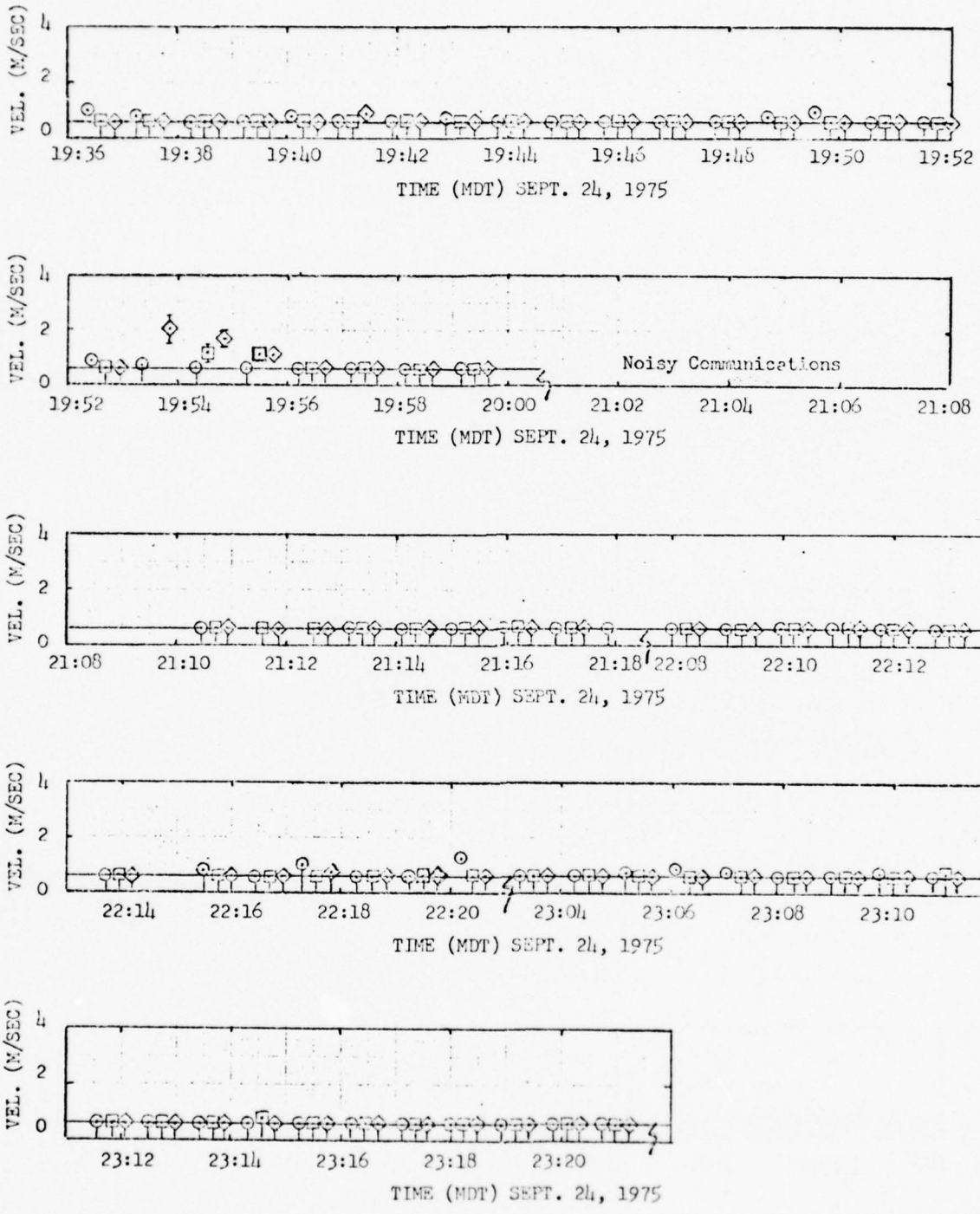

Figure 6-f. Anemometer velocity readings as a function of time (MDT).

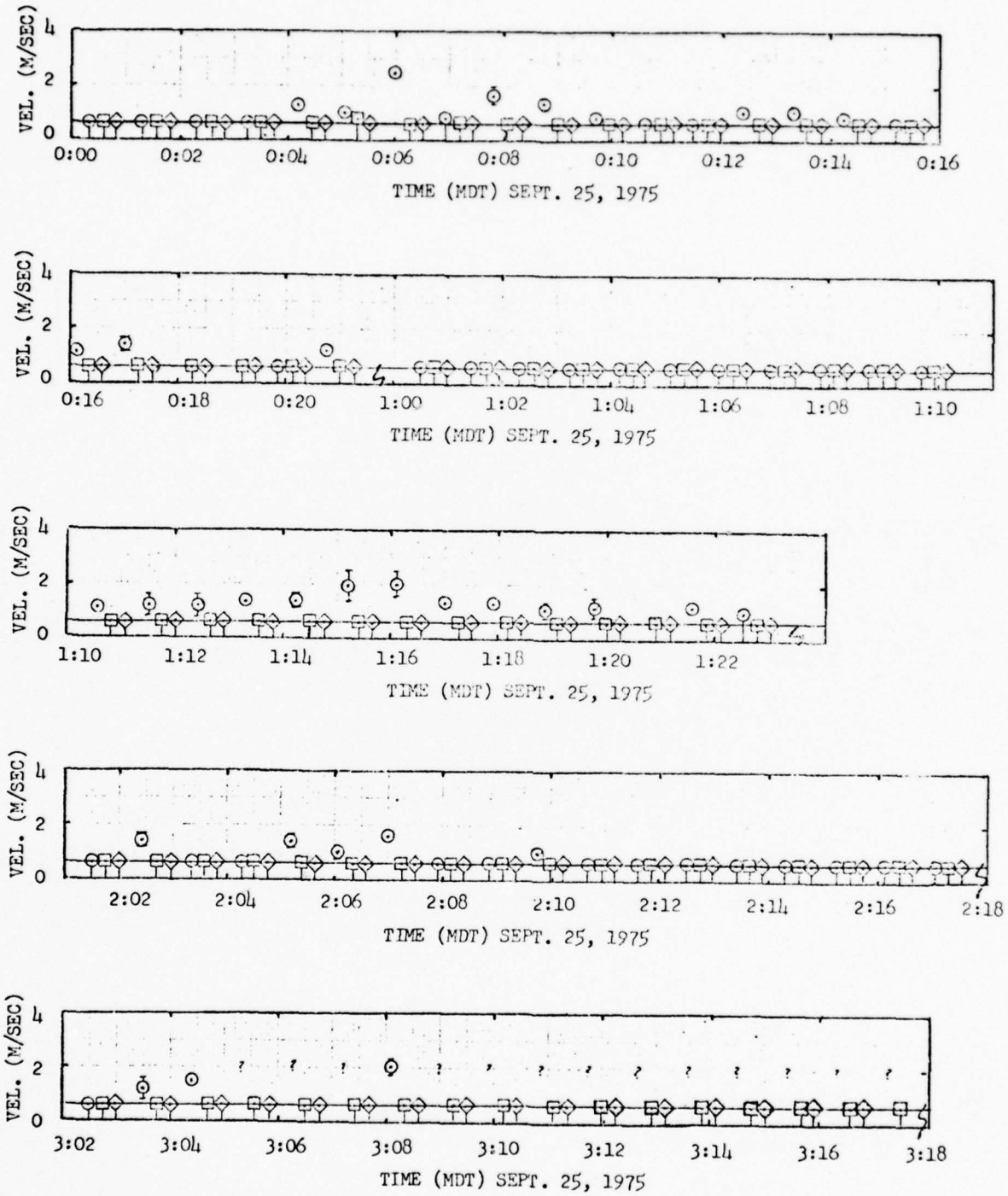

Figure 6-g. Anemometer velocity readings as a function of time (MDT).

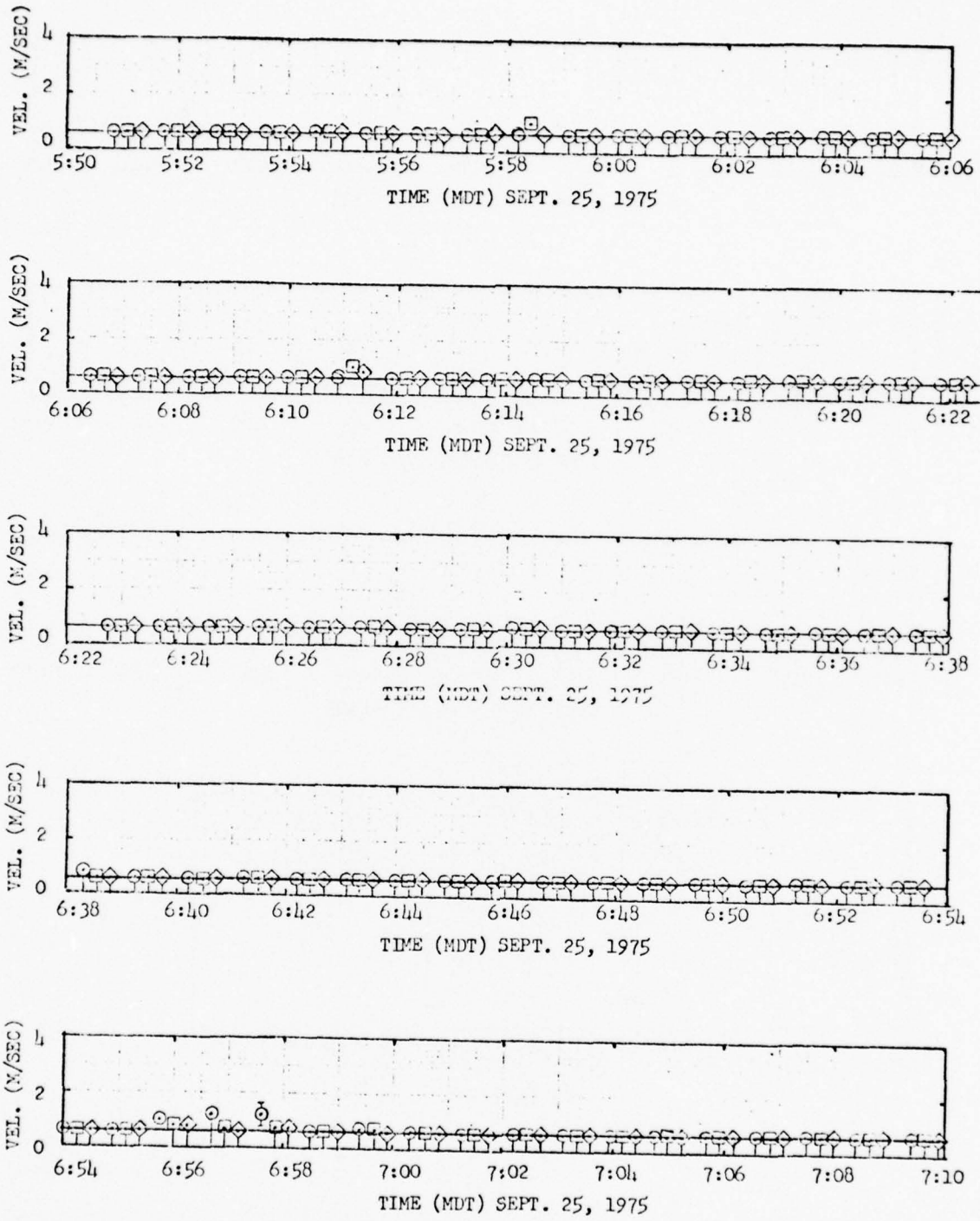

Figure 6-h. Anemometer velocity readings as a function of time (MDT).

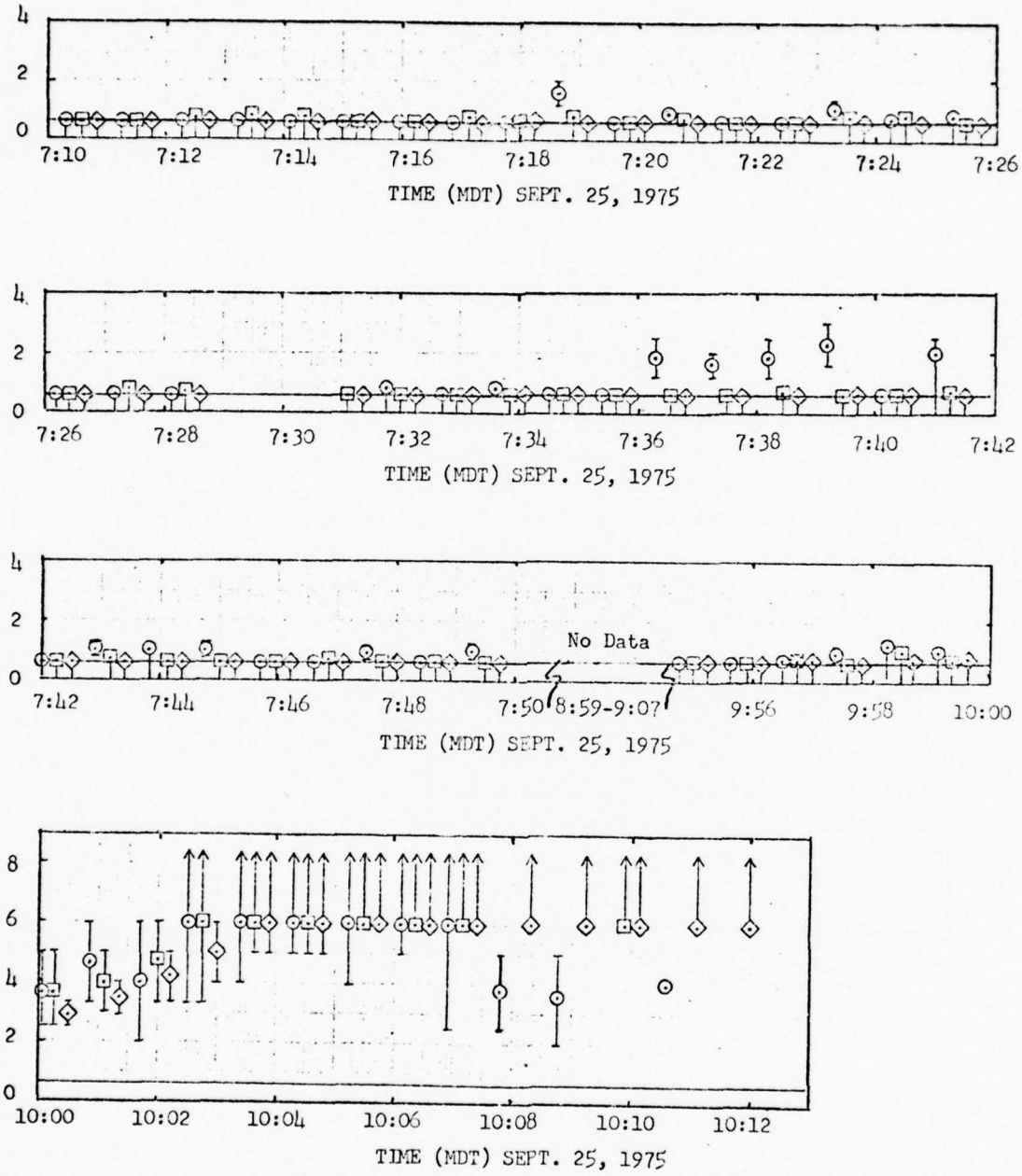

Figure 6-i. Anemometer velocity readings as a function of time (MDT)

REFERENCES

1. Williamson, P. Roger, "Effects of Wind Shear and Turbulence on Measurements in the Stratosphere," paper presented at the 1974 Spring Meeting of the American Geophysical Union, Washington, DC.

2. Lilienfeld, Pedro, et al., 1967, "Ion Tracer Anemometer for the Measurement of Low Density Air Flow," Rev. Sci. Instrum. 38(3):405-409.

3. Petriw, Andrew, "Directional Ion Anemometer," U. S. Patent 3,706,938, December 1972.

4. Desai, Prateen V., and William C. Johnston, 1971, "Corona Discharge Anemometer and Its Operational Hypothesis," Rev. Sci. Instrum. 42(5): 595-600.

5. Petriw, Andrew, 1970, "Directional Ion Anemometer," R&D Report, ECOM-3379, US Army Electronics Command, Fort Monmouth, NJ.

CHAPTER 5

MEASUREMENTS OF NET ATMOSPHERIC IRRADIANCE IN THE 0.7- TO 2.8-MICROMETER INFRARED REGION

Roberto Rubio
Atmospheric Sciences Laboratory, WSMR, NM

Mike Izquierdo
University of Texas at El Paso, El Paso, TX

ABSTRACT

The objective of this experiment was to measure atmospheric irradiance within the 0.7- to 2.8-micrometer infrared wavelength region from a balloon platform at altitudes ranging from 5 to 39 kilometers. An Epply precision spectral pyranometer pointed in a general downward direction and equipped with a 7-degree field of view field stop was successfully employed to collect irradiance data for a period of 34 hours on 23, 24, and 25 September 1976. The results showed that at low solar zenith angles and in the absence of clouds the atmospheric irradiance values usually remained within 2.2×10^{-2} cal/cm^2 min and 2.6×10^{-2} cal/cm^2 min. Clouds attenuated the irradiance down to magnitudes below 4×10^{-4} cal/cm^2 min which was the combined noise level of the pyranometer and associated electronics. At high solar zenith angles, specular reflections of sunlight which entered the pyranometer's field view caused enhancements of the measured irradiance to reach magnitudes greater than the instrument could measure (3.5×10^{-2} cal/cm^2 min). No significant variations in irradiance were detected with changes in altitude above 5 kilometers or terrain viewed; therefore, the background intensity is attributed to the radiant emittance of the lower atmosphere.

INTRODUCTION

The existence and causes of naturally occurring atmospheric infrared light emission with intensity magnitudes greater than those of the normal background have been important to the military services since the advent of remote sensing reconnaissance and surveillance systems. To supplement existent, but insufficient, data on atmospheric near infrared light emission or reflections, the experiment to be described in this report was designed as part of project STRATCOM VI-A. STRATCOM VI-A was a high-altitude balloon project consisting of a multi-instrument atmospheric-sensing payload designed to make simultaneous measurements of solar and atmospheric radiation, atmospheric composition, and the thermodynamic structure in the 5- to 40-kilometer altitude interval. The specific objective of this particular STRATCOM VI-A experiment was to acquire atmospheric irradiance data within the 0.7- to 2.8-micrometer wavelength region and to attempt to identify the cause of any intensity enhancements detected during the balloon flight.

INSTRUMENTATION

An Epply precision spectral pyranometer with an RG8 light filter (0.7- to 2.8-micrometer window) was used to measure atmospheric irradiance. A field stop machined to limit the field of view to 7 degrees was attached to the pyranometer. Inclusion of the field stop reduced the pyranometer sensitivity to 0.38 millivolt/(cal/cm^2 min). Thus to provide a voltage signal sufficiently large to telemeter, the sensor output was amplified by two cascaded operational amplifiers enclosed in a temperature controlled container. The combined electronics noise level was measured to be 0.1 microvolt; this value is equivalent to an irradiance level of 4×10^{-4} cal/cm^2 min. Based on previous data [1] rounded off to the next higher order of magnitude, the Epply pyranometer sensitivity and its viewing solid angle of 0.01 steradian, the maximum anticipated irradiance level was calculated to be 3×10^{-2} cal/cm^2 min. This corresponds to an equivalent pyranometer output voltage of approximately 10 microvolts. Accordingly, the total gain of the operational amplifiers was set to accentuate the sensor output voltages between 0.1 and 10 microvolts. Because of the high amplifier gain employed, sensor output voltages above 13.3 microvolts saturated the modulation signal; therefore, all irradiance data which produced a sensor output voltage larger than 13.3 microvolts were electronically limited to the corresponding value of 3.5×10^{-2} cal/cm^2 min.

The pyranometer and its appendage were located at the bottom side of the balloon's instrumentation platform. Its optical axis pointed toward the earth at an angle of 17.6 degrees below the horizontal plane defined by the platform base. All irradiance data were recorded after the payload platform had been lowered 300 meters below the balloon.

IRRADIANCE DATA

Net atmospheric irradiance data were intermittently recorded for a period of approximately 34 hours. During balloon ascension, the pyranometer sensed slanted atmospheric path lengths ranging from 17.5 to 130 kilometers. The first data sample (Fig. 1(a), 2312 MST), recorded at an altitude of 5.3 kilometers, corresponds to the 17.5-kilometer slant path; while the eighth data sample (Fig. 1(b), 0230 MST), recorded at an altitude of 39 kilometers, corresponds to the 130-kilometer path. During this balloon climb phase, the irradiance background magnitudes did not vary as a function of the observed path length, as can be seen in Figs. 1(a) and 1(b). This is attributed to the fact that when the initial data sample was obtained, the pyranometer was already sensing a large majority of the air mass and most of the precipitable water vapor, both of which were located in the region of the atmosphere with the highest temperature where the bulk of the atmosphere's radiant emittance occurs. Other than the third data sample, obtained at 0005 MST, 24 September, the irradiance remained within 2.3×10^{-2} cal/cm^2 min and 2.6×10^{-2} cal/cm^2 min. The abrupt decrease in intensity to less than 4×10^{-4} cal/cm^2 min recorded at 0005 MST was probably produced by cloud attenuation of the low-altitude atmospheric radiance. However, due to the lack of precise information on cloud locations at 0005, it cannot be unequivocally stated that a cloud obscured the pyranometer's field of view.

Investigation of the balloon's projected ground trajectory and the type of earth surface terrain traversed by this trajectory revealed that variations in the recorded irradiances were uncorrelated to changes in the type of observed terrain. Observed terrains consisted of flat desert, semibarren mountains, forrested mountains and valleys, and small lakes. Calculation of the earth's radiant emittance, at a temperature of 25°C, and unity emissivity, within the 0.7- to 2.8-micrometer region, yielded an irradiance value of 1.5×10^{-4} cal/cm^2 min. This intensity is below the operating signal threshold of the instrumentation employed here. Thus the small changes in irradiance brought about by changes in terrain temperatures and emissivities went undetected.

Measurements recorded during the balloon's first float altitude of approximately 39 kilometers covered the time interval from 0256 MST to 1142 MST, 25 September. Within this time span, the atmosphere was sensed during night, sunrise, and daylight hours. The recorded data are shown in Figs. 1(c), 1(d), and 1(e). Irradiance levels generally remained between 2.3×10^{-2} cal/cm^2 min and 2.6×10^{-2} cal/cm^2 min without any noticeable variations during sunrise. Orientation of the pyranometer's field of view was such that it never faced the sun directly. The intensity enhancement expected at sunrise was that due to the clear sky atmospheric scattering of the near infrared light. However, a post-flight computation based on the data of [1] indicated that the additional

irradiance due to clear sky atmospheric scattering of 0.7 to 2.8 micrometers energy was 3×10^{-4} cal/cm^2 min or less, clearly a magnitude less than the instrument's noise level. The gradual decreases in intensity registered at 0330 MST and 0451 MST are attributed to the attenuation effects of clouds entering the pyranometer's field of view. While the sky on the morning of 24 September may be described as generally clear (less than 0.1 coverage), the afternoon was characterized by increased cloudiness which intermittently obscured the pyranometer's field of view.

In the time frame from 1030 MST to approximately 1850, eight irradiance data samples were acquired while the balloon descended from 38 to 27.4 kilometers. The last of these samples was 2 hours long so that not only this experiment but also other STRATCOM experiments would record continuous data during sunset. The irradiance amplitudes did not change appreciably during sunset. All the variations observed were comparable to the small changes already recorded throughout most of the flight when the amplitudes were centered about 2.4×10^{-2} cal/cm^2 min. In contrast, before sunset, beginning at 1631 MST large variations in irradiance levels were observed. Because of the increased cloudiness on this afternoon and with the sun's attainment of a high zenith angle, cloud specular reflection of sunlight entered the pyranometer's field of view and enhanced the irradiance amplitudes to values greater than 3.5×10^{-2} cal/cm^2 min. These enhancements are shown in Figs. 1(f) and 1(g). As previously mentioned, values greater than 3.5×10^{-2} cal/cm^2 min are not plotted because the electronics became saturated at this magnitude. Consequently, it may be stated only that the values registered at 1630 MST and 1821 MST were greater than 3.5×10^{-2} cal/cm^2 min. Since preflight calculations of solar energy scattering (diffused light) of 0.7 to 2.8 micrometers light from sunlit clouds yielded a maximum irradiance of only 3×10^{-2} cal/cm^2 min, it is maintained that the enhancements recorded at 1636 MST and 1821 are indeed specular cloud reflections. When clouds were in the pyranometer's field of view, the balloon platform's slow motion caused the pyranometer to sense in sequence either solar specular reflections or atmospheric irradiance attenuated by the same clouds. This process effectively introduced the irradiance fluctuations recorded in Figs. 1(f) and 1(g). At sunset all enhancements ceased.

During the remainder of the balloon flight, eight more samples were obtained as the balloon rose to 39 kilometers. Most of these data, plotted in Figs. 1(h), 1(i), and 1(j) were recorded at night. Other than the decreases in irradiance recorded at 2004 MST and 2114 MST on 24 September and at 0550 MST on 25 September, the intensity levels did not significantly deviate from 2.5×10^{-2} cal/cm^2 min. Sunrise effects were again found to be negligible. All values recorded after 0558 MST, last data point in Fig. 1(j), also remained close to a value of 2.5×10^{-2} cal/cm^2 min.

CONCLUSIONS

Net lower atmosphere 0.7- to 2.8-micrometer irradiance data were successfully recorded for a period of 34 hours from altitudes ranging from 5.3 to 39 kilometers. An irradiance background level which usually remained between 2.3×10^{-2} cal/cm^2 min and 2.6×10^{-2} cal/cm^2 min existed during both day and night. This irradiance level is in general agreement with data reported by K. YA. Kondratyev [2] when only that fraction of energy due to the near infrared is obtained from Kondratyev's total irradiance. Since no appreciable variations in irradiance with increases in altitude were observed between 5.3 and 39 kilometers, it is concluded that the aforementioned irradiance levels are maintained by air mass in the lower atmosphere. Changes in the radiant emittance of the earth's surface terrain were too small to be detectable. Clouds entering the sensor's field of view acted as attenuators of the lower atmosphere irradiance. More importantly, it was established that the existence of clouds located in a position to specularly reflect sunlight into a sensor can cause intensity enhancement well above the background irradiance.

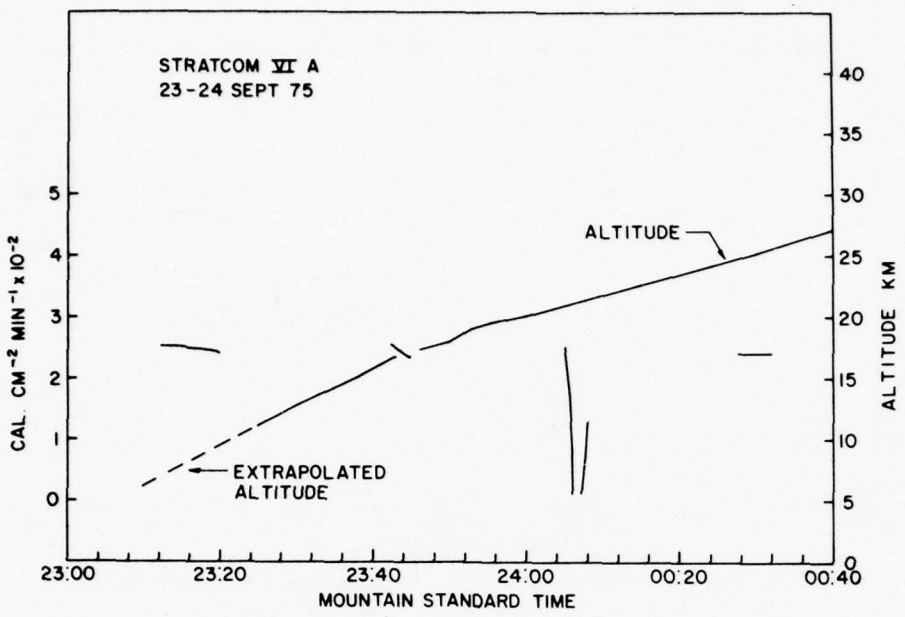

FIGURE 1 (a) NET ATMOSPHERIC RADIATION WITHIN THE 0.7 TO 2.8 MICRON REGION AS A FUNCTION OF TIME AND ALTITUDE.

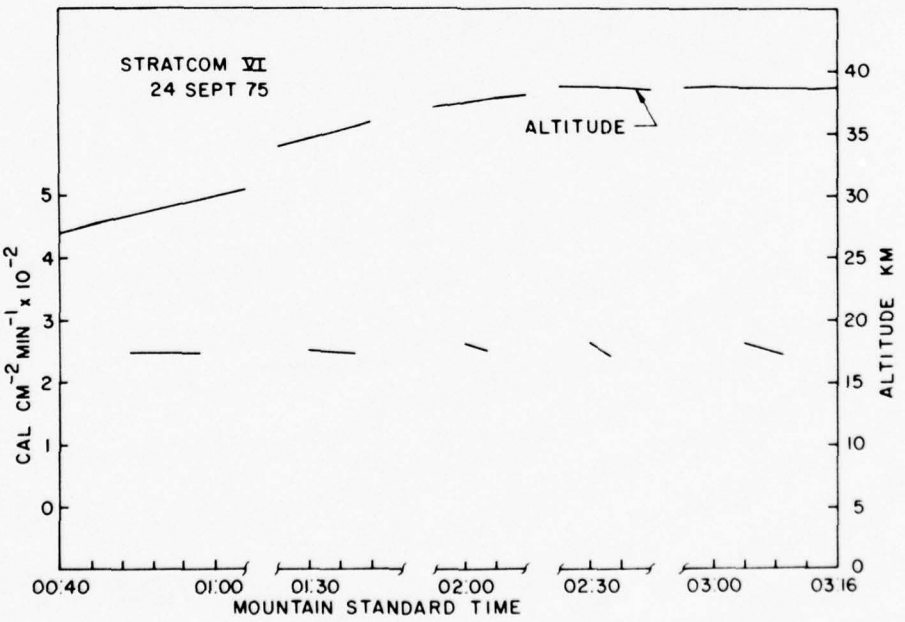

FIGURE 1 (b) NET ATMOSPHERIC RADIATION WITHIN THE 0.7 TO 2.8 MICRON REGION AS A FUNCTION OF TIME AND ALTITUDE.

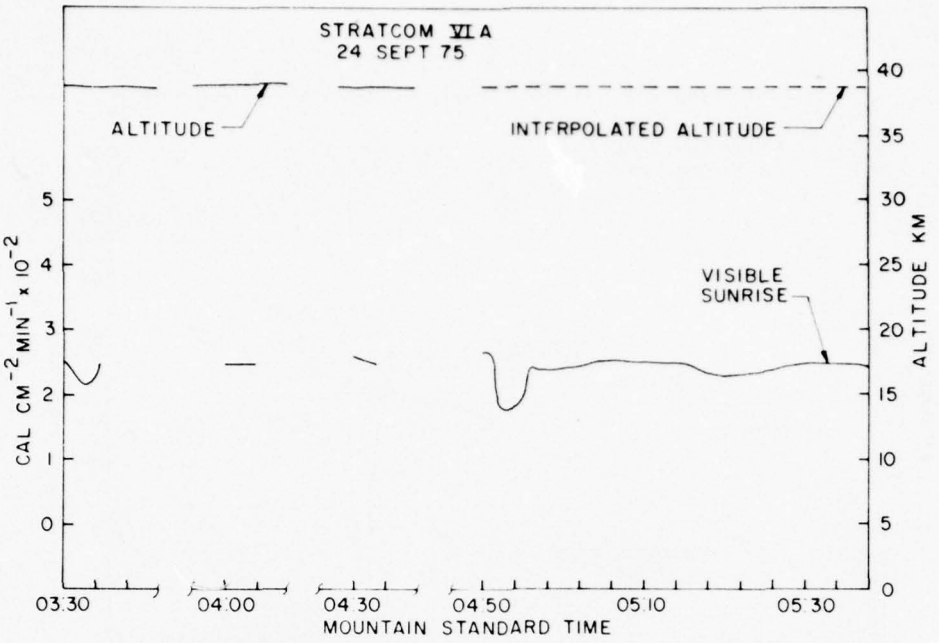

FIGURE 1 (c) NET ATMOSPHERIC RADIATION WITHIN THE 0.7 TO 2.8 MICRON REGION AS A FUNCTION OF TIME AND ALTITUDE.

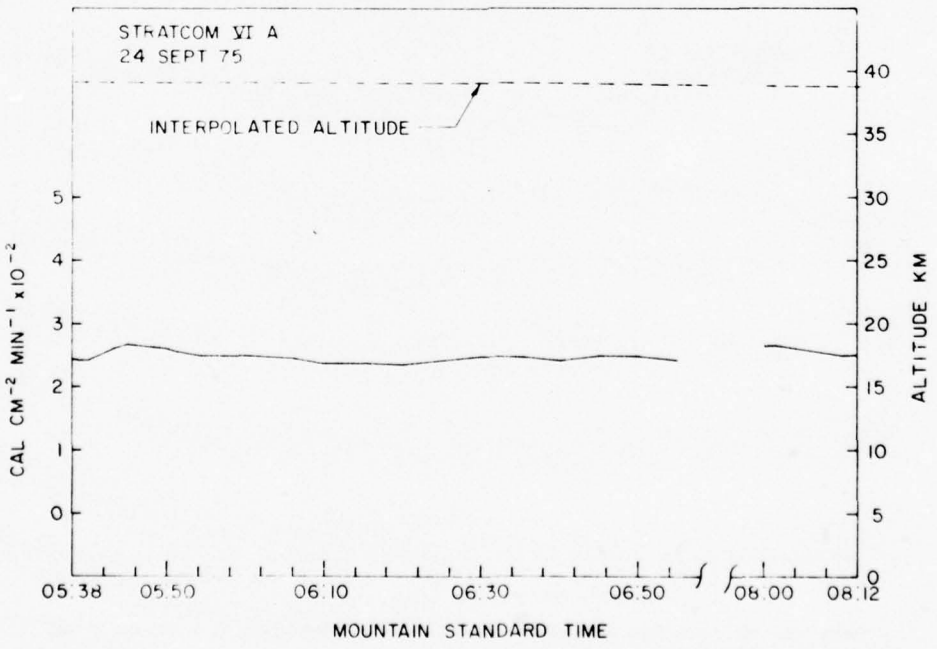

FIGURE 1 (d) NET ATMOSPHERIC RADIATION WITHIN THE 0.7 TO 2.8 MICRON REGION AS A FUNCTION OF TIME AND ALTITUDE.

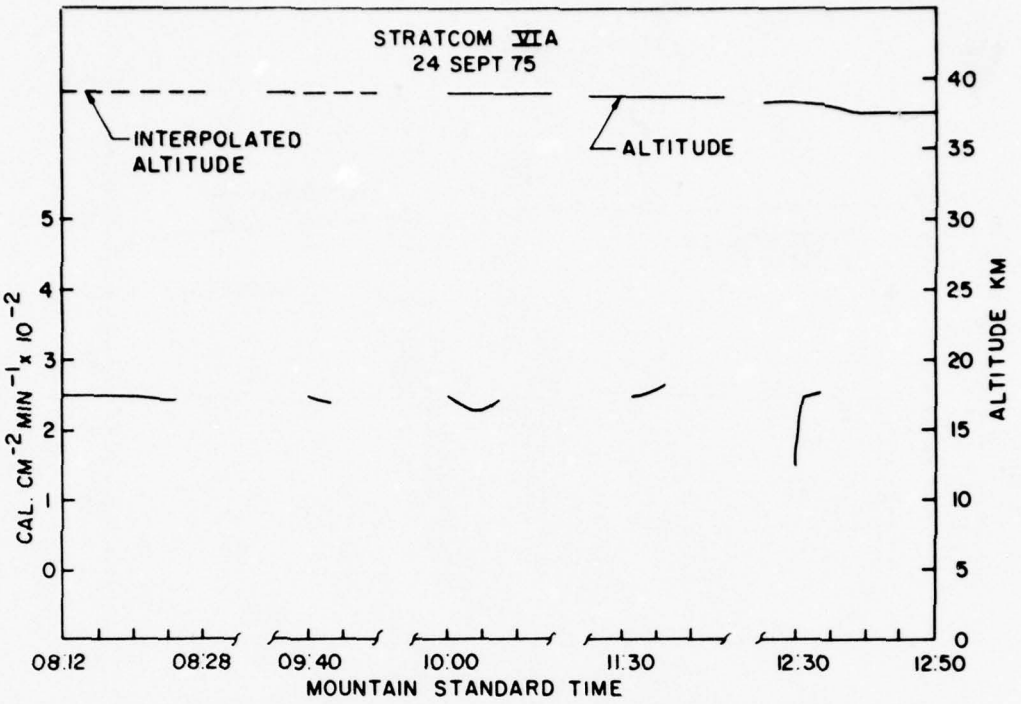

FIGURE 1 (e) NET ATMOSPHERIC RADIATION WITHIN THE 0.7 TO 2.8 MICRON REGION AS A FUNCTION OF TIME AND ALTITUDE.

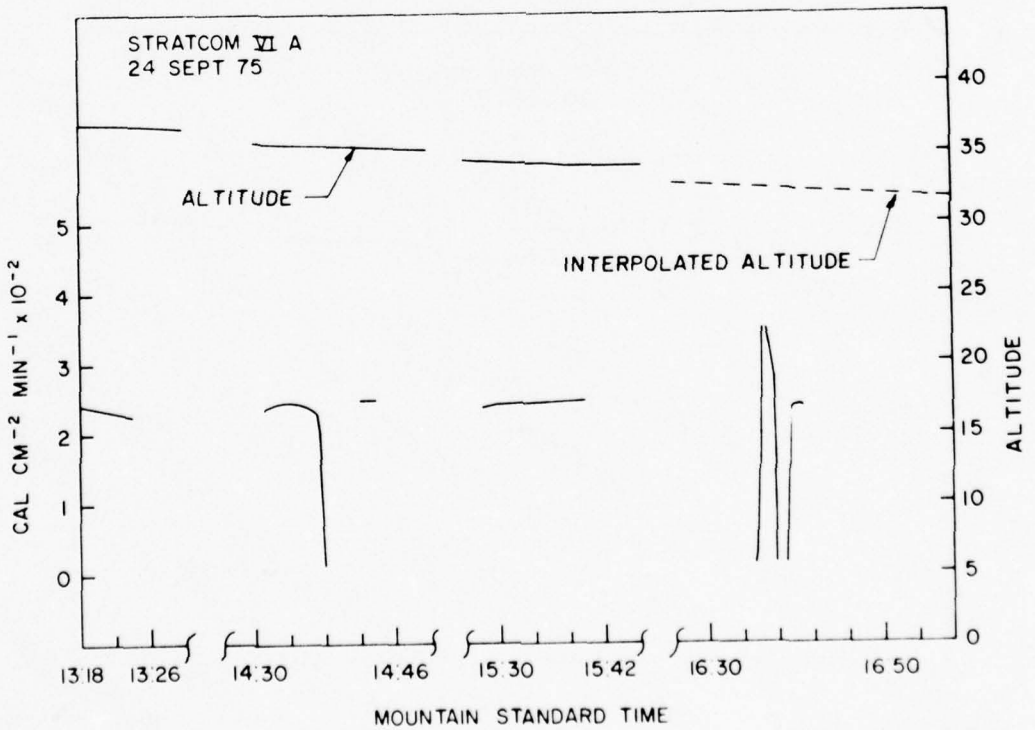

FIGURE 1 (f) NET ATMOSPHERIC RADIATION WITHIN THE 0.7 TO 2.8 MICRON REGION AS A FUNCTION OF TIME AND ALTITUDE

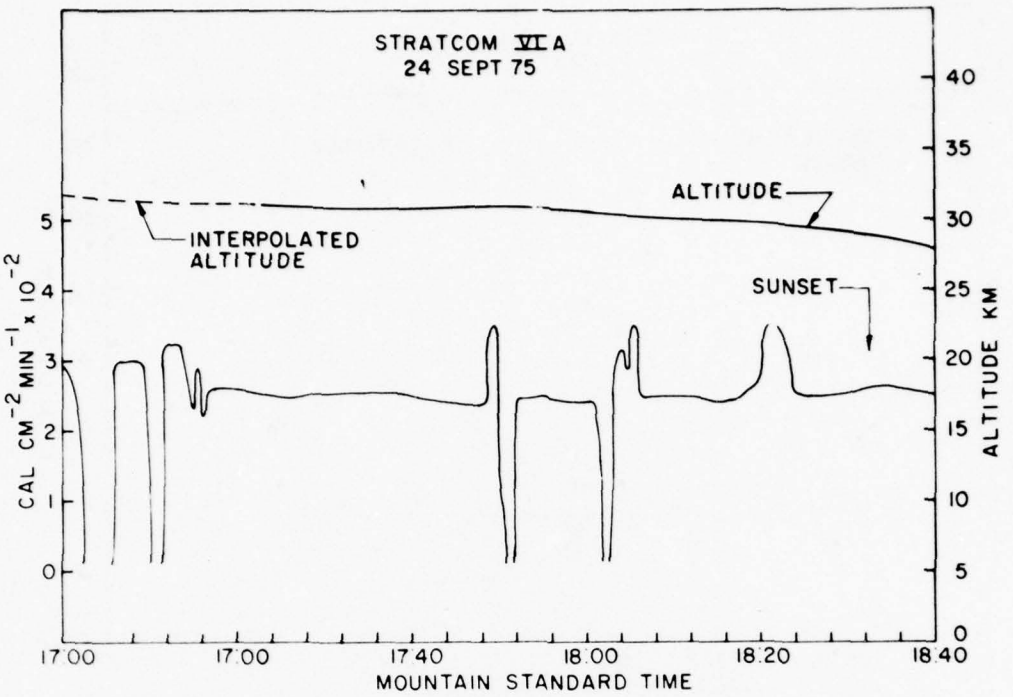

FIGURE 1 (g) NET ATMOSPHERIC RADIATION WITHIN THE 0.7 TO 2.8 MICRON REGION AS A FUNCTION AND ALTITUDE

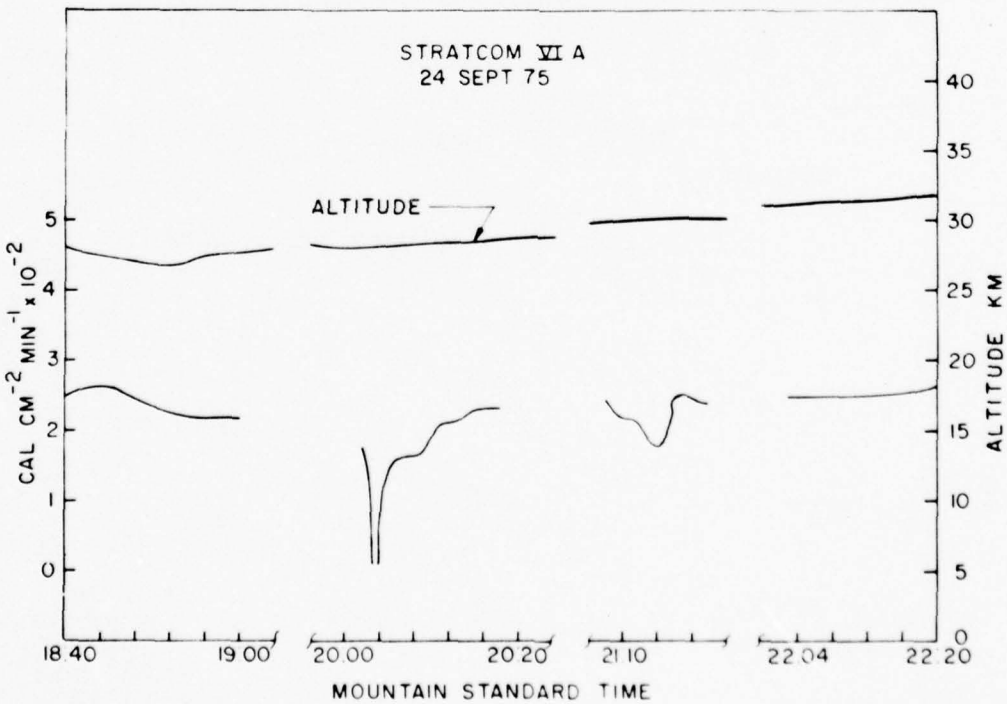

FIGURE 1 (h) NET ATMOSPHERIC RADIATION WITHIN THE 0.7 TO 2.8 MICRON REGION AS A FUNCTION OF TIME AND ALTITUDE

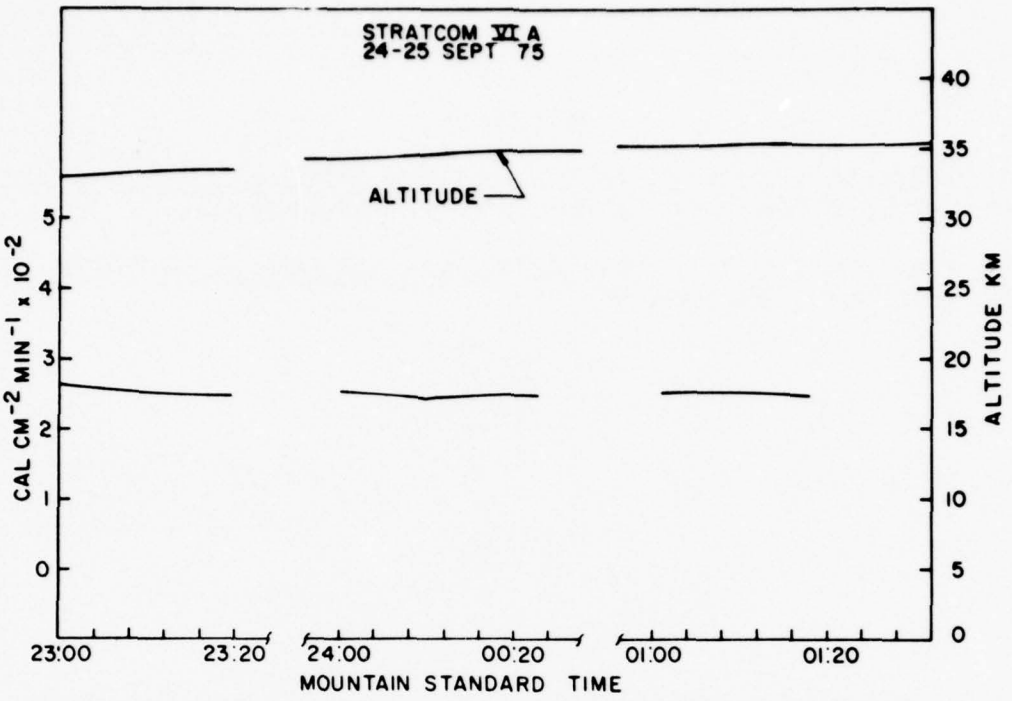

FIGURE 1 (i) NET ATMOSPHERIC RADIATION WITHIN THE 0.7 TO 2.8 MICRON REGION AS A FUNCTION OF TIME AND ALTITUDE.

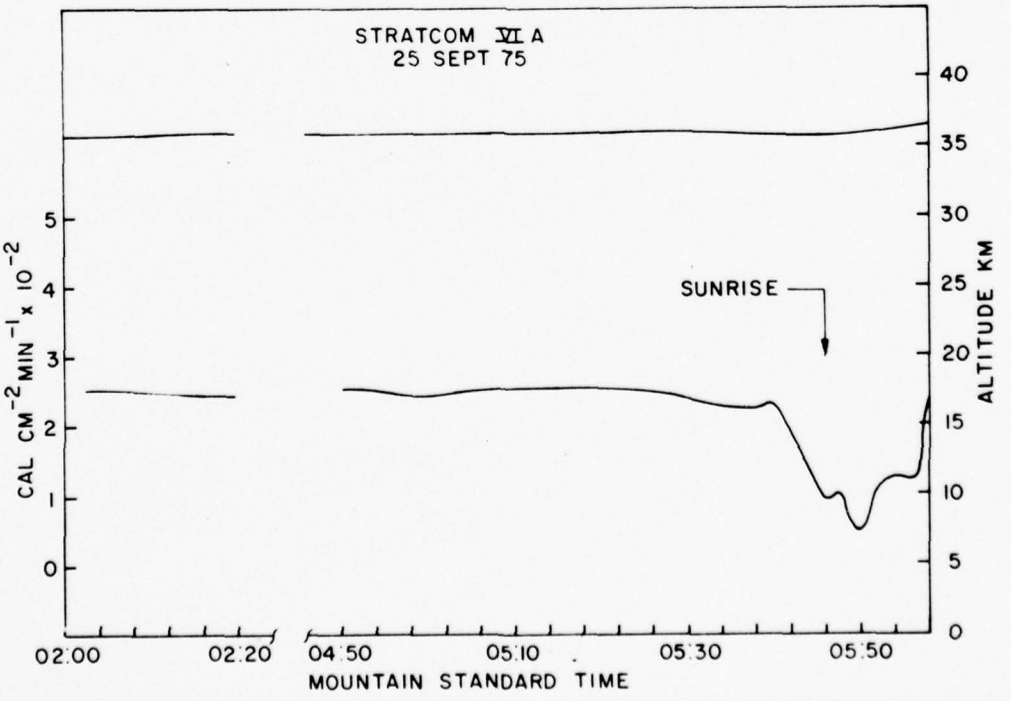

FIGURE 1 (j) NET ATMOSPHERIC RADIATION WITHIN THE 0.7 TO 2.8 MICRON REGION AS A FUNCTION OF TIME AND ALTITUDE.

REFERENCES

1. Wolfe, W. L., Editor, 1965, Handbook of Military Infrared Technology, Chapter 5, US Government Printing Office, Washington, D.C.

2. Kondratyev, K. YA., 1969, Radiation in the Atmosphere, Chapter 9, Academic Press, New York, NY.

CHAPTER 6

MEASUREMENT OF 200-400 nm SOLAR UV FLUXES AT ALTITUDES UP TO 40 km

Frederick A. Hanser
Bach Sellers
Jean L. Hunerwadel
Panametrics, Inc., Waltham, MA

ABSTRACT

Solar uv fluxes in the 200-400 nm range have been measured at up to 40 km altitude. A filter-wheel uv spectrophotometer was used to make measurements at ten wavelengths over this range. Flux versus solar zenith angle data were obtained for two sunrises and one sunset. After payload cutdown a vertical profile of solar uv flux was measured to below 20 km. A good measurement of the 220 nm solar flux in the ozone-oxygen atmospheric window was made. The result of $3.93 \times 10^{-6} W/(cm^2\text{-nm})$, together with other measurements, indicates some dependence of the 220 nm solar flux on sunspot number.

INTRODUCTION

The uv spectrophotometer (UVS) flown on the STRATCOM VI-A balloon payload was originally developed to measure high-altitude solar uv fluxes from an aircraft as part of the Climatic Impact Assessment Program (CIAP) [1]. The UVS gave measurements of the solar uv flux in the 200-400 nm region at altitudes up to 130 kft [2]. Of particular interest are the measurements at 220 nm, a window in the atmospheric transmission lying between the peak of the ozone absorption at 250 nm and the strong oxygen absorption below 180 nm. This wavelength region is extremely important for the photochemistry of the upper atmosphere, particularly the 50-150 kft region. The photolysis of many important pollutants, the chlorofluoromethanes in particular [3], is due primarily to the solar uv in this 220 nm window.

The altitude dependence of the 220 nm solar flux has been only poorly measured ([4], p 5). Balloon measurements reported in [5] are questionable because the reported absolute solar fluxes are a factor of 3 lower than all other reported measurements, including the UVS data from STRATCOM VI-A. Higher altitude (175-225 kft) rocket measurements have been reported [6]. Satellite measurements of solar uv radiation show that for wavelengths less than 300 nm the sun becomes increasingly variable [7]. The 220 nm flux data obtained on STRATCOM VI-A, combined with a number of other solar flux measurements, suggest that the 220 nm solar flux increases

with increasing solar activity as measured by sunspot number. Measurement of the 220 nm solar flux as a function of both altitude and time in solar cycle is thus a very important part of upper atmosphere experiments.

The remaining nine solar uv flux measurements are used mostly to obtain information about the ozone layer and certain other photochemical reactions. The 280-330 nm region can be used to calculate the total ozone along the air path to the sun for very thin to very thick layers. The 330-400 nm measurements provide a check on UVS operation since the sun has a stable, well-known output at these wavelengths, and they are not significantly affected by ozone. The UVS thus measures an important part of the solar spectrum, a part necessary to understand the upper atmosphere.

INSTRUMENT DESCRIPTION

The UVS is basically a narrow-band transmission filter photometer. A set of ten filters on a stepping wheel in front of a calibrated uv photomultiplier measures the solar irradiance over the range 200-400 nm. A flat diffuser in front of the filters provides response over a large range of solar zenith angles with only minimal orientation requirements. For future flights a conical diffuser and vertical mounting of the UVS should eliminate all requirements for sun-seeking orientation. A more detailed description of the basic UVS is given in [1]. The wavelengths of the ten filter sets used are given in Table 1. To fly the UVS on a balloon for a prolonged period of time required several design changes to the basic instrument. The changes include increased thermal insulation, selection of the filter wheel sample rate by ground command, and the mounting configuration.

The basic instrument is equipped with an internal ON/OFF temperature control maintaining all components at a constant +20°C. Power requirement for this control is 50 W at 28 V, when on. Due to power restrictions on this flight, the heater control had to be disconnected, subjecting the instrument to the temperature extremes of the tropopause and midstratosphere.

To maintain a reasonable thermal isolation between the ambient environment and the inside of the instrument, the basic UVS was placed in an insulated cylindrical container, allowing for 3 in. of polyethylene insulation all around the instrument. Figure 1 shows an outline drawing of the instrument package. To minimize the effect of heat radiation at float altitude, the outside was painted with a high reflectivity/low emissivity vinyl epoxy paint. To maintain low outgassing properties, the package was pressure sealed with O-rings.

The instrument package was mounted on a sun-seeking platform with its centerline at 45° from the vertical. Since the half angle of the optics of the UVS is 75°, light reflection from the balloon had to be obscured with an optically black shield.

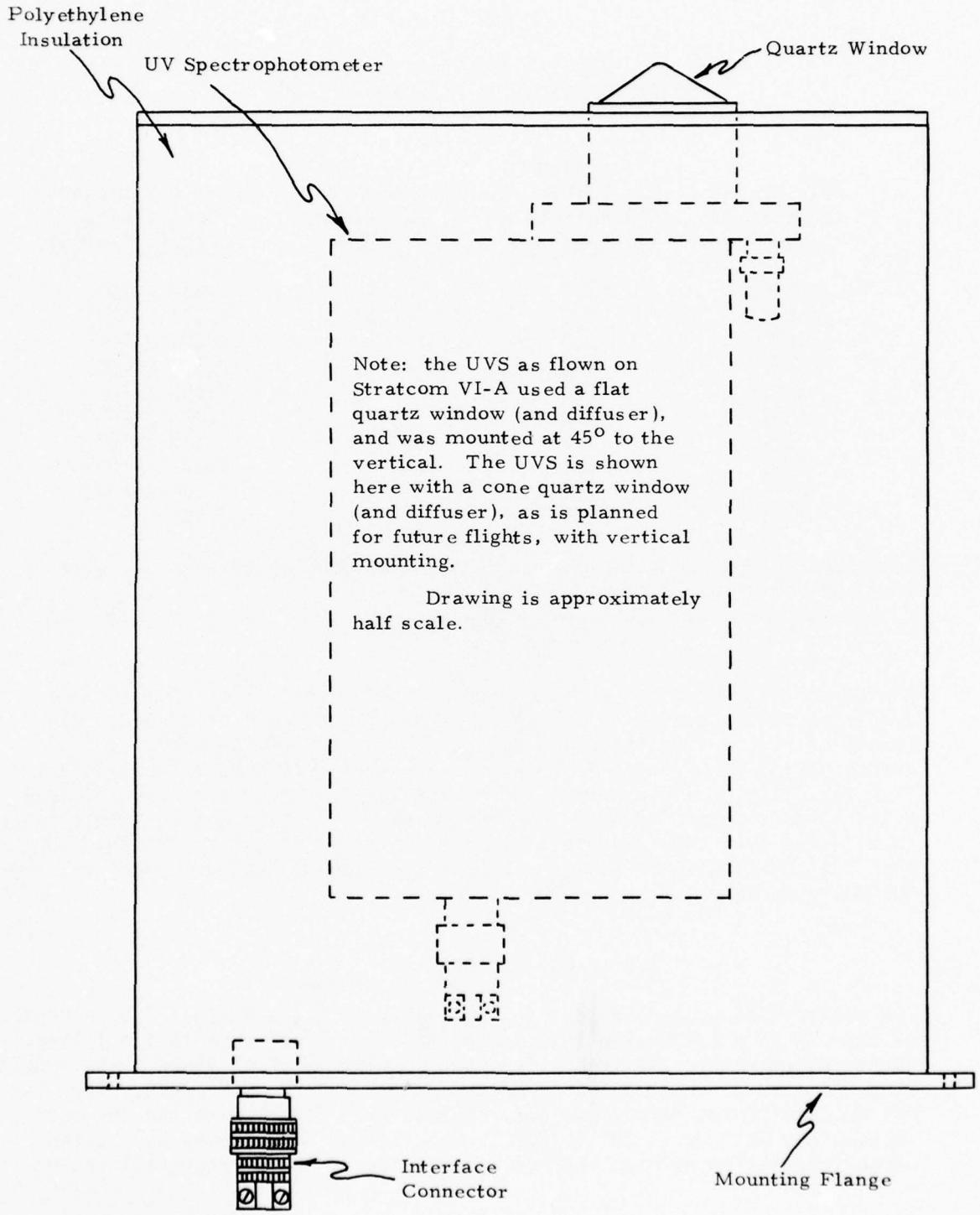

Fig. 1. Outline Drawing of UVS Mounted Inside Thermally Insulating Container.

TABLE 1

UVS CALIBRATION SENSITIVITIES
FOR THE STRATCOM VI-A BALLOON FLIGHT

Filter Set Wavelength (nm)	Single Filter Bandwidth (nm)	Number of Filters Used	Solar Calibration Sensitivity $\{A/[W/(cm^2\text{-}nm)]\}$
393.0	26.4	1	3.324×10^{-3}
363.0	28.0	1	1.947×10^{-3}
329.2	2.2	2	9.802×10^{-3}
319.3	2.0	2	2.337×10^{-2}
310.3	1.8	2	2.485×10^{-2}
305.3	2.0	2	3.871×10^{-2}
297.8	3.0	2	7.535×10^{-2}
290.7	2.4	2	1.673×10^{-1}
287.3	1.8	2	2.984×10^{-2}
220.*	28.0	3	3.508

**At high altitudes the average wavelength detected by the set of three 214.0 nm filters is 220 nm.*

The basic instrument has a fixed sample rate of the filter wheel of one sample per sec, completing one spectrum scan in a total of 12 sec. Although this is desirable during ascent and descent of the payload, it is unnecessarily fast during long periods at relatively constant altitude. Therefore, the design was modified to include a sample rate of one sample every 10 sec, completing one scan in 120 sec. The appropriate sample rate is selected by a simple contact closure, external to the instrument. On this balloon flight the sample rate was selected by ground command via the telemetry uplink.

UVS CALIBRATION

The calibration procedure has been described in [1] and [8]. The response of the UVS to a calibrated Standard of Spectral Irradiance (SSI)* is measured and corrected for the difference in solar spectral shape. The result is a calibration constant in $A/[W/(cm^2\text{-}nm)]$ for each filter set. The UVS was calibrated before and after the balloon flight with the internal temperature monitor at 25° to 30°C. Most filter sets showed only a few percent variation between the two calibrations. The average calibration

**A 200 W tungsten-iodine quartz envelope lamp calibrated by EG&G, Inc., Electro Optics Division, Salem, MA. The calibration is traceable to the National Bureau of Standards.*

is listed in Table 1, and this was used for the data reduction. Also listed are the single filter bandwidths and the number of filters used in each set. The 393 and 363 nm filters are both used with neutral density 4 filter.

During the balloon flight the UVS cooled significantly during the nights, and operated with internal temperatures as low as -40°C. The UVS operated under these conditions, but the calibration validity was suspect at the lowest temperatures. Consequently, the UVS was calibrated after the flight at several temperatures between -40° and +30°C. Small corrections to the 25° to 30°C calibrations are required at the lower temperatures, and these were made during data analysis [2].

The SSI is calibrated over the range 250 nm to 2500 nm. For calibration of the 220 nm set (3 x 214.0 nm filters), the SSI spectrum below 250 nm was calculated from a 3100°K blackbody spectrum normalized to the 250 nm calibration intensity. This extrapolated spectrum yields a calibration for the 220 nm filter set which is accurate to about 50%. To improve the 220 nm calibration accuracy, the SSI relative spectrum was measured by using the calibrated uv photomultiplier from the UVS and several broadband filters. This effectively transfers the uv photomultiplier calibration, which extends below 200 nm, to the SSI. Using this method the SSI intensity at 220 nm was found to be within 10% of the extrapolated blackbody spectrum. The 220 nm calibration is thus improved to about 20% absolute error. The errors in the other filter calibrations are less than 10%.

ANALYSIS OF FLIGHT OPERATION

The scientific payload with the UVS on board was launched from Holloman AFB near midnight MDT, or 0600 GMT, on 23-24 September. The balloon reached its float altitude range (126-128 kft) at 0315 MDT and remained in that range for 10 hours, then slowly descended to approximately 100 kft at 1900 MDT. During this period, uv data were obtained from sunrise to sunset with a filter sampling rate of 1 per sec for most of the day. The instrument was turned on continuously at sunrise and sunset but was on an intermittent schedule of 3 min ON every 30 min during the day. Because of thermal problems with the drive mechanism for the sun-seeking platform, the UVS was not pointed at the sun at all times; therefore, valid data were obtained only sporadically during the sunrise hours. A detailed evaluation of these data is given in the next section.

During the night the payload reached a minimum of $\sim$90 kft, and the UVS was turned on periodically in an attempt to keep the inside temperature at reasonable levels. The computer model study made at Sandia Laboratories of the internal temperature conditions versus time indicated a minimum temperature of -5°C. According to our on-board monitor, with a range of +50° to -5°C, this objective was not achieved since the monitor saturated at -5°C sometime after reaching $\sim$90 kft that night. The low internal temperature is no problem during the night, since the UVS is not operational during this period anyway. However, the low temperature did require gain corrections on the next day, 25 September, and all through the final parachute descent.

Fortunately for this experiment, the multiplexed monitor output exhibits a temperature coefficient of its cycle time, which in no way influences the data, but which could later be used during a postcalibration. The largest correction factor encountered is ~2.5% and occurs at sunrise on 25 September. At approximately 1000 MDT of the same day, the payload was cut down and began its parachute descent. From sunrise to just before cutdown the filter sample rate was 0.1 per sec and the instrument was turned on periodically. Prior to cutdown a ground command was sent which turned the instrument continuously ON and selected a filter sample rate of 1 per sec. The flight was terminated at ∿0439 MDT. As during the previous day, the sun-seeking platform was inoperative for periods of time, restricting the data gathering capability of the UVS. This problem with the platform is more serious during descent where data gaps occur over large altitude ranges due to the relatively fast descent rate. The flight data are discussed and tabulated in the next sections.

DATA REDUCTION PROCEDURE

The basic data reduction procedure for the UVS has been described in [1], [8], and [9]. For altitudes above about 20 km, the effects of Rayleigh scattering become quite small, and so the analysis procedure is simplified. However, the large temperature variations experienced by the UVS on the STRATCOM VI-A flight require additional corrections to the data because of voltage level and calibration shifts.

The UVS data for a complete cycle consists of 10 uv filter measurements for the wavelengths listed in Table 1, a dark current measurement, and two calibration points from the set(1,2), (3,4), (5, CALB), and (CALA, 0). The values 0, ---, 5 are nominal voltage calibrations to correct for any shifts that might be introduced in signal transmission and processing, while CALA and CALB are light calibration points to monitor the photomultiplier-log amplifier gain.

The simplified form of the UVS data analysis has been described in [2]. Basically, the voltage outputs of the log-amplifier are converted to a current and corrected for temperature shifts. If $i_m(\lambda)$ is this temperature corrected current, and i_d the dark current, then the measured solar flux is

$$F_m(\lambda) = [i_m(\lambda) - i_d] \Big/ [S_p(\lambda) R(\theta_{sd}, \lambda) \cos\theta_{sd}] - B_\ell(\lambda) \qquad (1)$$

where $S_p(\lambda)$ is the calibration constant from Table 1, $R(\theta_{sd})$ is the diffuser relative angular response, and θ_{sd} is the sun line-diffuser normal angle. Values for θ_{sd} were calculated from the balloon location, as obtained from tracking radar data, and sun location data from [10]. The leakage flux correction $B_\ell(\lambda)$ is obtained from the 363 nm flux measurement as described in [2]. The result (1) is then corrected for log-amplifier - PM

gain shifts as measured by the calibration light. The final, corrected fluxes are accurate to about 10% when the leakage flux $B_{\ell}(\lambda)$ in (1) is less than 25% of $F_m(\lambda)$.

For some wavelengths the residual ozone above the balloon can be calculated from

$$t_{O_3}(\lambda) = \frac{-\cos\theta}{\mu_{O_3}(\lambda)} \ln\left\{\frac{F_{corr}(\lambda)}{F_o(\lambda)} \; F_{tm}\right\} \qquad (2)$$

The result (2) is most accurate for values of the bracket between about 0.3 and 0.05. The factor F_{tm} in (2) is a normalization to the 363 and 393 nm flux measurements, and is additionally used for the 220 nm flux normalization. The solar zenith angle is θ, while the ozone absorption coefficient is $\mu_{O_3}(\lambda)$, and $F_o(\lambda)$ is the unattenuated solar flux.

RESULTS

As mentioned earlier, *STRATCOM VI-A was launched during the night of* 23-24 September 1975 and was at float altitude of 127 kft by 0400 MDT (1000 GMT). Radar contact was lost between 0545 MDT and 1100 MDT (1145 to 1700 GMT) during the first sunrise. The balloon was at 127 kft near 34° N latitude, 107° W longitude, from about 0400 MDT to 0545 MDT, and at 128 kft near 34° N latitude, 107° W longitude, from 1100 MDT to 1130 MDT, when the slow descent began. It thus seems quite likely that during the first sunrise the balloon was at 127.5 kft near 34° N, 107° W, and the UVS data have been analyzed using this balloon location. For all other times the radar tracking data have been used for the balloon location.

The UVS data can be conveniently separated into four groups: sunrise on 24 September, sunset on 24-25 September, sunrise on 25 September, and parachute descent after cutdown on 25 September. The sunset data span 2 days in GMT and hence are listed as 24-25 September. All times listed with the UV data are in GMT (hours-minutes). Although the UVS was mounted on a rotating platform with a sun sensor, it generally took more than an hour after sunrise for the mechanism to warm up sufficiently for proper operation; therefore, the sunrise uv data are limited to chance payload rotations which pointed the UVS at the sun.

The solar flux data for the four periods listed above are given in Tables 2 through 5. Fluxes were calculated as described in the preceding section. All 220 nm fluxes have been normalized to the 393 and 363 nm measurements, except where no corresponding measurements are available. The fluxes are for an area perpendicular to the sun-earth line, and do not include any backscattered light from the lower atmosphere and the earth's surface. The sun-earth distance for 24-25 September is 1.003 au, so solar uv fluxes not attenuated by ozone or oxygen are effectively normalized to 1 au. The

Table 2
Stratcom VI-A
UVS Solar Flux Data for Sunrise on Sept. 24, 1975

GMT (hrs-min)	Altitude (kft)	Sun zenith angle (deg)	Flux (W/(cm^2-nm)) at wavelength λ (nm), on an area normal to the sun-earth line*									
			393	363	329.2	319.3	310.3	305.3	297.8	290.7	287.3	220
1244	127.5	93.6	6.42-5	4.25-5	7.23-6	1.06-6	1.68-8	(1.20-8)	-	-	-	-
1249	127.5	92.5	1.07-4	9.03-5	4.57-5	(5.06-6)	(7.59-8)	(8.60-8)	-	-	-	-
1352	127.5	79.6	-	-	-	-	-	-	-	-	-	8.92-8
1509	127.5	64.1	1.18-4	1.11-4	1.18-4	7.47-5	6.26-5	5.38-5	3.56-5	2.12-5	(1.15-5)	8.77-7
1521	127.5	61.7	1.18-4	1.19-4	1.19-4	7.88-5	6.13-5	5.65-5	3.65-5	2.40-5	(1.26-5)	1.05-6
1642	127.5	47.3	1.22-4	1.11-4	1.20-4	8.00-5	6.65-5	5.99-5	4.02-5	3.10-5	(1.46-5)	1.41-6
1705	128.0	43.5	1.19-4	1.13-4	1.20-4	7.96-5	6.48-5	6.11-5	4.10-5	3.16-5	(1.57-5)	1.44-6
1834	126.1	34.7	1.09-4	9.85-5	1.06-4	7.05-5	5.88-5	5.42-5	3.38-5	2.80-5	(1.29-5)	1.37-6

*6.42-5 ≡ 6.42 x 10^{-5}. Numbers in parentheses are for measurements where the leakage flux is greater than 25% of the solar flux measurement, and so have increased uncertainty. Blanks indicate either that no measurement was obtained because of payload rotation, or the flux is too low to measure reliably.

Table 3
Stratcom VI-A
UVS Solar Flux Data for Sunset on Sept. 24-25, 1975

GMT (hrs-min)	Altitude (kft)	Sun zenith angle (deg)	Flux (W/(cm^2-nm)) at wavelength λ (nm), on an area normal to the sun-earth line*									
			393	363	329.2	319.3	310.3	305.3	297.8	290.7	287.3	220
1933	124.8	35.1	1.16-4	1.00-4	1.10-4	6.96-5	6.20-5	5.47-5	3.41-5	2.71-5	(1.29-5)	1.23-6
2023	122.1	39.6	1.18-4	1.09-4	1.17-4	7.61-5	6.16-5	5.43-5	3.52-5	2.29-5	(1.14-5)	9.87-7
2137	116.7	50.8	1.35-4	1.22-4	1.34-4	8.40-5	6.80-5	5.74-5	3.51-5	1.39-5	(9.11-6)	5.20-7
2238	111.8	62.0	1.22-4	1.18-4	1.19-4	7.00-5	5.38-5	4.15-5	2.27-5	3.79-6	(6.43-6)	1.32-7
2334	106.6	73.1	1.37-4	1.23-4	1.23-4	7.43-5	4.64-5	2.78-5	(1.41-5)	(8.18-7)	-	1.36-8
2341	106.0	74.5	1.31-4	1.21-4	1.24-4	7.12-5	4.26-5	2.44-5	(1.31-5)	(6.88-7)	-	8.84-9
0003	104.1	78.9	1.44-4	1.26-4	1.26-4	6.90-5	3.38-5	1.76-5	(9.40-6)	(5.35-7)	-	(1.89-9)
0010	103.5	80.2	1.32-4	1.19-4	1.16-4	5.71-5	2.70-5	1.23-5	(7.00-6)	(4.53-7)	-	(9.79-10)
0022	102.5	82.6	1.32-4	1.22-4	1.17-4	5.72-5	2.11-5	7.83-6	(5.08-6)	(3.89-7)	-	(3.84-10)
0035	101.5	85.2	1.27-4	1.15-4	1.05-4	4.60-5	1.12-5	2.84-6	-	(2.49-7)	-	-
0046	100.9	87.4	1.26-4	1.14-4	9.67-5	3.12-5	3.96-6	7.86-7	-	-	-	-
0059	100.4	90.1	1.19-4	9.25-5	6.04-5	(8.34-6)	(1.91-7)	(1.38-7)	-	-	-	-
0110	99.6	92.2	5.54-5	3.63-5	8.59-6	(7.86-7)	-	(1.70-8)	-	-	-	-
0119	98.3	94.0	9.34-7	4.37-7	1.26-7	(1.02-8)	6.11-9	3.97-9	-	-	-	-

*See footnote for Table 2

Table 4
Stratcom VI-A
UVS Solar Flux Data for Sunrise on Sept. 25, 1975

GMT (hrs-min)	Altitude (kft)	Sun zenith angle (deg)	Flux (W/(cm^2-nm)) at wavelength λ (nm), on an area normal to the sun-earth line*									
			393	363	329.2	319.3	310.3	305.3	297.8	290.7	287.3	220
1251	118.4	95.1	1.17-7	8.58-8	4.50-8	(1.15-8)	1.49-9	4.14-10	-	-	-	-
1308	120.8	91.5	1.30-4	1.08-4	6.68-5	(1.19-5)	(2.54-7)	(1.40-7)	-	(8.83-9)	-	-
1318	122.1	89.6	1.38-4	1.23-4	1.03-4	3.76-5	-	-	-	-	-	-
1322	122.6	88.6	1.41-4	1.26-4	1.19-4	5.67-5	1.39-5	-	-	-	-	(8.54-10)
1327	123.1	87.6	-	-	-	-	-	-	-	-	-	(1.35-9)
1329	123.4	87.1	-	-	-	6.98-5	3.15-5	1.28-5	-	-	-	-
1333	123.7	86.3	1.39-4	1.15-4	-	-	-	-	-	-	-	-
1337	123.9	85.6	-	-	-	7.16-5	3.88-5	1.99-5	-	-	-	-
1339	124.0	85.1	-	-	-	-	3.84-5	2.25-5	(1.35-5)	-	-	-
1342	124.1	84.5	1.43-4	1.25-4	1.09-4	-	-	-	-	-	-	-
1344	124.3	83.9	1.03-4	-	-	-	-	-	-	-	-	1.91-8
1349	124.8	82.9	1.25-4	9.71-5	-	-	4.80-5	2.88-5	(1.55-5)	1.24-6	-	3.17-8
1558	130.2	57.1	1.18-4	1.10-4	1.22-4	7.71-5	6.59-5	5.79-5	3.97-5	3.01-5	(1.47-5)	1.41-6
1600	130.1	56.8	1.15-4	1.12-4	1.18-4	7.85-5	6.36-5	5.60-5	3.81-5	3.05-5	(1.44-5)	1.44-6

*See footnote for Table 2

Table 5
Stratcom VI-A
UVS Solar Flux Data for Parachute Descent on Sept. 25, 1975

GMT (hrs-min)	Altitude (kft)	Sun zenith angle (deg)	Flux (W/(cm^2-nm)) at wavelength λ (nm), on an area normal to the sun-earth line*									
			393	363	329.2	319.3	310.3	305.3	297.8	290.7	287.3	220
[1600	130.1	56.8	1.15-4	1.12-4	1.18-4	7.85-5	6.36-5	5.60-5	3.81-5	3.05-5	(1.44-5)	1.44-6]
(Cut-down)												
1602	106.2	56.4	-	-	1.18-4	6.91-5	4.74-5	3.90-5	2.58-5	3.26-6	-	-
1603	91.0	56.2	9.96-5	1.02-4	1.21-4	7.01-5	3.98-5	2.39-5	(1.39-5)	(6.89-7)	-	7.22-9
1604	83.3	56.0	1.18-4	1.05-4	9.73-5	5.93-5	2.99-5	1.40-5	(8.57-6)	(5.27-7)	-	(2.61-9)
1606	73.9	55.7	1.18-4	1.03-4	9.52-5	5.64-5	2.38-5	1.02-5	(7.77-6)	(4.03-7)	-	(1.63-10)
1607	68.6	55.5	1.05-4	1.02-4	8.38-5	4.34-5	2.11-5	7.69-6	(4.16-6)	(3.29-7)	-	-
1608	62.3	55.3	9.66-5	9.85-5	1.01-4	4.99-5	2.03-5	7.41-6	(6.12-6)	(3.53-7)	-	-
1610	55.9	55.0	8.97-5	9.75-5	1.00-4	4.93-5	1.79-5	6.52-6	(6.05-6)	(3.34-7)	-	-
(1613	45.2	54.3	9.26-5	8.99-5	8.18-5	2.90-5	1.67-5	5.56-6	(4.86-6)	(3.15-7)	-	-).

*See footnote for Table 2.

uncertainty in the fluxes is ±10%, except for the 220 nm flux which is ±20%. Numbers in parentheses have larger uncertainties because of large corrections for leakage flux at longer wavelengths. Blanks in the tables indicate either fluxes too weak to measure with the UVS, or that payload rotation did not give a sun view for that particular filter set.

Plots of solar flux versus solar zenith angle for some of the sunset data of 24-25 September, from Table 3, are given in Fig. 2. Since the balloon was descending from 125 to 98 kft, the increasing attenuation with solar zenith angle is greater than if the balloon were at a constant altitude. Comparison of the data in Tables 2 and 3 shows greater attenuation for the lower altitude sunset data when compared at about equal solar zenith angles (compare also with the data in Table 4). The 320 to 300 nm region also shows a modified "umkehr" effect for solar zenith angles greater than 90°, where the ratio of solar fluxes [e.g., F(305.3)/F(393)] first decreases with increasing zenith angle, and then flattens and increases slightly beyond 90°.

Some of the parachute descent data of Table 5 are plotted in Fig. 3. Here the attenuation is due primarily to the increasing ozone above the UVS as it descends through the ozone layer. The data below about 60 kft have more than a 10% uncertainty, since Rayleigh scattering becomes increasingly important at low altitudes. The 305.3 nm data show that the ozone layer lies mostly between 70 and 110 kft.

The high-altitude data can be used to obtain an absolute value for the solar flux at 220 nm. This is done by plotting the measured intensities against the attenuation path length on a semilog plot and extrapolating to zero path length. The attenuation path length should be proportional to the local atmospheric pressure divided by the cosine of the solar zenith angle, provided that the oxygen/ozone ratio remains constant. Appropriate portions of the 24 September sunrise and 24-25 September sunset data are plotted in Fig. 4, along with the best-fit lines for data with $P/\cos\theta$ less than 20 mb. The pressures were taken from the mid-latitude spring-fall model of [11]. The 24 September sunrise data have a nearly constant oxygen/ozone ratio, while the 24-25 September sunset data have this ratio decreasing as the balloon descends. This accounts for the different slopes in Fig. 4. The zero pressure intercept is 2.93×10^{-6} W/(cm^2-nm) to 0.5% for both lines. The unattenuated solar flux at 220 nm (averaged over ±5 nm, effectively) is thus measured to be 3.93×10^{-6} W/(cm^2-nm) ±20% at 1 au on 24-25 September 1975.

The solar flux at 220 nm has been measured by a number of other groups over the past several years. Variations in the measurements are frequently larger than the quoted errors. The 220 nm flux given above is low compared to other recent measurements. Satellite data on solar uv show that variability increases as the wavelength decreases [7]. To check the variability of the solar 220 nm flux, the measurements of a number of groups have been compared with sunspot number, a measure of solar activity. In [12] the Zürich sunspot numbers $\ddot{R}z$ for 24-25 September 1975 are given as 0. Solar flux measurements in [13] are an average for 16 May 1973 and 23

September 1972, for which Rz is 33 and 65. Graphical results indicate that the flux at 220 nm was about 10% different on these two dates, so the average has been raised and lowered by 5% to give effective fluxes for those two dates. Ackerman et al. [14] give an average flux measurement for data from 10 May 1968, 19 April 1969, and 3 October 1969, for which Rz is 117, 128, and 99. Since the data in [14] are difficult to separate according to date, the average flux at 220 nm has been used with the average Rz. Measurements in [15] are for June 1970, when Rz was 168. The measured fluxes and sunspot numbers are listed in Table 6 and plotted in Fig. 5.

TABLE 6

SOLAR FLUX AT 220 nm VERSUS ZÜRICH SUNSPOT NUMBER

Solar Flux at 220 nm (±5 nm) [W/(cm^2-nm)]	Zürich Sunspot Number	Date of Measurement	Data Source and Comments
3.93×10^{-6}	0	24-25 Sep 75	Present results
4.39×10^{-6}	33	16 May 73	[13] - average
4.91×10^{-6}	65	23 Sep 72	Separated (see text)
9.16×10^{-6}	115	10 May 68 19 Apr 69 3 Oct 69	[14] - average Rz for 3 dates
5.78×10^{-6}	168	15 Jun 70	[15]

The data in Fig. 5 show a general rise in the 220 nm solar flux with increasing Rz. A possible peaking may exist near Rz = 100, but the data are too few to show this with certainty. The Rz values in Fig. 5 are daily averages, but for the 220 nm region it may be better to use Rz averaged over a solar rotation. The data in [7] show that below 200 nm the solar uv flux varies significantly in a solar rotation, while at longer wavelengths the variations are more long-term. Thus the 27-day-averaged Rz may be a better index of solar uv variability for wavelengths greater than 200 nm.

Future measurements of the 220 nm flux, particularly during the coming years as the sunspot cycle goes from minimum to maximum, will produce data of considerable interest by fixing more precisely the variability of the solar flux in this region. The variation of solar flux with altitude measured under this program will make it possible to check radiation transport model predictions. Finally, the calculation of ux flux at any altitude and point in the solar cycle can then be made with confidence and reasonably well known limits on the accuracy.

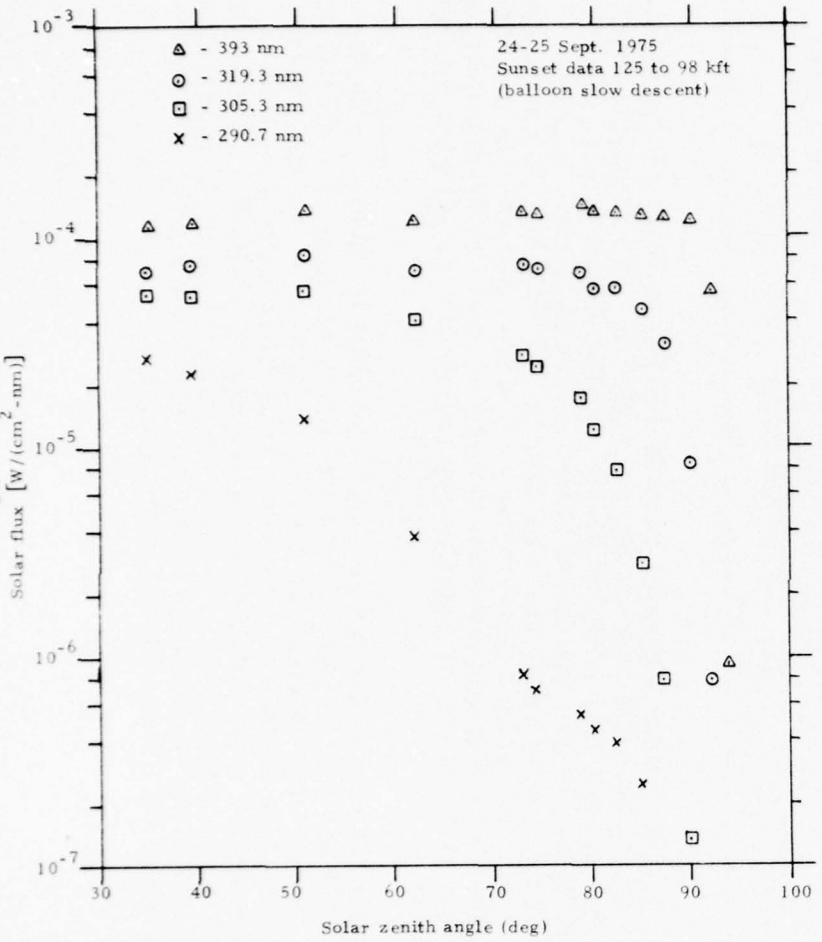

Figure 2. Plot of Solar Flux vs. Solar Zenith Angle at Selected Wavelengths for Sunset on 24-25 Sept. 1975.

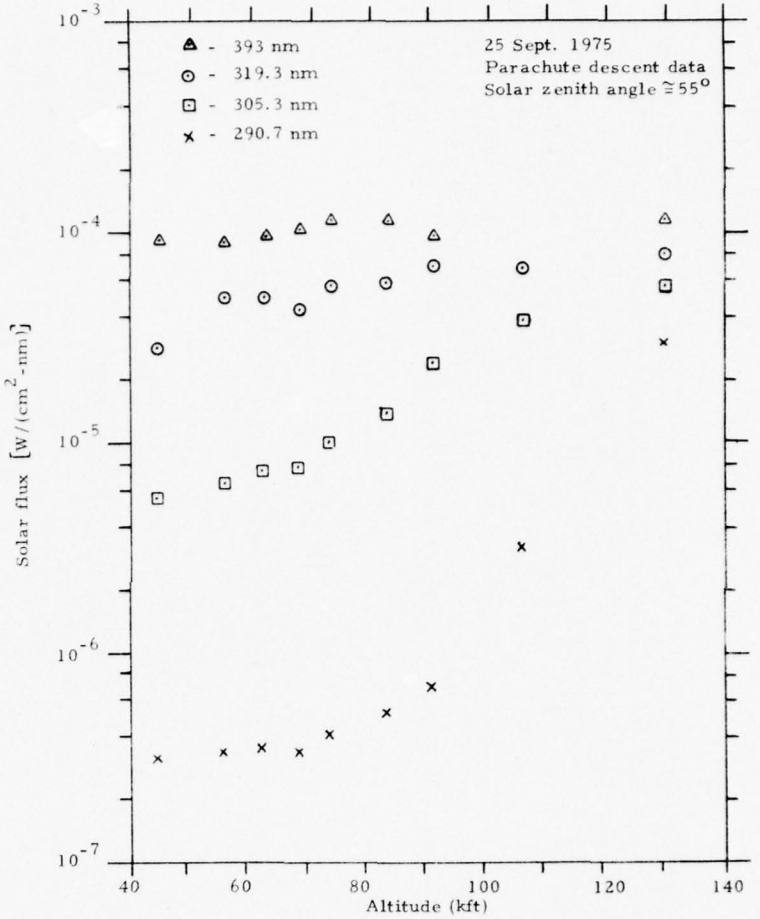

Figure 3. Plot of Solar Flux vs. Altitude at Selected Wavelengths for Parachute Descent on 25 Sept. 1975.

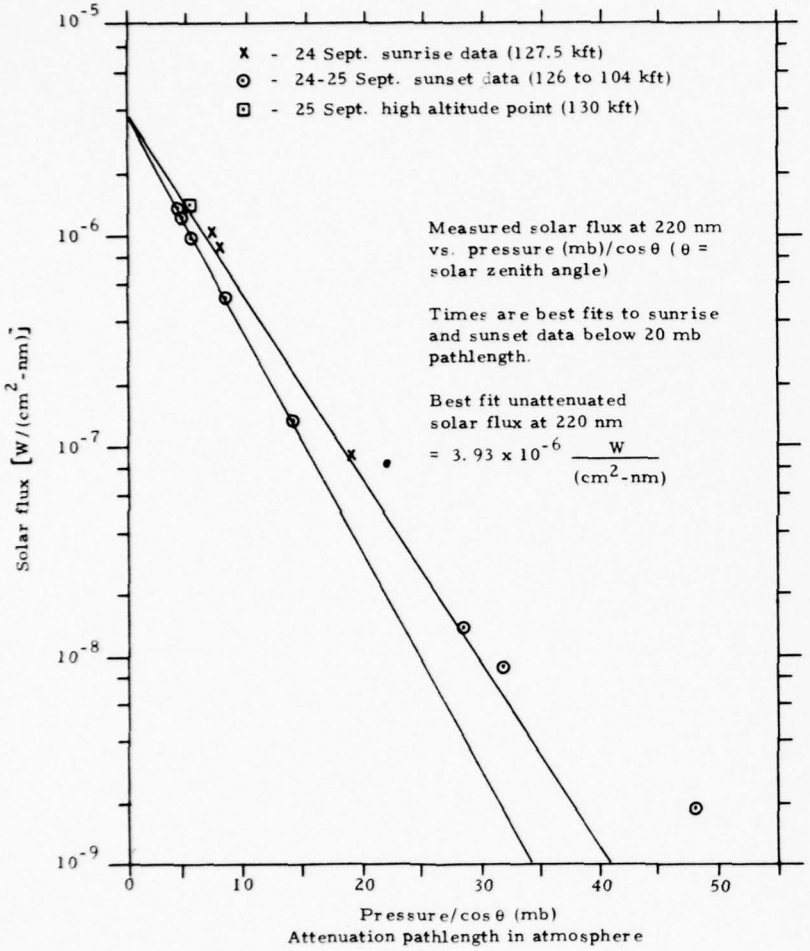

Figure 4. Plot of Measured Solar Flux at 220 nm vs. Attenuation Pathlength in Atmosphere.

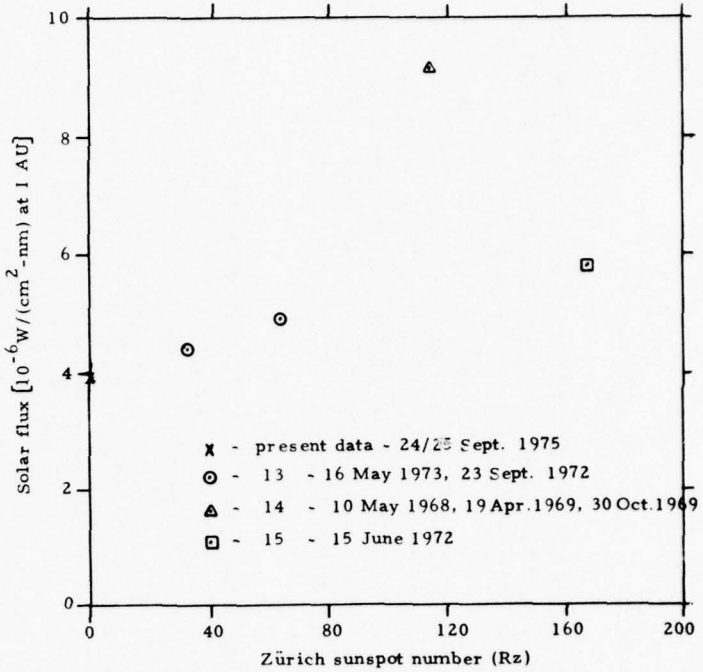

Figure 5. Plot of Solar UV Flux at 220 nm vs. Sunspot Number

CONCLUSIONS

The uv spectrophotometer operated successfully on the STRATCOM VI-A balloon flight and returned much good data on stratospheric solar uv fluxes. The dependence of the solar uv fluxes on solar zenith angle at 30-40 km was measured, and the vertical profile to below 20 km was measured during the parachute descent. One of the few reliable measurements of solar uv in the important high-altitude 220 nm atmospheric window was made, giving a solar flux of 3.93×10^{-6} W/(cm^2-nm)(at 220 nm) at 1 au during solar minimum (Rz = 0). Comparison with other measurements shows a trend of increasing solar flux at 220 nm with increasing solar activity (Rz - sunspot number).

The UVS gave a considerable amount of data on solar uv flux versus zenith angle for the 24-25 September sunset period. The two sunrise data sets are more sparse because of the warmup requirement for the solar pointing mechanism. Efforts will be made to eliminate this problem on future balloon flights by using a conical diffuser [1] and mounting the UVS in a vertical position. This removes the requirement for solar pointing, and thus any problems associated with the pointing mechanism.

During portions of the flight, the UVS temperature was considerably lower than had been predicted by theoretical models. Although the UVS continued to operate properly, it was necessary to include small temperature-induced gain shifts into the data reduction procedure to obtain maximum accuracy. It would be desirable to use the UVS internal heaters to avoid this problem if sufficient power were available on future flights.

REFERENCES

1. Hanser, F. A., B. Sellers, and J. L. Hunerwadel, 1975, "Design, Fabrication and Flight of a UV Spectrophotometer Aboard a WB57F High Altitude Aircraft for the CIAP Flight Series," Report PANA-UVS-7, Summary Report for Contract No. N00014-73-C-0316.

2. Sellers, B., F. A. Hanser, and J. L. Hunerwadel, 1976, "STRATCOM VI-A UV Flux and 30-65 km Low-Background Betasonde Air Density Measurements," Report PANA-AIR-1, Final Report for Contract No. DAAD07-75-C-0124.

3. Rowland, F. S., and M. J. Molina, 1975, "Chlorofluoromethanes in the Environment," Rev. Geophys. Space Phys. 13:1-35.

4. Tousey, R., 1966, "The Radiation from the Sun," The Middle Ultraviolet: Its Science and Technology, ed. A. E. S. Green, 1-39, Wiley, NY.

5. Brewer, A. W., and A. W. Wilson, 1965, "Measurements of Solar Ultraviolet Radiation in the Stratosphere," Quart. J. Roy. Meteor. Soc. 91: 452-61.

6. Tisone, G. C., 1972, "Measurements of the Absorption of Solar Radiation by O_2 and O_3 in the 2150-A Region," J. Geophys. Res. 77:2971-4.

7. Heath, D. F., 1973, "Space Observations of the Variability of Solar Irradiance in the Near and Far Ultraviolet," J. Geophys. Res. 78:2779-92.

8. Sellers, B., F. A. Hanser, and J. L. Hunerwadel, 1973, "Design, Fabrication and Flight of an Ultraviolet Interference-Filter Spectrophotometer Aboard a WB57F High Altitude Aircraft," Report PANA-UVS-1, Annual Report for Contract No. N00014-73-C-0316.

9. Hanser, F. A., and B. Sellers, 1974, "Solar UV Fluxes and Ozone Overburdens Obtained from UVS Measurements on the CIAP Airstream Flight Series of June 1973, September 1973, November 1973, and January 1974," Report PANA-UVS-4, Annual Report for Contract No. N00014-73-C-0316.

10. The American Ephemeris and Nautical Almanac for the year 1975, US Government Printing Office, Washington, DC, 1973.

11. US Standard Atmosphere Supplements, 1966, US Government Printing Office, Washington, DC, 1966.

12. Solar-Geophysical Data, issued monthly by US Dept of Commerce, NOAA, Environmental Data Service, Boulder, CO.

13. Simon, P., 1974, "Balloon Measurements of Solar Fluxes between 1960Å and 2300A," Proceedings of the Third Conference on the Climatic Impact Assessment Program, A. J. Broderick, and T. M. Hard, eds., DOT-TSC-OST-74-15, 137.

14. Ackerman, M., D. Frimount, and R. Pastiels, 1971, "New Ultraviolet Solar Flux Measurements at 2000Å Using a Balloon Borne Instrument," New Techniques in Space Astronomy, eds. Labuhn and Lust, 251, Reidel, Dordrecht, Holland.

15. Broadfoot, A. L., 1972, "The Solar Spectrum 2100-3200Å," Astophys. J. 173:681-9.

CHAPTER 7

STRATOSPHERIC OZONE DENSITY AS MEASURED BY A CHEMILUMINESCENT SENSOR DURING THE STRATCOM VI-A FLIGHT

Jagir S. Randhawa
Atmospheric Sciences Laboratory, WSMR, NM

M. Izquierdo
Carlos McDonald
Zvi Salpeter
University of Texas at El Paso, El Paso, TX

ABSTRACT

Ozone concentration was measured by the chemiluminescent technique during the STRATCOM VI-A balloon flight flown from Holloman Air Force Base, New Mexico, on 23 September 1975. More than 30 hours of data were collected as the balloon floated at various altitudes in the stratosphere. A diurnal variation in ozone above the ozone peak was observed in the 27 to 40 km region. Wet stratospheric photochemistry is used as a guide to explain the diurnal change in ozone.

INTRODUCTION

Ozone, a minor constituent of the upper atmosphere, is not distributed uniformly. Its concentration has been measured by rocket-borne [1] as well as balloon-borne sensors [2-5]. These instruments do not stay for long periods in the atmosphere; they are flown with rockets and small radiosonde balloons and hence are not capable of measuring temporal variation in ozone concentration. To observe the effect of solar radiation on the ozone concentration at various altitudes during the day and also during sunset and sunrise, a chemiluminescent sensor was flown with the STRATCOM VI-A payload.

EXPERIMENT

The STRATCOM VI-A balloon was launched on 23 September 1975 at 2300 MST from Holloman Air Force Base near Alamogordo, New Mexico. It reached the float altitude of 38.5 km at 0300 MST on September 24. The balloon floated at this altitude through sunrise at 0530. At 1200 it drifted downward to an altitude of 27.4 km by 1900 MST (sunset occurred at 1828 MST). Shortly after 1900, the balloon started ascending as the ballast was dropped, and reached an altitude of 36 km at 0200 on 25 September. It stayed at this altitude until sunrise at 0456 MST. As the sun heated the balloon, it ascended to an altitude of 39.8 km at 0715 MST. The ozone sensor and some other sensors were turned off at 0500 MST to conserve power for the remaining experiments; therefore, no ozone data were obtained after that time. The flight was terminated at 0900 MST. Figure 1 shows the altitude plotted against time of the flight.

An electrochemical (mast) ozonesonde was also released on 24 September 1975 (1100 MST) from White Sands Missile Range, New Mexico, for comparison purposes.

RESULTS

The solid line on Figure 2 shows the ozone profile as obtained by the chemiluminescent sensor on its first ascent; the dotted line shows electrochemical sonde data. The times shown on the figure indicate the balloon altitude and the corresponding ozone concentration.

Figure 3 shows Figure 2 data and the descent data of ozone concentration along with the time the balloon reached that altitude. Note that between 27 and 38 km a difference in ozone concentration was observed between the nighttime ascent and the afternoon descent.

Figure 4 shows the descent data obtained on the afternoon and evening of 24 September and the ascent data on the night and early morning of 25 September. Figure 5 shows the composite data of the complete flight. Both times the ascent data were obtained during nighttimes and the ozone concentration measured is in good agreement.

The transition through sunrise on 24 September at a constant altitude is shown in Figure 6.

ANALYSIS

During the balloon ascent, up to 25 km, there is good agreement between the chemiluminescent and electrochemical sensors. From 27 to 35 km, the two nighttime ascents are in very good agreement. The descent data in the afternoon shows a marked increase in ozone concentration although it follows the same gradient as ascent.

The diurnal change can possibly be explained by wet photochemistry. During descent, the ozone concentration curve (Figure 4) from noon (point 1) to sunset (point 2) should correspond closely to the undisturbed daytime values since the sensors were descending away from the wake of the balloon.

The daytime production of ozone is primarily due to the following reactions [6]:

$$O_2 + h\nu\ (< 2424\text{Å}) \rightarrow O + O \quad (1)$$

$$O + O_2 + M \rightarrow O_3 + M \text{ (twice)} \quad (2)$$

$$\text{Net } 3O_2 \rightarrow 2O_3$$

The destruction reactions of O_3 are as follows:

$$O_3 + h\nu\ (< 3100\text{Å}) \rightarrow O_2 + O \quad (3)$$

$$O_3 + O \rightarrow O_2 + O_2 \quad (4)$$

$$\text{Net } 2O_3 \rightarrow 3O_2$$

The NO_x destruction reactions:

$$NO_2 + h\nu\ (< 4000\text{Å}) \rightarrow NO + O \quad (5)$$

$$NO + O_3 \rightarrow NO_2 + O_2 \quad (6)$$

$$NO_2 + O \rightarrow NO + O_2 \quad (7)$$

$$N_2O + O(^1D) \rightarrow 2NO \quad (8)$$

The HO_X destruction reactions:

$$H_2O + O(^1D) \rightarrow 2HO \quad (9)$$

$$CH_4 + O(^1D) \rightarrow CH_3 + HO \quad (10)$$

$$HO + O_3 \rightarrow HO_2 + O_2 \quad (11)$$

The net gain in ozone is the difference between the destruction and the production reactions.

The sunset transition occurred from sunset at 1828 MST to 2004 MST (point 2 to point 3). During the transition, the balloon slowed down until it reached its lowest altitude and then slowly started ascending. In reference to the ozone chemistry, during the sunset transition, UV sunset first occurs at the shortest wavelengths. Consequently, the ozone production by Equations (1), (2), and (5) is no longer active. However, all the remaining destruction reactions of O_3 by NO_X and HO_X remain. At the sensor location, the destruction reactions of O_3 were probably enhanced due to the presence of water vapor. However, this enhanced destruction of O_3 in the vicinity of the ozone sensor is not very apparent because the balloon was descending into air with a higher concentration of ozone.

As the night progressed from point 3 to point 4, the ascending cold balloon and payload package acted as sinks of water vapor, and the balloon temperature was essentially that of the air temperature. Hence the disturbance by the balloon and payload should be minimal, and the measured values of ozone by the sensors should correspond to the nighttime equilibrium values of the undisturbed atmosphere. Consequently, a comparison of the ozone measurements of the daytime descent (point 1 to point 2) and the nighttime ascent (point 3 to point 4) shown in Figure 4 shows a diurnal change in the ozone above the ozone peak.

The nighttime decrease in the ozone profile may be explained by the absence of the daytime production and destruction reactions, the nighttime equilibrium of O_3 being primarily established by Equations (2) and (4) since NO and HO are essentially depleted. Another possible explanation could be the subsidence of the O_3 layer. However, this explanation is unlikely because of the meteorological conditions existing at that time.

During twilight, as the scattered light increased (Figure 6), ozone concentration slowly decreased from its nighttime equilibrium. At twilight, as the sky receives scattered UV in the region between 3100Å and 4000Å, ozone is destroyed by NO_X reactions. This destruction of ozone may have caused the ozone concentration decrease. At sunrise when energies of wavelengths less than $\lambda < 3100$Å start arriving at the balloon and payload platform, causing water vapor to be released from the platform, the destructive reactions of HO_X plus NO_X accelerate the reduction

of ozone [7]. Additional ozone is produced as the wavelength radiation less than 2424Å becomes available at the platform altitude [Equation (1)] and the formation of ozone exceeds its destruction. This increase is shown by the change in slope in Figure 6 at about 0600 MST.

Model calculations for sunrise transition [8] were made for 25, 30, 35, and 40 km altitudes and are plotted in Figure 6. The changes in ozone concentration during that transition period for 25 and 30 km indicate a slight decrease until sunrise and then a slight increase. For 35 km the trend is opposite, i.e., an increase during the night and then a decrease. The 40 km calculation shows the same trend as for 35 km, but the amplitude is large. An additional calculation made for 40 km altitude which included large amounts of water vapor (10^3 times the normal) is also plotted on the same figure. The effect of large amounts of water vapor in the model is quite significant.

The diurnal variation in ozone concentration as observed between 27 and 40 km (Figure 4) is consistent with the model calculation made with additional water. Thus it is apparent that the ozone sensor was measuring ozone in the wake of the balloon during both ascents, while during descent the measurements were not in the wake of the balloon. The sunrise effect, however, could not be explained on the model calculation and may be a clue to significant processes not yet included in these models.

CONCLUSIONS

A diurnal change in the ozone concentration was observed in the region between 27 and 40 km during this balloon flight. These observations are consistent with the model calculations made with additional water vapor and indicate that the balloon was outgassing throughout most of the flight.

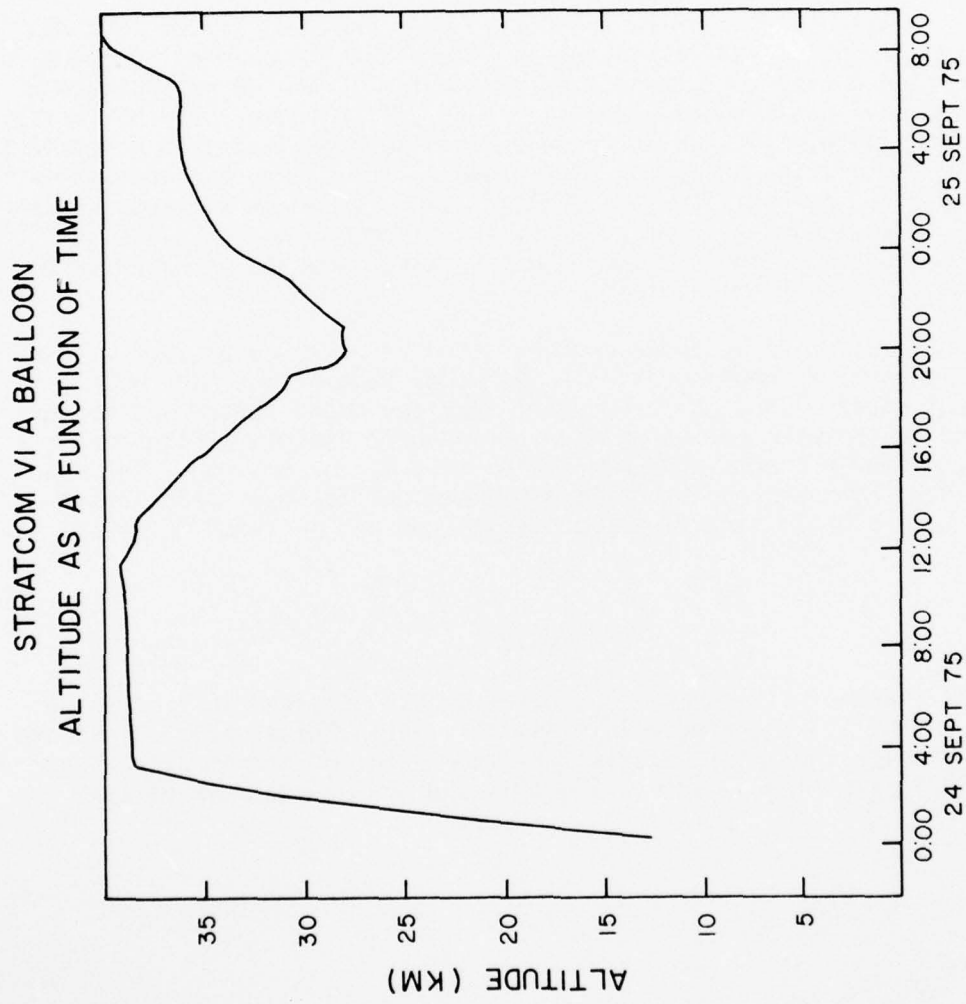

Figure 1. Balloon altitude as a function of time.

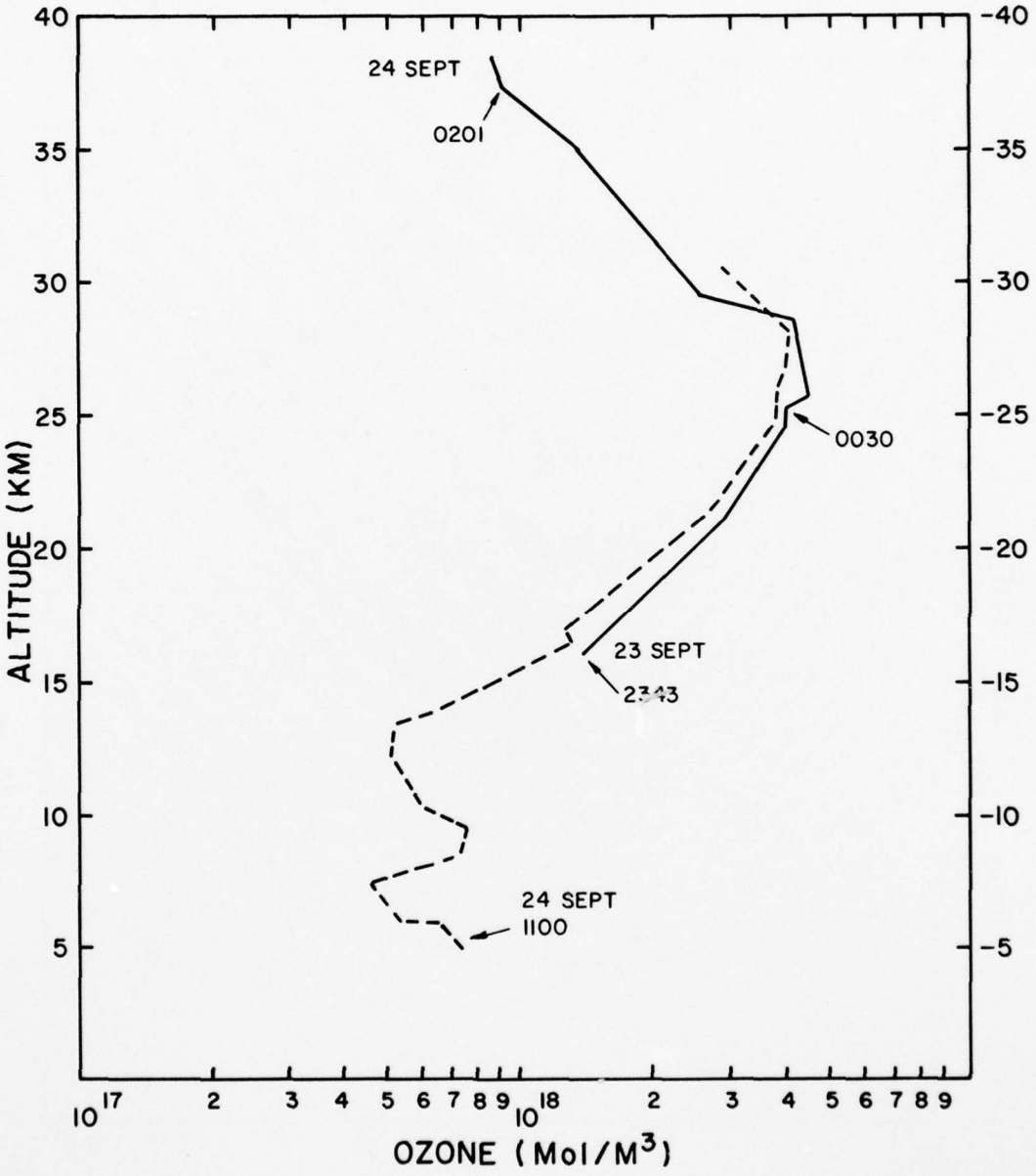

Figure 2. Ozone concentration measured by the chemiluminescent sensor as the balloon ascended through troposphere and stratosphere (solid line). Electrochemical (mast) ozonesonde profile (dotted line) is also shown.

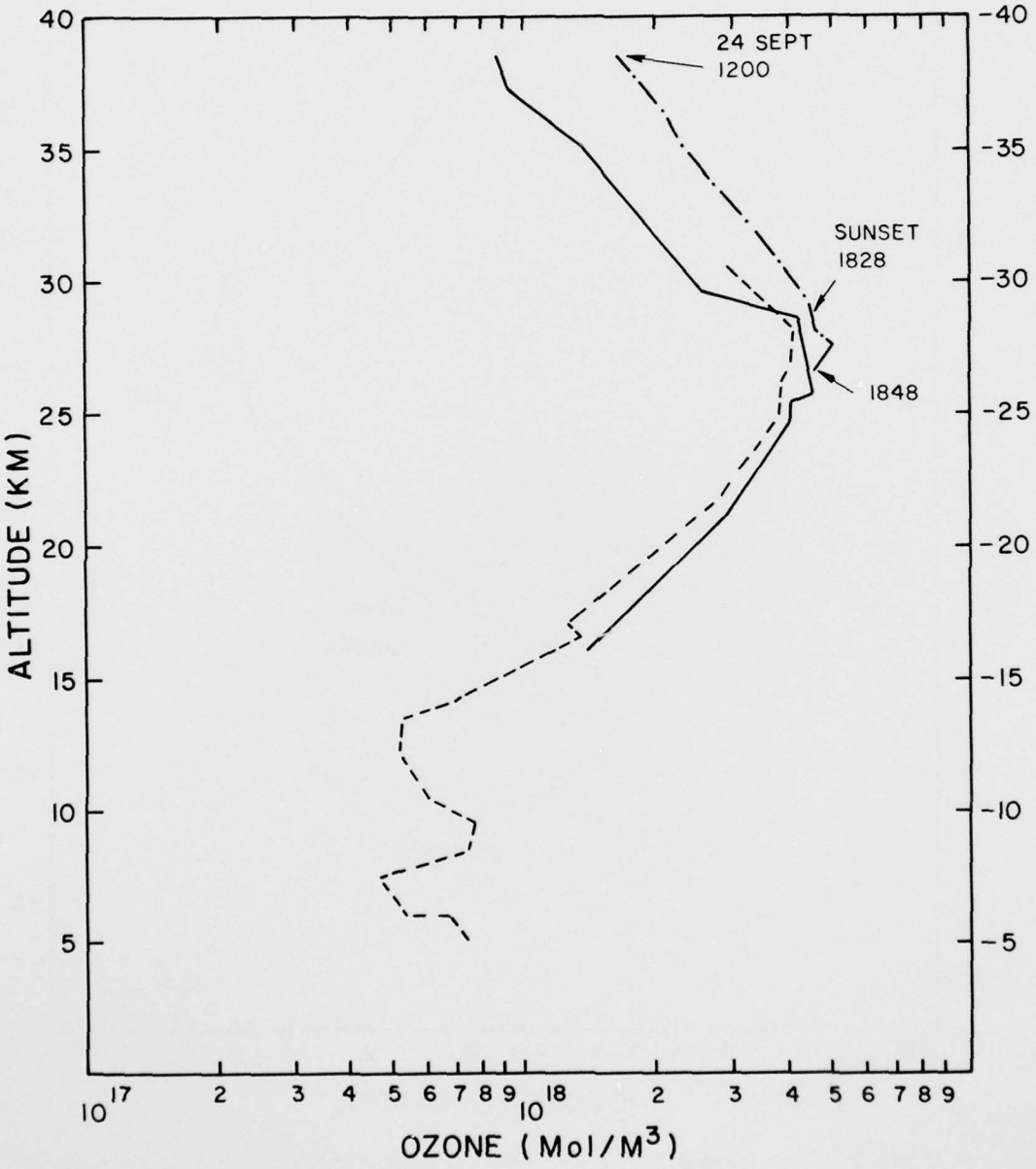

Figure 3. Same as Figure 2 plus ozone concentration measured by chemiluminescent sensor as the balloon descended in the afternoon of 24 September 1975 (dashed dotted line).

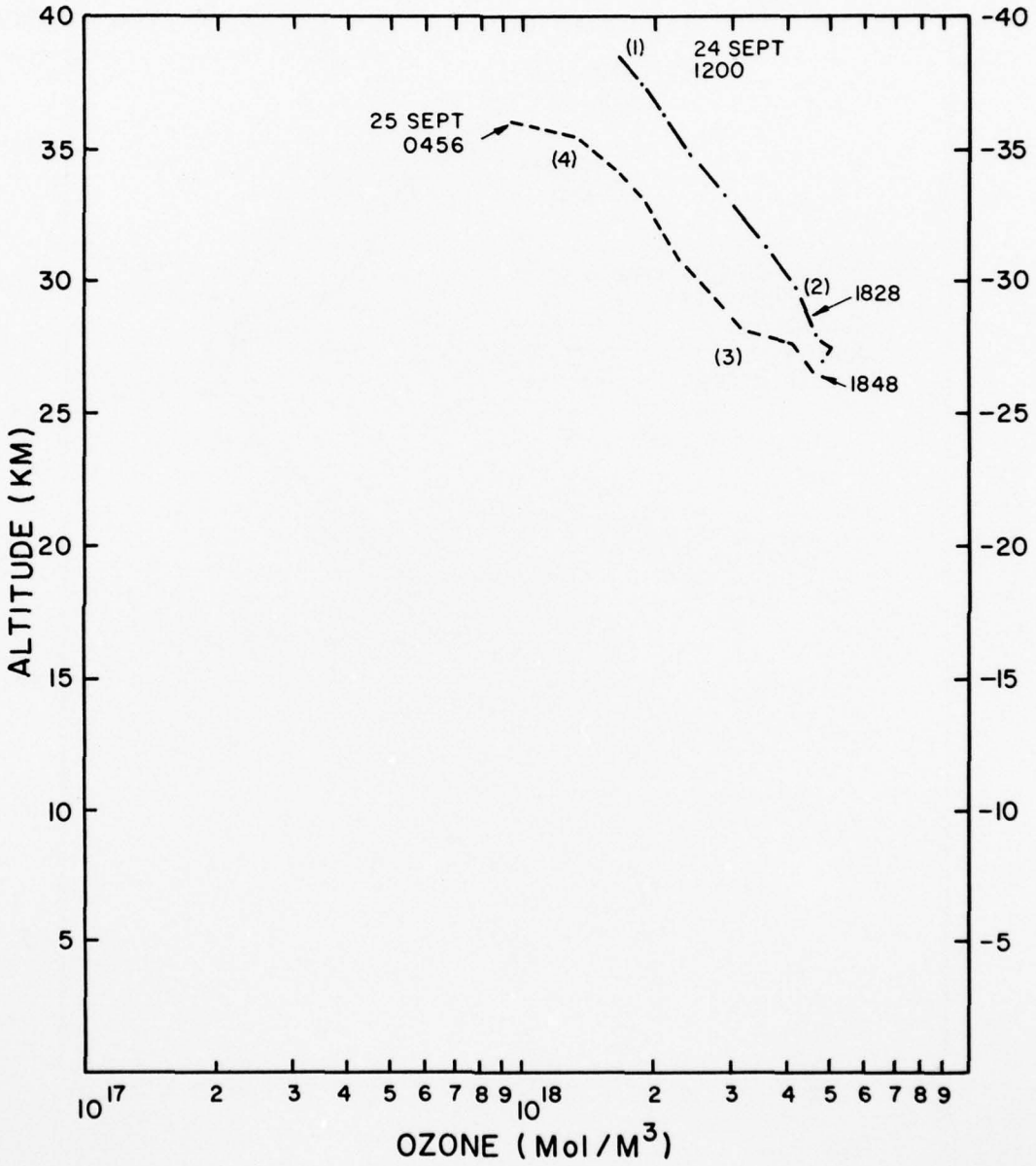

Figure 4. Ozone concentration as measured by the chemiluminescent sensor on its descent (dashed dotted line) and the second ascent (dashed line).

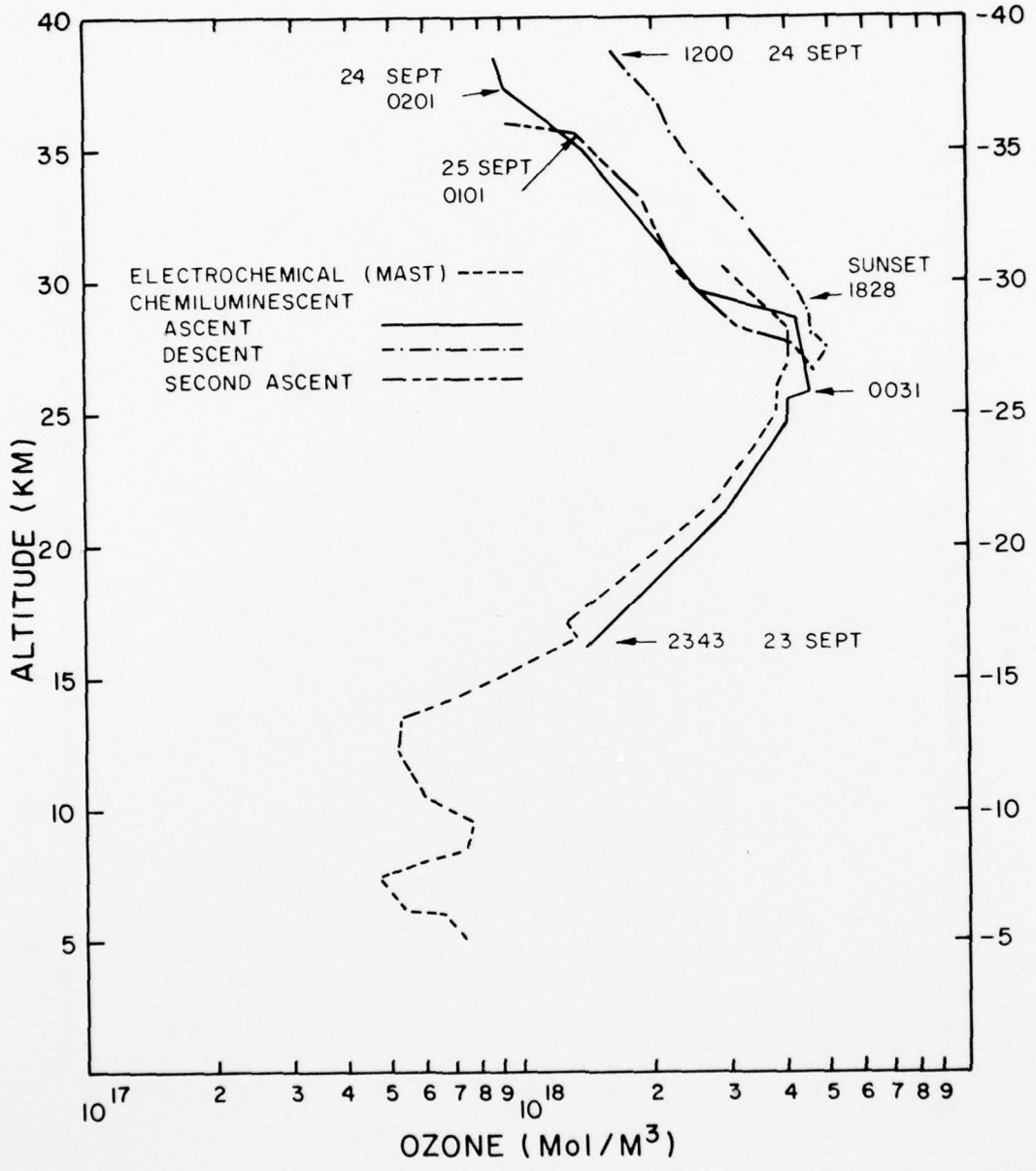

Figure 5. Composite profiles of ozone concentration as measured by the chemiluminescent sensor on STRATCOM VI-A flight. Electrochemical profile is also shown.

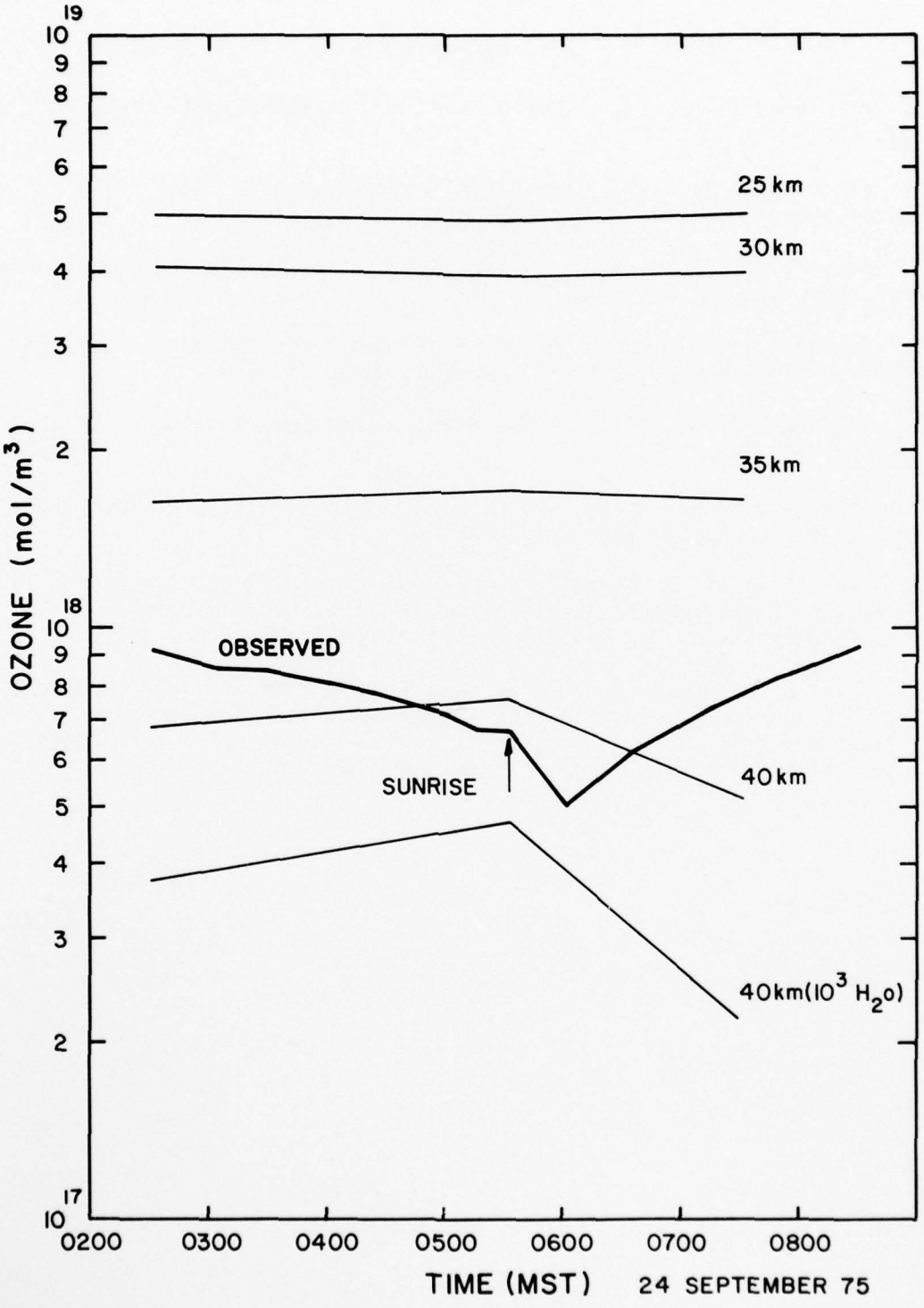

Figure 6. Sunrise effect as observed by the chemiluminescent sensor. The balloon was floating at a constant altitude of 38.6 km. Model calculation for 25, 30, 35, and 40 km are also plotted. An additional profile at 40 km contained 10^3 times the normal water vapor in the calculation.

REFERENCES

1. Randhawa, J. S., 1967, "Ozone Sonde for Rocket Flight," Nature, 213, 53.

2. Regener, V. H., 1964, "Measurement of Atmospheric Ozone with Chemiluminescent Method," J. Geophys. Res., 69, 3795.

3. Brewer, A. W., and J. R. Milford, 1960, "The OXFORD-KEW Ozone Sonde," Proc. Roy. Soc. A, 256, 470.

4. Randhawa, J. S., 1969, "Ozone Measurements from a Stable Platform Near the Stratopause Level," J. Geophys. Res., 74, 4588.

5. Randhawa, J. S., 1971, "Ozone Measurements Near Sunrise," Nature Physical Science, 233, 101.

6. Johnston, H. S., 1975, "Global Ozone Balance in Natural Stratosphere," Reviews of Geophysics and Space Physics.

7. Lin, S. C., T. M. Donahue, R. J. Cicerone, and W. L. Chameides, 1976, "Effect of Water Vapor on the Destruction of Ozone in Stratosphere Perturbed by CIX or NO_X Pollutants," J. Geophys. Res., 81, 3111.

8. Ballard, H. N., Jose M. Serna, and Frank P. Hudson, 1977, "Calculation of Selected Atmospheric Composition Parameters for the Mid-Latitude, September Stratosphere," R&D Report, ECOM-5818, Atmospheric Sciences Laboratory, White Sands Missile Range, New Mexico.

CHAPTER 8

MEASUREMENTS OF WATER VAPOR CONCENTRATIONS DURING THE STRATCOM VI-A EXPERIMENT

Philip Goodman
Panametrics, Inc.
221 Crescent Street
Waltham, MA 02154

ABSTRACT

Measurements of water vapor concentrations were obtained for three different locations on the platform introduced into the stratosphere by the STRATCOM VI-A experiment. Two of these locations were on the gondola, one in the inlet to the ozone instrument and one near the inlet to the mass spectrometer. A third measurement was made by a sensor suspended 130 ft below the gondola. All measurements were made by Al_2O_3 humidity sensors positioned on mounts which were capable of maintaining the sensor temperature at +25°C during measurements. Results obtained from the suspended sensor at the end of the experiment corresponded to an ambient concentration of 0.8 ppm_w. Since this result was in reasonable accord with expectation for unperturbed stratospheric water vapor concentration, it validated the much higher concentrations measured during earlier portions of the flight. These results are discussed in terms of the balloon trajectory, outgassing dynamics, and sensor location on the experimental platform.

INTRODUCTION

The H_2O molelcule is an all-pervasive constituent of virtually every scientific experiment. Water is present in the stratosphere by virtue of its introduction into the stratosphere through the tropical tropopause Hadley cell circulation patterns. It may also be introduced into the stratosphere by thunderstorm penetrations through the tropopause, by methane oxidation, and, perhaps, by numerous other source mechanisms as yet not totally identified. The experimental measurement of atmospheric constituents conducted from a balloon platform is subject to still another source of water vapor because the water molecule is also carried aloft by absorption on the platform surfaces. Water vapor is therefore known to be naturally present in the stratosphere but its volume concentration may be enhanced by orders of magnitude in the vicinity of any platform introduced into the stratosphere in order to make aeronomic studies.

Water vapor plays a significant role in the determination of the radiation balance of the earth. The H_2O molecule, as well as numerous radicals derived therefrom, such as OH, HO_2, etc., also participate importantly in the photochemical aeronomic reactions which determine the concentration of numerous other chemical species present in trace and larger amounts in the stratosphere. Water vapor introduced into the stratosphere by an experimental platform such as STRATCOM VI-A can therefore perturb the local environment of the platform as well as perturb measurement of other stratospheric parameters for which instrumentation aboard the platform is provided. Measurement of the local water vapor concentration in the platform environment can therefore provide a means for correcting other experimental measurements.

Aluminum oxide sensors were flown aboard the STRATCOM V experiment. Improved sensors of the Al_2O_3 type were flown aboard the STRATCOM VI-A experiment for the same reasons. In addition, a single sensor intended to measure the unperturbed stratospheric ambient during the balloon flight was flown during STRATCOM VI-A. The results of these measurements are presented in this report.

EXPERIMENTAL

Al_2O_3 sensors utilized aboard STRATCOM V experiment were of the type that exhibited negligible dependency of sensor output upon ambient temperature. Although this characteristic is very desirable, such sensors are susceptible to failure as a result of abrasion of the thin Al_2O_3 layer present on the sensor surface by the mechanical contact arm utilized to make contact with one of the sensor electrodes. These sensors also occasionally fail because ice accumulates under the mechanical contact arm. Following STRATCOM V a new type of sensor was developed which was considerably more rugged than the earlier version but which exhibited a dependence of sensor output upon temperature. For some sensors, the output was independent of temperature from +25° to about -30°C whereas for other sensors the absence of a temperature dependence extended only to about -10°C. To compensate for the temperature dependency of the water vapor measurement, such sensors were mounted on heated surfaces which maintained the sensor temperature at a constant 25°C provided that heater power was supplied. Circuitry suitable for controlling the surface temperature of the sensor mount was developed, constructed, and flown aboard the STRATCOM VI-A. Sensors of this improved type are shown in Fig. 1.

The water vapor sensors were of the Al_2O_3 type such as were described earlier in [1]. The sensors utilized on heated sensor mounts were substantially of the same construction except for the addition of a more abrasion resistant Al_2O_3 coating over a portion of the sensor surface. This tougher coating permitted a larger mechanical contact pressure to be exerted on the sensor surface without causing penetration through the oxide layer and consequent sensor shorting. The higher mechanical pressure also minimized the occurrence of open sensors resulting from failure of the mechanical arm to maintain electrical contact with the vacuum deposited gold electrode on the sensor surface.

Three such sensors were deployed on the gondola, and one sensor of the same type was deployed by means of a let-down reel which suspended the sensor 130 ft below the gondola. The let-down reel was activated when the balloon altitude reached about 10,000 ft. A fifth sensor, of the older STRATCOM V type, was installed at the top of the balloon. The older type was utilized for this installation because heater power was not available at this location.

One of the gondola mounted sensors was positioned in the inlet tubing to the ozone sonde and therefore monitored the water vapor content of the ambient air sampled by the ozone sonde. A second sensor was positioned near the exit of the gas stream passing through the ozone sonde and a third was located near the inlet to the mass spectrometer.

The electronic circuitry utilized for the sensors positioned on the gondola and atop the balloon was identical with that which was utilized for STRATCOM V and described in [1]. This circuitry is, however, sensitive to cable capacitance and would have been inoperative if it had been used in conjunction with a 130 ft long cable. Consequently, circuitry was constructed specifically for this flight which was insensitive to cable capacitance (and length). This circuitry is similar to that utilized in the Panametrics Model 2000 hygrometer. However, two simultaneously operative channels were provided which gave higher sensitivity over different ranges than would have been obtainable had only a single data channel been employed. In addition to the sensor impedance measuring circuitry, each heated sensor was also provided with a temperature monitor to assure that sensor temperature was maintained at 25°C when the heaters were operative. Temperature control circuitry performed satisfactorily during the entire flight for all the sensors and will not be discussed further.

The heater enclosed in the sensor mount had a resistance of 70 ohms and was powered by a 24 V supply. The heater was insulated from the case. No significant interference from the heater operation was observed during preflight calibration and checkout.

Usable data was obtained from three of the four heated sensors. These data will be discussed below. The cause of the failure of the fourth sensor, located on the gondola ring at the exit of the ozone sonde, was not determinmed but could have resulted from either sensor or electronic circuitry malfunction. The unheated sensor positioned atop the balloon provided data during balloon ascent. However, this data indicated that a layer of ice formed on the surface of the sensor because frost points measured were greatly in excess of the ambient temperature. This ice apparently ultimately resulted in sensor failure since usable sensor data transmission ceased shortly after attainment of float altitude.

RESULTS AND DISCUSSION

Measured sensor impedances were converted to frost point data by means of calibration curves determined for each individual sensor in the laboratory prior to flight.

The reduced data obtained is shown in Fig. 2. Included in this figure as curve 1 is the altitude-time profile of the STRATCOM VI-A experiment. Also shown in Fig. 2, as curve 2, is the temperature-time profile for the experiment. Curves 3, 4, and 5 represent the data obtained from the three heated sensors as discussed above. Curve 3 represents the condition present in the inlet to the ozone sonde utilized aboard the experiment; curve 4 represents the ambient condition in the very near vicinity of the instrument package during the flight. The data obtained from the sensor suspended 130 ft below the instrument package, termed the reel-down sensor, is shown in curve 5 of Fig. 2.

The initial impression that one gains from inspection of the data shown in Fig. 2 is that the environment of STRATCOM VI-A is exceedingly wet. It is therefore important to note initially that the final data obtained for the reel-down sensor just prior to sunrise on the second day of the experiment does not indicate a wet environment. These data, which show a frost point of -104°C, are consistent with the model of the unperturbed stratosphere currently accepted. The water vapor concentration at the float altitude corresponds to an ambient concentration of approximately 0.8 ppm_w. Although this concentration is slightly lower than the generally accepted 2-3 ppm, it is not unreasonably so and is consistent with other measurements made at this approximate altitude. The fact that the final data obtained by the reel-down sensor were not approached asymptotically, but are consistent with expectation for the unperturbed stratosphere, tends to validate the preceding data obtained with the same sensor. In addition, these observations make the data obtained with the other two sensors of the same type more credible.

Returning therefore to the beginning of the flight, let us first examine the data obtained for the sensor present in the inlet to the ozone sonde as shown in curve 3 of Fig. 2. Starting from an extremely wet value at 1100 GMT, the sensor indicates a rapid decrease from approximately -27°C frost point to about -40°C frost point. The general course of the subsequent data obtained during the entire duration of the balloon trajectory can be represented approximately as a very slow decrease from about -40°C to about -45°C frost point. The slight oscillations in the steady decrease as observed during the major portion of the flight do not appear to be correlatable with balloon ascent or descent motions. The data obtained do suggest that the air sampled by the ozone instrument was exceedingly wet, the indicated concentration corresponding to approximately 100,000 ppm_w or about 10% water or more. Comparing this result with the data shown by curve 4 representing the gondola package ambient, at about 0800 GMT on the second day, one sees that the probable major source of this high water vapor concentration in the ozone inlet is the inlet tubing itself. The indicated concentration for curve 3 is approximately 30 times as great as the indicated concentration for the gondola ambient at the same time. This observation is supported by a detailed examination of the data obtained from the sensor in the ozone inlet tubing. Oscillations were observed for the data obtained from this sensor only during the period of time when the ozone instrument pump was operative. These oscillations are

not demonstrable on the time scale shown in Fig. 2, nor were such oscillations present for other sensors when the pump was operative. However, the oscillations were not detected when the pump was not operative. It is therefore suggested that turbulence caused in the air flow during operation of the pump resulted in significant desorption from the tubing walls and that this turbulence caused a real oscillation in the ambient being sampled by the ozone instrument.

Data obtained for the sensor monitoring the gondola environment was received only for that portion of the flight commencing at sunset on the first day (curve 4 in Fig. 2). During this portion of the flight the balloon was ascending from approximately 91,000 ft to about 118,000 ft at which altitude float was achieved. During the ascent the near package environment dried off considerably from its initially extremely wet condition. At sunset the near package environment had a water vapor concentration approximately 5% of that at the ozone instrument inlet, whereas upon achievement of float altitude the water vapor concentration in the near package environment had decreased to approximately 3% of the water vapor concentration present in the ozone inlet.

During the interval from about 0915 to 1050 GMT, no data during the float was received. Upon resumption of data reception at 1050 GMT, the apparent water vapor concentration in the gondola environment had dropped considerably, i.e., by a factor of about 4. This decrease in water vapor concentration was coincident with the achievement of float altitude and the persistent absence of the sun's radiation. Following sunrise at 1240 GMT, the balloon altitude increased rapidly. However, the gondola environment did not change measurably in water vapor concentration until about 1350 GMT at which time the water vapor concentration in the vicinity of the gondola started to increase. This behavior suggests that the major portion of the water vapor environment is contributed by desorption of water vapor from the balloon itself. If desorption from the packaging and instrumentation carried aboard the gondola were the major source of water vapor, then an increase should have been observed upon the incidence of sunrise or shortly thereafter, whereas the actual observation is that the onset of an increase in water vapor concentration is not observed until approximately 1 hour after sunrise. Attribution of the balloon skin as being the major source of water vapor contamination is consistent with the observations made during the STRATCOM V experiment as well as being consistent with the very wet conditions measured at sunset when data for the gondola environment was first received. Presumable outgassing of water vapor from the balloon skin, as well as some outgassing from the gondola package, resulted in the very high concentration initially measured in curve 4. This outgassing was induced by constant irradiation by the sun during the preceding day.

It is to be noted that the data shown in curve 4 for conditions when the heater was operative at about 1200 GMT on the second day do not differ from the subsequent data that was obtained when the heater was inoperative. It is therefore apparent that the sensor shows a negligible dependence upon temperature over the range from approximately +25° to -32°C.

The behavior shown in curve 5 of Fig. 2 which represents the data obtained from the reel-down sensor, positioned approximately 130 ft below the gondola, is the most puzzling and difficult to interpret. When data was initially obtained shortly before sunrise of the first day, the balloon was at float. Presumably the water vapor concentration in the immediate environment of the sensor was rapidly decreasing. This is shown by the data initially recorded. This decrease continued until reasonably dry conditions were recorded at approximately 1350 GMT. At this time power was no longer provided to the reel-down sensor until 1520 GMT. At that time a comparatively dry, but not truly ambient condition, was measured.

During most of the remainder of the daylight float on the first day, as well as a substantial portion of the initial descent, the reel-down sensor provided data, but under unheated conditions. These data were not consistent with the data for the same sensor when operating at +25°C. It was therefore concluded that, for this sensor, the output was more dependent upon ambient temperature than it had been for the sensor depicted in curve 4 of Fig. 2. As a result, data from the reel-down sensor when it was not at +25°C are omitted from curve 5 in Fig. 2.

When power was once again applied at about 2230 GMT, the frost point reading was considerably wetter than it had been earlier despite the fact that the balloon was descending at this time. It was expected that the sensor would have been sampling free ambient air. Nevertheless, the environment 130 ft below the gondola continued to get even wetter until the balloon reached approximately 100,000 ft in altitude. At that time the balloon descent rate increased significantly. Coincident with the increase in the balloon descent rate, the frost point at the reel-down sensor position decreased again until a comparatively dry condition was achieved at about 0200 GMT.

The most puzzling part of the data obtained and shown in curve 5 is the apparent increase in the frost point recorded by the reel-down sensor during the descent on the first day in daylight hours. The sensor had been lowered to 130 ft below the gondola with the expectation that ambient stratospheric air would be sampled during some portions of the balloon flight. Despite these expectations, it is apparent that extremely wet conditions were recorded by this sensor under almost all balloon dynamic conditions. It is to be noted that the balloon descent rate from about 125,000 ft down to 100,000 ft is extremely slow, averaging approximately 70 ft/min. It appears that, accompanying this slow descent rate, the envelope of water vapor generated by the desorption from the balloon skin in daylight hours is sufficiently large as to significantly affect the reel-down sensor even at the distance that it was located from both the balloon and the gondola package. This interpretation is supported by noting that, when the balloon descent rate increased at approximately 0100 GMT on the second day to a descent rate of 200 ft/min, then the frost point measured by the reel-down sensor decreased rapidly even during daylight hours.

AD-A049 030 ARMY ELECTRONICS COMMAND FORT MONMOUTH N J F/G 4/1
STRATOSPHERIC COMPOSITION BALLOON-BORNE EXPERIMENT 23-26 SEPTEM--ETC(U)
OCT 77 H N BALLARD, F P HUDSON

UNCLASSIFIED ECOM-5830 NL

2 OF 2
ADA049 030

END
DATE FILMED
2-78
DDC

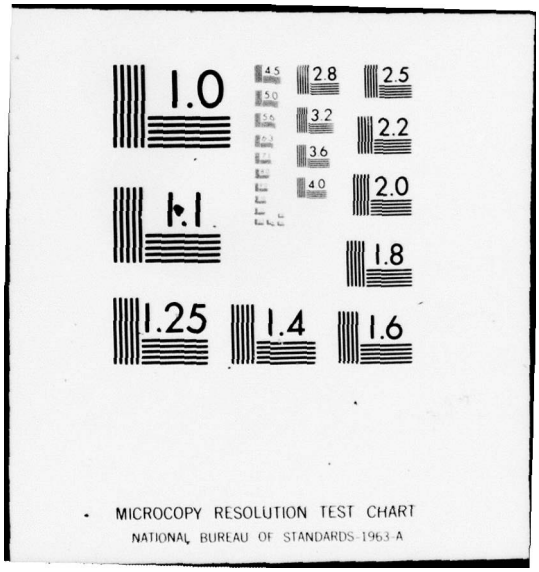
1.0
1.1
1.25
1.4
1.6
1.8
2.0
2.2
2.5
2.8
3.2
3.6
4.0
4.5
5.0
5.6
MICROCOPY RESOLUTION TEST CHART
NATIONAL BUREAU OF STANDARDS-1963-A

Following sunset, and commencing at about 0150 GMT, the balloon ascended in darkness with the reel-down sensor in the wake of the balloon during ascent. A slight but not very significant decrease in frost point was measured during this ascent. Presumably the balloon and/or the instrument package was outgassing and losing still more water during this second ascent to altitudes of about 120,000 ft. The slow decrease in frost point during nighttime hours of the second day, from about 0200-0900 GMT, is therefore considered to be associated with the wake of the balloon during ascent which provided a slowly decreasing water vapor environment for the reel-down sensor.

The final data points obtained by the reel-down sensor were noted at 1200 GMT of the second day, prior to sunrise. The balloon had then achieved a float altitude so that the reel-down sensor was no longer subjected to the water vapor present in the wake of the ascending balloon. Under these conditions a frost point of -104°C was recorded which, as noted earlier, corresponded to a 0.8 ppm_w water vapor concentration at the float altitude.

CORRELATION WITH OZONE DATA

The four ozone profiles as a function of altitude, generated during the initial ascent, during the descent and ascent in the middle portion of the flight, and during the final descent were examined to determine if any effects attributable to water vapor could be detected. Ozone profiles at altitudes of 28 km and higher were substantially identical during the first ascent and descent and, in the overlap region, also agreed well with the Mast ozone sonde results. However, the ozone concentration decreased rapidly by about 35% at the end of the first descent which was also coincident with sunset. The subsequent profile data (both second ascent and descent) was approximately parallel to, but 35% lower than, the first two profiles measured.

Water vapor data for the ozone inlet was obtained only for the first descent and second ascent. Average frost points measured during the first descent were approximately -41°C and about -44°C during the second ascent. The water vapor pressure during the second ascent was therefore about 30% lower than it had been for the first descent.

Any attempt to ascribe a causal relationship to the commonality in magnitude and direction of the changes in both ozone and water vapor concentrations would be highly speculative. This would be especially difficult because the first observation of an ozone concentration decrease was sharp and rapid, was coincident with sunset, and was not accompanied by any observed sharp decrease in water vapor concentration. Nevertheless, the possibility that a causal relationship exists, whether it be of chemical or experimental origin, would appear to deserve further investigation.

SUMMARY

Measurements of water vapor concentrations were made by three Al_2O_3 water vapor sensors positioned at various locations around an instrument package carried aloft during the STRATCOM VI-A experiment. Two of these sensors were located in the immediate vicinity of the gondola package, one being positioned in the inlet tube to the ozone sonde of the package, the second being positioned to monitor the near package environment. A third sensor was suspended at the end of a 130 ft cable hanging below the gondola package. All sensors could be maintained at +25°C to eliminate any possible effects of ambient temperature upon the frost point measurement. Data showed wet conditions in the vicinity of the gondola, corresponding to about 10% water vapor in the inlet to the ozone sonde and a factor of 20-30 lower in the environment of the gondola. The water vapor concentration at the latter location was still greatly in excess of the ambient. The sensor suspended 130 ft below the gondola also measured unexpectedly wet conditions during most of the flight which was attributed to a large envelope of water vapor outgassed principally from the balloon skin. However, at the conclusion of the flight, prior to descent, this envelope decreased in volume so that measurement of the ambient by the suspended sensor corresponded to a water vapor concentration of 0.8 ppm_w.

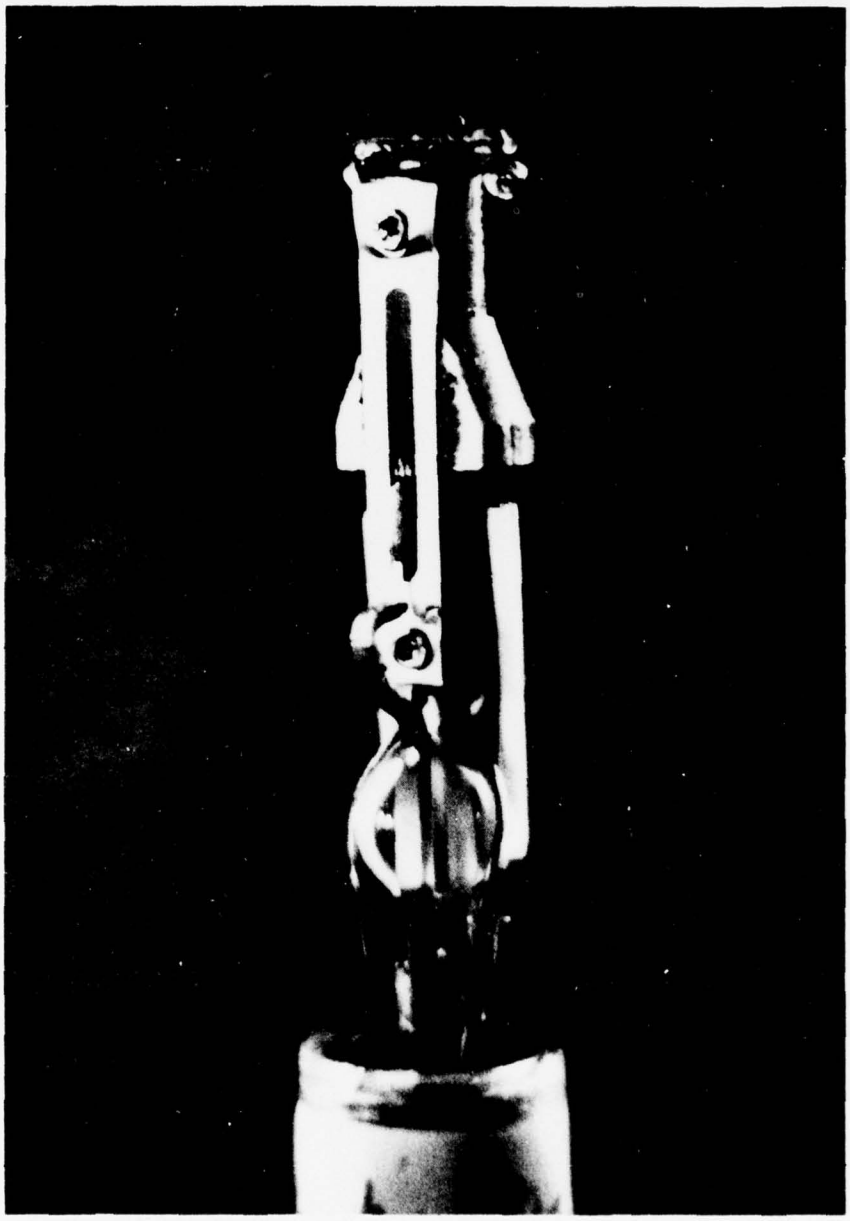

Figure 1. Photograph of Al_2O_3 humidity sensor mounted on constant temperature surface.

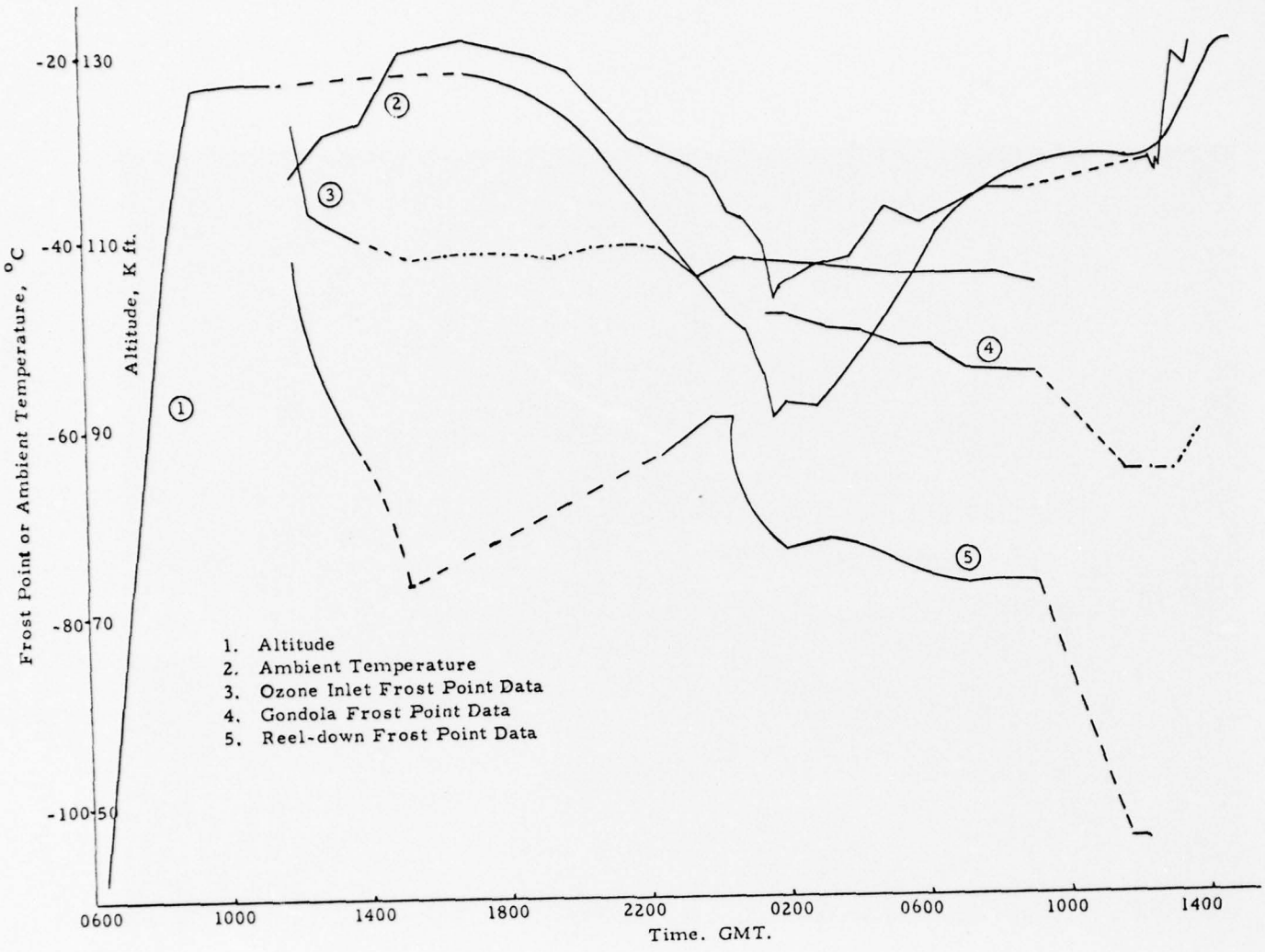

Figure 2. Variation of frost point at three locations during STRATCOM VI-A flight along with altitude and temperature.

REFERENCES

1. Goodman, P. "Water Vapor Measurements During a 48 km Balloon Flight," Final Report, Contract No. DAAD07-72-C-0306, August 1973.

CHAPTER 9

CRYOGENIC COLLECTION OF WHOLE AIR ABOARD STRATCOM VI-A

L. E. Heidt
W. H. Pollock
R. A. Lueb
National Center for Atmospheric Research, Boulder, CO*

ABSTRACT

Whole air samples were collected on a balloon launched from Holloman Air Force Base, NM. Three altitudes were sampled by using a low temperature air sampler. Values for N_2O, $CFCl_3$, CF_2Cl_2, CH_4, H_2, CO and CO_2 are reported. A brief description of the sampler and the analysis technique is given.

INTRODUCTION

Over the last several years considerable effort has been directed toward the analytical measurements of the trace gases in the stratosphere. Whole air samples have been collected and measured by Ehhalt et al. [1,2,3]. Other trace gas measurements have been made by Goldman et al. [4] and Murcray et al. [5]. Recent controversies over the destruction of the ozone layer by the chlorofluoromethanes and nitrous oxide make it necessary that additional measurements be made for these trace gases. Measurements of these gases have been made by Heidt et al. [6], Hester et al. [7], Krey et al. [8], and Schmeltekopf et al. [9]. This paper presents some of the first measurements of these trace gases above 33 km.

THE SAMPLING SYSTEM

Stainless steel cylinders, 29.5 cm long and 3.8 cm diameter, are connected to a common manifold through a bellows-sealed stainless steel high-vacuum valve which is driven by a 28 V dc motor (Fig. 1). Each motor drives its valve through a clutch which insures proper torque for leak-tight closure. When the collected samples are allowed to warm to room temperature, pressures up to 20 atm are attained. For safety, a stainless steel rupture disk is welded into each sample cylinder extension tube

*The National Center for Atmospheric Research is sponsored by the National Science Foundation.

(Fig. 2). Each cylinder has been pressure-tested to 170 atm without permanent deformation while the rupture disk burst pressure is set at 102 atm. The extension tube extends 10 cm beyond the mounting flange into the sample cylinder as an added precaution to prevent back diffusion of the noncondensables.

The stainless steel Dewar, which is commercially available, is filled with liquid Ne to 6 cm below the top flange before flight. This keeps the liquid Ne level below the extension tubes whose temperature thus remains sufficiently above liquid Ne temperature to prevent the plugging of the extension tubes by solid air. Ullage gas pressure in the Dewar is maintained at 0.5 atm above ambient by relief valves to prevent freezing of the cryogen at pressures below the triple point of neon during flight. The cold Ne boiloff gas is warmed to ambient temperatures in a black aluminum ballast tank and vented away from the gondola.

The flexible inlet line extends 6 m below the gondola to avoid possible contamination sources in the payload. The line is capped with a stainless steel rupture disk which is burst after reaching float altitude, exposing a clean inlet. This is accomplished by temporarily opening a motor-driven valve connecting the inlet line to a stainless steel cylinder containing high pressure dry N_2 gas (Fig. 1). This procedure is designed to prevent absorption of H_2O vapor in the baked-out inlet line before launch and during the ascent through the moist troposphere. A number of auxiliary measurements (pressure, temperature, flow rates, etc.) are performed during the flight and telemetered to the ground [Lueb et al., 10]. Telemetry and launch and recovery support were provided by Sandia Laboratories and AFGRL, respectively.

The sampling system, telemetry, batteries, and other experiments were housed in hermetic containers mounted on the gondola frame. The gondola was reeled down 200 m below the balloon to minimize contamination from the outgassing of the large balloon surface. The entire system was allowed to float at maximum altitude for approximately 6 hours to allow outgassing of gondola and balloon. After completion of the float, three samples were taken: the first at 38.7 km, the second at 36 km, and the third at 33 km.

SAMPLE ANALYSES

When the samples were returned to the laboratory, they were individually attached to a high-vacuum-pumping system with a built-in precision pressure gauge and volume-calibrated manifold. Since the volumes of the individual tubes had been calibrated prior to use, the total volume of each sample collected could be determined from the pressure measurement. At this time, two aliquots of the sample were withdrawn. One was used for the gas chromatographic analyses and one was stored for future use.

Molecular Hydrogen and Neon

The concentrations of molecular H_2 and Ne are measured with a gas chromatograph equipped with a radio frequency (RF) glow discharge detector. The H_2 and Ne are resolved from the other components in air in a 6 mm OD x 3 m long stainless steel "column" packed with Linde 5A molecular sieve. Details of this technique, together with sensitivity and calibration information, were published by Heidt and Ehhalt [11]. The natural concentration of Ne remains constant (18.18 ppm/v) over the altitude range of our collections. Our measurements of Ne, therefore, serve to prove that the sample was not fractionated during collection or handling.

Methane and Carbon Monoxide

The technique for measuring the concentrations of CH_4 and CO is similar to that used for H_2 and Ne. The detector used, however, is a hydrogen flame ionization detector (FID). Also, after separation of CO from CH_4 on a 5A molecular sieve column, the CO is converted to CH_4 by passing it over a nickel catalyst using the H_2 which feeds the detector flame for conversion. As the FID is extremely sensitive for hydrocarbons, the sensitivity for CO is greatly enhanced.

Chlorofluoromethanes

The chlorofluoromethanes, CCl_2F_2 and CCl_3F, are measured with a third gas chromatograph equipped with a porasil (silica beads) column and an electron capture detector (ECD). Since the ECD is extremely sensitive to chlorine, it can be used to detect concentrations of only a few parts per trillion (ppt). In addition, nitrous oxide (N_2O) is now being measured in each of the samples with the ECD.

Nitrous Oxide and Carbon Dioxide

The air sample remaining in each collection tube is then used for the determination of N_2O and CO_2. The collection tube is attached to a vacuum system and cooled to liquid nitrogen temperature, and the O_2 and N_2 is pumped away. The total volume of O_2 and N_2 is measured with a gas meter attached to the exhaust port of the vacuum pump. The liquid N_2 cryogen is then replaced with dry ice. This insures that the H_2O is quantitatively retained in the collection tube while the N_2O and CO_2 are transferred by a Toepler pump into a special volume-calibrated McLeod gauge in which the gas volume is determined. Thus, from the volume of this gas fraction (which is essentially CO_2) and the volume of stratospheric air measured with the gas meter, a CO_2 mixing ratio is calculated for each sample.

A second measurement of the N_2O mixing ratio is determined by mass spectrometric analysis. The N_2O/CO_2 ratio in the O_2 mixture is measured by comparing the ratio of the peak heights at mass 30 and 44 to those for a set of standard N_2O/CO_2 mixtures covering the concentration range of interest, including pure CO_2. The peak height ratio of mass 30 is directly proportional to the N_2O mixing ratio in the CO_2. Details of this technique have been published by Ehhalt et al. [2] and Moore [12].

RESULTS

TABLE 1

BALLOON FLIGHT STRATCOM VI-A

24 September 1975

Altitude (km)	CO (ppmb)	H_2 (ppmv)	CH_4 (ppmv)	N_2O (ppbv)	CO_2 (ppmv)	$CFCl_3$ (pptv)	CF_2Cl_2 (pptv)
38.7	88	0.45	0.52	20	324	5	9
36.0	135	0.55	1.03	73	320	6	20
33.0	44	0.44	0.91	95	323	11	44
*	±3	±0.02	±0.04	±5	±3	±1	±2

**Measurement errors*

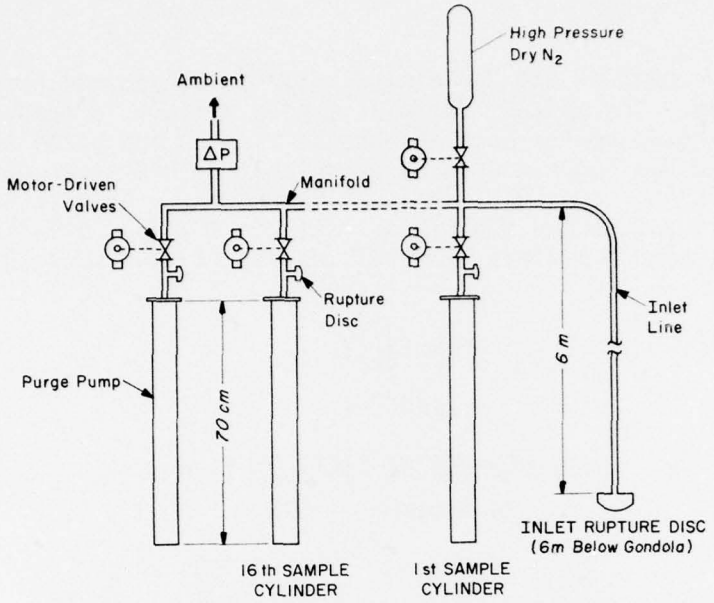

Figure 1. Schematic of the basic components of the balloon-borne low temperature sampler for the 16 tube system. However, the system flown consisted of only 4 tubes arranged in concentric circle with a common manifold. The sample tubes are submerged in liquid neon in a stainless steel Dewar. No provision was made for a purge pump.

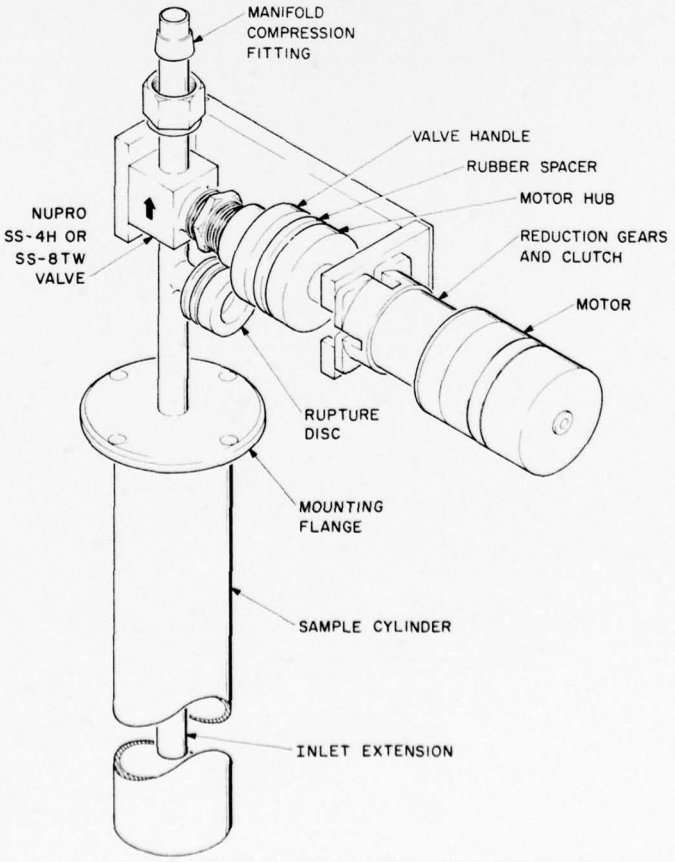

Figure 2. Sample cylinder with motor-driven valve. Note the rupture disk and inlet extension into the cylinder.

REFERENCES

1. Ehhalt, D. H., L. E. Heidt, R. A. Lueb, and N. Roper, 1974, "Vertical Profiles of CH_4, H_2, CO, N_2O and CO_2 in the Stratosphere," Prog. III CIAP Conference, Boston, MA: 153-160.

2. Ehhalt, D. H., L. E. Heidt, R. A. Lueb and E. A. Martel, 1975, "Concentrations of CH_4, CO, CO_2, H_2, H_2O, and N_2O in the Upper Stratosphere," J. Atmospheric Sci. 32: 163-169.

3. Ehhalt, D. H., L. E. Heidt, R. A. Lueb, and W. Pollock, 1975, "The Vertical Distribution of Trace Gases in the Stratosphere," Pageoph, 113: 389-402.

4. Goldman, A., D. G. Murcray, F. H. Murcray, W. J. Williams, J. N. Brooks, and C. M. Bradford, 1973, "Vertical Distribution of CO_2 in the Atmosphere," J. Geophys. Res. 78: 5273.

5. Murcray, D. G., A. Goldman, F. H. Murcray, W. J. Williams, J. N. Brooks, and D. B. Barker, 1973, "Vertical Distribution of Minor Atmospheric Constituents as Derived from Airborne Measurements of Atmospheric Emission and Absorption Infrared Spectra," Proc. II CIAP Conference, ed. A. J. Broderick. US Department of Transportation, DOT-TSC-OST-73-4.

6. Heidt, L. E., R. Lueb, W. Pollock, and D. H. Ehhalt, 1975, "Stratospheric Profiles of CCl_3F and CCl_2F_2," Geophy. Res. Lett. 2: 445-447.

7. Hester, N. E., E. R. Stephens, and O. C. Taylor, 1975, "Fluorocarbon Air Pollutants III," Environ. Sci. and Technol.: 875-876.

8. Krey, P. W., R. J. Lagomarsind, and J. J. Frey, 1976, "Stratospheric Concentrations of CCl_3F in 1974," J. Geophy. Res. 81: 1557-1560.

9. Schmeltekopf, A. L., P. O. Goldan, W. R. Henderson, W. J. Harrop, T. L. Thompson, F. C. Fehsenfeld, H. I. Schiff, P. J. Crutzen, I. S. A. Isaksen, and E. E. Fergusen, 1975, "Measurements of Stratospheric CCl_3F, CCl_2F_2, and N_2O," Geophy. Res. Lett. 2: 393-396.

10. Leub, R. A., D. H. Ehhalt, and L. E. Heidt, 1975, "Balloon-Borne Low Temperature Air Sampler," Rev. Sci. Instr. 46: 702-705.

11. Heidt, L. E., D. H. Ehhalt, 1972, "Gas Chromatographic Measurement of Hydrogen, Methane, and Neon in the Air," J. Chromatogr. 69: 103-113.

12. Moore, H., 1974, "Isotopic Measurement of Atmospheric Nitrogen Compounds," Tellus, XXVI: 169-174.

CHAPTER 10

ELECTRICAL CONDUCTIVITY MEASUREMENTS IN THE MIDDLE STRATOSPHERE

J. D. Mitchell
Electrical Engineering Department
The University of Texas at El Paso
El Paso, TX 79968

C. L. Croskey and L. C. Hale
Ionosphere Research Laboratory
The Pennsylvania State University
University Park, PA 16802

ABSTRACT

A blunt probe for measuring polar electrical conductivity was flown on the STRATCOM VI balloon experiment launched from Holloman Air Force Base (HAFB), NM, on 23 September 1975. Electrical conductivity data were obtained during both the ascent and descent phases of the flight, as well as while the balloon was at float altitude. Negative electrical conductivity measurements made during the flight were observed to be larger in value than corresponding positive electrical conductivity data, thus indicating that the negative ions were comparatively more mobile. This was particularly noticeable during the ascent and float periods of the flight. The positive electrical conductivity measurements at float altitude (approximately 39 km) were typically in the range of $2\text{-}3 \times 10^{-13}$ mho/cm, which are consistent with previously obtained rocket-launched parachute-borne blunt probe data for that altitude.

During designated periods of the flight, a krypton discharge lamp (1236Å) was operated in conjunction with the blunt probe experiment in a configuration such that the probe could measure the lamp's ionization effects on the stratosphere. Enhancements in positive electrical conductivity were observed during the time intervals when the lamp was operating, with the increases in negative electrical conductivity being even larger.

After the cutdown of the scientific package, the electrical conductivity measurements were observed to decrease in value as the probe descended, with a value of approximately 2×10^{-14} mho/cm measured at the tropopause. The altitude dependence for electrical conductivity during the descent phase of the flight is in good agreement with representative data obtained from previously flown parachute-borne blunt probes.

INTRODUCTION

A blunt probe experiment for measuring electrical conductivity was conducted on the STRATCOM VI balloon flight launched from HAFB, NM. The blunt probe [1], an instrument more commonly employed with rocket systems, has been found diagnostically useful for studying electrical conductivity and its variations in the stratosphere. On this particular flight, the instrument was extended horizontally on an arm approximately 1 m from the rest of the scientific package. The probe's collector was directed downward so that it could be shielded from the sun, thus avoiding possible photoemission from its surface. Mounted beside the blunt probe was a krypton discharge ionization lamp (1236Å) which was commanded on and off from the ground. Thus, when the lamp was on, the blunt probe could be used to study the lamp's ionization effects on the atmosphere.

DATA

The electrical conductivity measurements for the STRATCOM VI balloon experiment are shown in Fig. 1. The lower two curves on the graph represent time-averaged values for electrical conductivity measured by the blunt probe when the krypton discharge lamp was off. The upper curve shows the balloon's altitude as a function of time.

The balloon was launched at approximately 2300 MST on 23 September 1975. The first conductivity measurements were obtained at 2345 MST ($Z \tilde{\approx} 11$ km), at which time the value for electrical conductivity was approximately 0.8×10^{-14} mho/cm. The negative electrical conductivity values for the balloon flight were generally larger than the corresponding positive electrical conductivity measurements, thus suggesting that the negative ions were comparatively more mobile than the positive ions. This was particularly evident during the ascent and float phases of the flight where the negative-to-positive electrical conductivity ratio was typically a factor of two.

The positive electrical conductivity values while the balloon was at float altitude ($Z \tilde{\approx} 39$ km) showed less variability than the negative electrical conductivity values and were typically in the range of $2\text{-}3 \times 10^{-13}$ mho/cm. These positive conductivity values are representative of daytime rocket-launched, parachute-borne blunt probe data (Fig. 2). Included in Fig. 2 are the range of float altitude values for positive electrical conductivity from three STRATCOM balloon experiments launched at HAFB as compared to parachute-borne blunt probe data obtained at White Sands Missile Range (WSMR), NM, on 22 May 1974.

As mentioned previously, a krypton discharge ionization lamp was cycled on and off during designated periods of the flight. An enhancement in positive electrical conductivity of typically a factor of two to three was observed when the lamp was on. The corresponding increase in negative electrical conductivity was considerably larger. These conductivity

enhancements are associated with either an increase in charge number density or ion mobility, or possibly both. The larger negative electrical conductivity values when the lamp was on suggest that possibly some free electrons were created by the lamp.

The balloon first began to descend at approximately 1000 MST on 24 September. During the descent, the electrical conductivity measurements decreased in value, with the decrease for negative electrical conductivity being significantly more noticeable. From approximately 1500 to 1900 MST while the balloon was still slowly descending, the values for the negative-to-positive electrical conductivity ratio ranged from 1.3 to 1.5, which are in general agreement with the negative-to-positive ion mobility ratio for light ions. After 2000 MST, the balloon began to ascend and, again, the curves for negative and positive electrical conductivity started to increase and diverge. This divergence continued while the balloon ascended until the scientific package was cut down at approximately 0900 MST on 25 September.

DISCUSSION

Blunt probe measurements obtained on balloon platforms are particularly useful for studying variations in electrical conductivity. In particular, sunrise variations, possible variations associated with vertical movement of the balloon package, and the altitude dependence of electrical conductivity will now be considered.

Positive ion conductivity variations during the early morning period have been observed on subsonic Gerdien condenser and blunt probe rocket experiments conducted at WSMR [2]. In Fig. 3, appreciable enhancements in positive electrical conductivity are seen above 30 km for a change in solar zenith angle from 90° to 53°. In particular, positive conductivity at 39 km increases during this time period by approximately a factor of six. Enhancements in positive electrical conductivity are also noticed during the sunrise period (approximately 0600 MST) for the balloon experiment, although they are not as large as for the rocket data. These conductivity enhancements during the sunrise period are thought to be primarily associated with an increase in positive ion mobility, possibly resulting from the photodissociation of larger positive ions into smaller, more mobile ions.

A rather unique feature of the STRATCOM VI electrical conductivity data is the divergence between the negative and positive electrical conductivity values during the ascent and float phases of the flight. The larger negative electrical conductivity values measured during these periods possibly result from the collection of some high mobility, negatively charged particles associated with the balloon package. The negative conductivity values come into better agreement with the rocket-launched parachute-borne blunt probe data during the descent phases of the flight where the airflow is directed against the downward oriented blunt probe.

The altitude dependence for electrical conductivity is probably best demonstrated by the data obtained after cutdown when the scientific balloon package is descending on a parachute (Fig. 4). Electrical conductivity data after cutdown were obtained from 37 km down to 17 km, with a value of approximately 2×10^{-14} mho/cm measured at the tropopause. No distinguishable differences were observed between the values for negative and positive electrical conductivity. The altitude dependence for the data in this region is inversely proportional to that for neutral number density, which is consistent with what has been previously observed with parachute-borne blunt probes [3]. General agreement is observed between the balloon electrical conductivity data and the parachute-borne blunt probe conductivity profile obtained at WSMR on 22 May 1974. There is also good agreement below 30 km between the balloon conductivity data (Fig. 4) and the Gerdien condenser positive ion conductivity data (15 July and 26 September 1975) in Fig. 3. The differences above 30 km are presumably due to differences in solar zenith angle as was discussed earlier.

CONCLUSIONS

A blunt probe experiment flown on the STRATCOM VI balloon experiment measured positive and negative electrical conductivities during both the ascent and descent phases of the flight, as well as while the balloon was at float altitude. Positive electrical conductivity data measured at float altitude were typically in the range of $2\text{-}3 \times 10^{-13}$ mho/cm, which are consistent with parachute-borne blunt probe data. Negative electrical conductivity measurements made during the flight were observed to be larger than corresponding positive electrical conductivity values, thus indicating that the negative ions were comparatively more mobile.

Enhancements in electrical conductivity were observed when a krypton discharge ionization lamp was operating, with the increases in negative electrical conductivity being larger than the corresponding enhancements in positive electrical conductivity.

After cutdown when the scientific package was descending on a parachute, the electrical conductivity measurements were observed to decrease with a value of approximately 2×10^{-14} mho/cm measured at the tropopause. The altitude dependence for electrical conductivity during this descent was in good agreement with representative data obtained from rocket-launched parachute-borne blunt probe experiments.

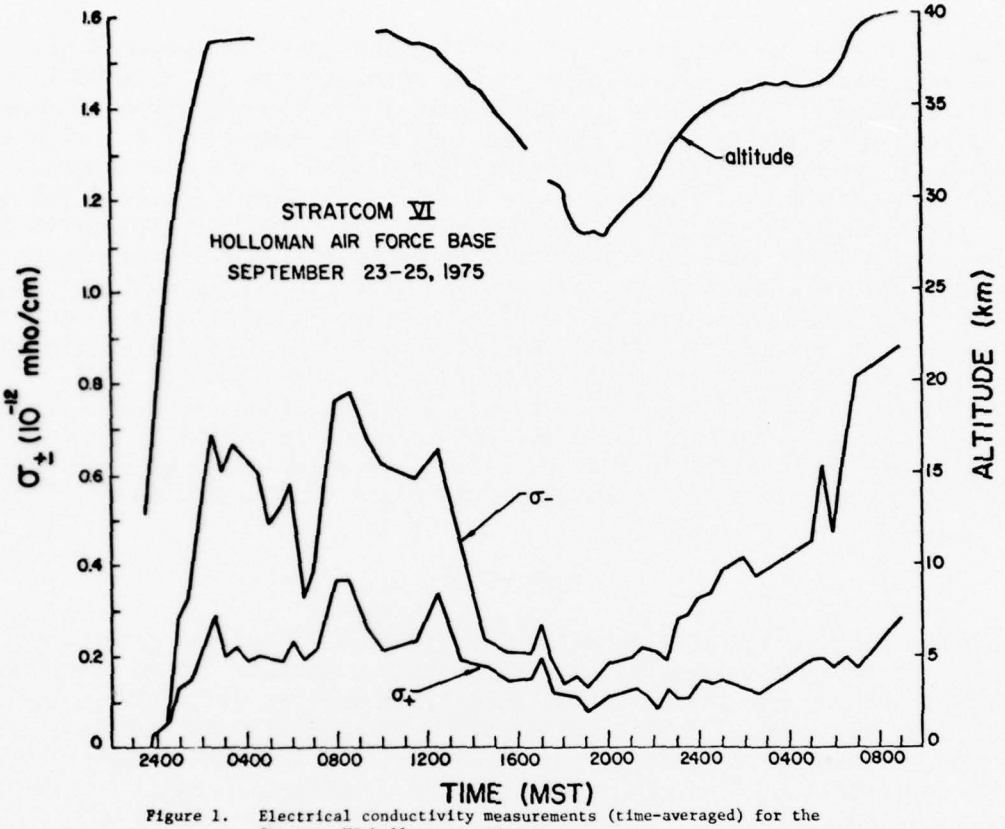

Figure 1. Electrical conductivity measurements (time-averaged) for the Stratcom VI balloon experiment.

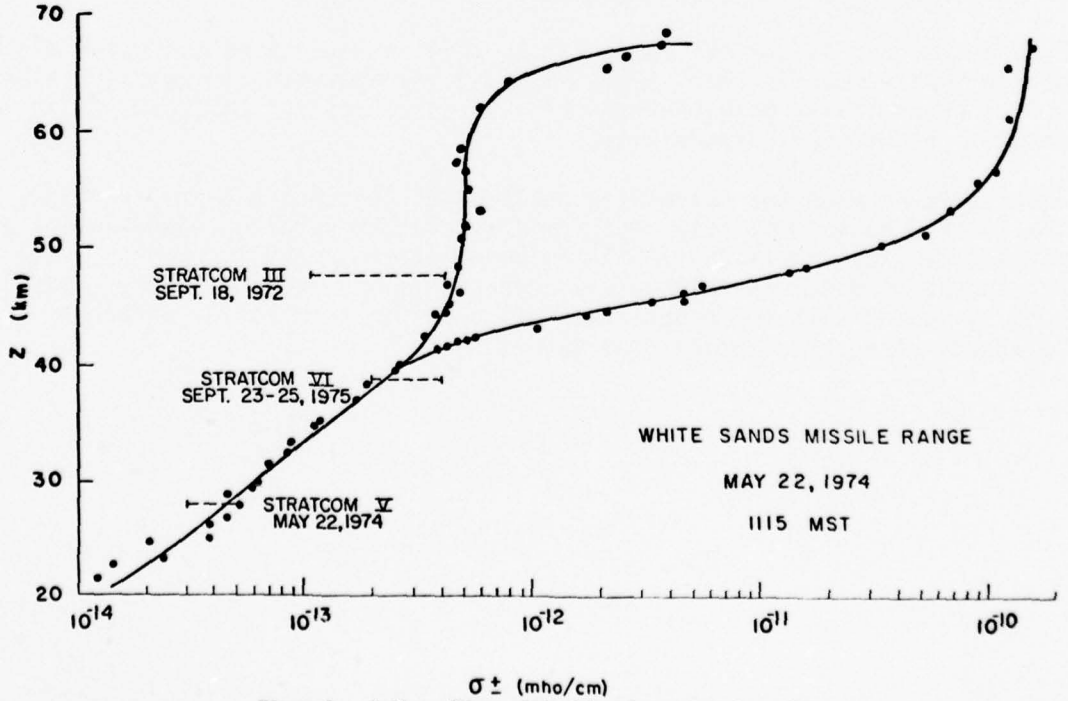

Figure 2. Balloon (float altitude) and parachute borne blunt probe electrical conductivity measurements.

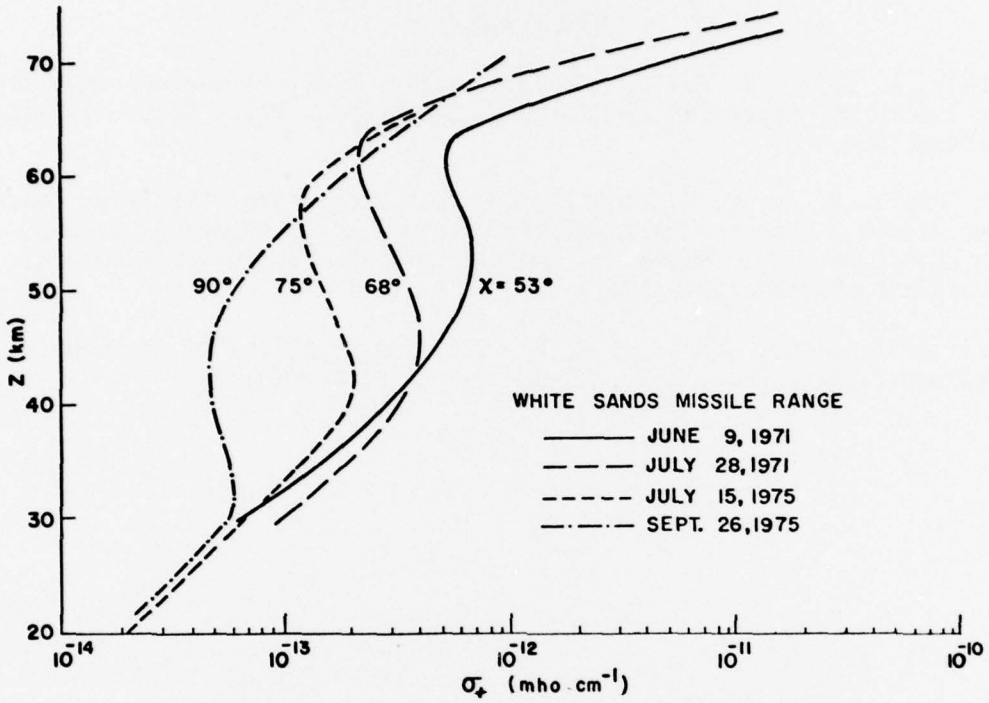

Figure 3. Parachute borne Gerdien condenser and blunt probe positive ion conductivity profiles during the early morning period.

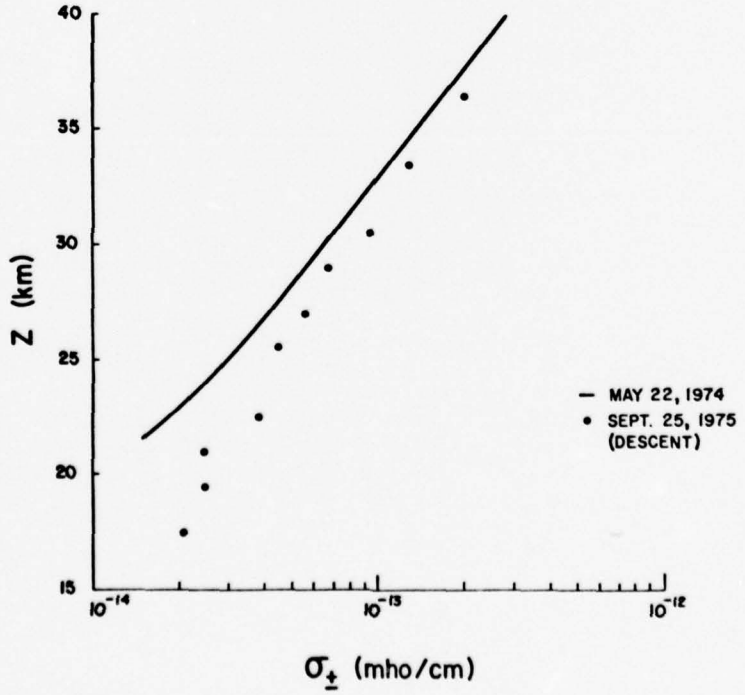

Figure 4. Electrical conductivity data for the Stratcom VI balloon experiment after cut down.

REFERENCES

1. Hale, L. C., D. P. Hoult, and D. C. Baker, 1968, "A Summary of Blunt Probe Theory and Experimental Results," Space Res., VIII, North-Holland, Amsterdam: 320.

2. Mitchell, J. D., R. S. Sagar, and R. O. Olsen, 1976, "Positive Ions in the Middle Atmosphere During Sunrise Conditions," Presented at the XIXth COSPAR Meeting, Session on Dynamics and Stratospheric-Ionospheric Interactions, Philadelphia, PA.

3. Mitchell, J. D., and L. C. Hale, 1973, "Observations of the Lowest Ionosphere," Space Res., XIII, Akademie-Verlag, Berlin: 471.

CHAPTER 11

MEASUREMENTS OF STRATOSPHERIC FLUOROCARBON DISTRIBUTIONS USING INFRARED TECHNIQUES (STRATCOM VI-B)

Walter J. Williams, John J. Kosters,
Aaron Goldman, and David G. Murcray
Department of Physics and Astronomy
University of Denver
Denver, CO

ACKNOWLEDGMENTS

The authors wish to acknowledge the assistance of John Van Allen in the reduction of the data and Carolyn Bauer in the preparation of the figures. Acknowledgment is made to the National Center for Atmospheric Research, which is sponsored by the National Science Foundation, for computer time used in this research.

This research was supported in part by the National Science Foundation and in part by the Manufacturing Chemists Association.

ABSTRACT

Absorption bands of CF_2Cl_2, $CFCl_3$, and CCl_4 have been observed on infrared sunset solar spectra in the 800-1000 cm^{-1} region from 30 km altitude during a balloon flight made in September 1975. The infrared absorption bands were used to derive the distribution of these constituents in the upper troposphere and lower stratosphere. The results are compared with 1968 data and with current results of other authors.

INTRODUCTION

The controversy concerning the possible depletion of the ozone layer by the fluorocarbons has resulted in an increased interest in the measurement of these molecules in the lower stratosphere. Several measurements have been reported to date. (See the recent bibliography in Goldman [1].) In all of these cases the measurements have been made by collecting samples at various altitudes in the stratosphere or by in situ measurement techniques. Since many fluorocarbon molecules have strong infrared absorption bands, the possibility of using infrared spectroscopic techniques exists. These techniques have the advantage of being suitable for remote sensing of the constituents.

Examination of solar spectra obtained at sunset from 30 km during a balloon flight performed in 1968 showed absorption features in the 800 cm^{-1} - 1000 cm^{-1} region tentatively assigned to CF_2Cl_2 and $CFCl_3$ [2]. Solar spectra covering this spectral region were obtained at large solar zenith angles from 30 km during a balloon flight performed 26 September 1975 from Holloman AFB, NM. These spectra confirmed the earlier identification of the absorptions and demonstrated the possibility of using infrared spectroscopic techniques for the measurement of these molecules in the stratosphere.

INSTRUMENTATION

The instrumentation used to obtain the data consists of a biaxial pointing control for maintaining the solar radiation on the spectrometer entrance slit, a 1-1/4 m grating spectrometer system, a digital magnetic tape recording system for on-board recording of the data generated by the instrumentation, an FM/FM telemetry system as a backup data handling system, various battery packs for supplying the power required to run the units, and a gondola system for assembling the various units and protecting them when they are returned to the ground by parachute.

The various units, with the exception of the grating spectrometer, have been described in earlier articles [3]. The spectrometer system is a new unit which was completed just before the flight of 26 September 1975. The unit is a 1-1/4 m Czerny-Turner system equipped with a 20 by 20 cm Bausch and Lomb grating blazed at 16μm. The spacing of all optical components is controlled by invar rods to keep the unit in optical alignment over the temperature range encountered during the balloon flight. To compensate for some of the changes associated with different expansion coefficients of the glass optics and the invar, small aluminum spacers are used with the longer invar rods. This combination has resulted in an instrument that maintains alignment over a wide temperature range.

The optical system incorporates a beam splitter into the exit optics which brings the beams out to two Cu:Ge detectors. The proper choice of the beam splitter and filters over the detectors makes it possible to record two orders of the grating simultaneously. The radiation passing through the spectrometer system is double passed and interrupted by a tuning fork chopper after the first pass. The ac signals from the detectors are amplified and synchronously rectified.

FLIGHT DETAILS

The sensitivity of this technique for measuring minor constituents is greatly enhanced by making the measurements at large solar zenith angles (sunset or sunrise). Thus for this flight, primary emphasis was placed on obtaining data during the sunset. Accordingly, the launch was accomplished at 1548 MDT. The balloon ascended at an average ascent rate of 250 m/min reaching float altitude (29.8 km) at 1820 MDT. Balloon sunset occurred at 1930 MDT; however, the balloon remained at float until 2200 MDT when the flight was terminated. The equipment was recovered without incident and in good condition.

DATA REDUCTION

All systems worked very well and spectra were obtained from the ground through float and from float altitude through the sunset. For this flight the spectrometer was set to scan from 4.5μm to 6.5μm and from 10.0μm to 18.0μm. Because the fluorocarbons have strong absorption in the 10.0μm to 14.0μm region, primary emphasis has been placed on reducing the data in this region. Consequently, only data in this wavelength region are reported here.

Since the concentrations of the fluorocarbons in the stratosphere are in the parts per trillion range, the absorptions are only strong enough to be observed in the sunset spectra. The solar spectra obtained during sunset are shown in Fig. 1. The absorptions due to CF_2Cl_2, $CFCl_3$ and CCl_4 are indicated on the figure. Data taken at float altitude before sunset were used to determine the vacuum envelope and this envelope was used to reduce the data to percent transmission. These reduced data are given in Fig. 2. Also shown in this figure are laboratory spectra of small amounts of the various absorbers in the absorption cell to verify the identification of the absorption features.

ANALYSIS

CF_2Cl_2

Although this molecule has been the subject of several laboratory investigations, none of them were aimed at obtaining the data necessary for quantitative analysis of the observed solar spectra. In view of this a laboratory investigation to determine the band model parameters for the 920 cm^{-1} region was undertaken. The results of this investigation are in press [1]. Using these results, the authors estimated the amount of CF_2Cl_2 in the optical path for each spectrum. The air mass traversed by the solar radiation in reaching the spectrometer was determined for each record by using a computer program which includes refraction effects. The average mixing ratio of CF_2Cl_2 for each spectrum was then determined on the assumption of uniform mixing along the path. Because the mixing ratio decreases with altitude, this assumption slightly underestimates the mixing ratio that would be present at the minimum altitude along the path. Since the major portion of the optical path is traversed within 2 km of the minimum height, the mixing ratios can be taken as representative of those occurring at about a kilometer above the minimum height. The estimated mixing ratio versus altitude profile given in Fig. 3 is plotted on this basis. The values obtained from the 1968 spectra are included for comparison.

$CFCl_3$

The comments concerning the status of quantitative laboratory spectra for CF_2Cl_2 also apply to this molecule. The authors currently are performing a laboratory study of $CFCl_3$ similar to that for the CF_2Cl_2. This study has not been completed, but sufficient spectra have been obtained for preliminary analysis of the data obtained during this flight. These results and the 1968 results are also shown in Fig. 3. (Comments made concerning the path also apply for this molecule.)

CCl_4

The absorption due to this molecule is overlapped by absorptions due to O_3 and CO_2. Thus the major problem in determining the mixing ratio for the CCl_4 lies in separating absorptions due to the CCl_4 from those due to the O_3 and CO_2. In principle this separation is accomplished by using line-by-line theoretical calculations to match the CO_2 and O_3 absorptions outside of the overlap region and then using the calculated spectra for O_3 and CO_2 to remove their contributions to the overlap region of the spectra. Suitable laboratory data were not available for this molecule so laboratory data had to be run for this molecule as well. The preliminary results of this analysis are also given in Fig. 3.

DISCUSSION

The recent results of stratospheric measurements of CF_2Cl_2 and $CFCl_3$ published by other investigators are given in Table 1 along with results from this experiment. Examination of these data indicates that the data obtained during this flight fall within the range of values measured by other investigators using in situ techniques. In comparing results one must keep in mind the variability in concentration of these molecules with time, particularly the long-term increasing trend in concentration expected for CF_2Cl_2 and $CFCl_3$. This trend is evident in comparing data obtained in 1968 [3] with the present results. This comparison shows an increase in the stratospheric mixing ratio of these gases of $\sim$2.5 in the 7-year period.

The decrease with altitude of the $CFCl_3$ and CF_2Cl_2 mixing ratio shown in these data is in agreement with the theoretical prediction and with the other observations [4]. However, the CF_2Cl_2 falloff is not as well established from our data.

ACCURACY

The absolute accuracy achieved in the measurements of these molecules using this technique depends on two independent factors: (1) determination of the number of molecules of the gases of interest in the optical path traversed by the radiation, and (2) determination of the total number

of air molecules in the same optical path. The first depends on determining an appropriate relation between absorption and number of molecules (so-called "curve of growth") and the accuracy of the absorption measurement in the solar spectra due to the molecules of interest. The second depends mostly on the geometry of the path traversed by the radiation, which in turn is affected by the accuracy of biaxial pointing control.

The gases studied here are easy to handle in the laboratory so that the laboratory determination of the curve of growth can be obtained with the accuracy of the derived curve of growth parameters of the order of ±10%. It is easy to achieve accuracy in the calibration spectra because the laboratory measurements do not require diluting the gas down to the ppt range as required for calibrating the in situ techniques, but rather handling gas samples of the pure or nitrogen broadened gas at a few millimeters mercury of pressure. The determination of the amount of absorption in the solar spectra is a more difficult problem. The accuracy of such a determination depends on the particular molecule since a major uncertainty arises from the overlap of absorption due to the other atmospheric constituents. Thus the CF_2Cl_2 is weakly overlapped by HNO_3 and CO_2 and the $CFCl_3$ is relatively free of interference, although at a large solar zenith angle (upper tropospheric paths) water vapor contributes to the observed absorption. The CCl_4, on the other hand, is strongly overlapped by the O_3 and CO_2 absorptions, and auxiliary calculations are needed to remove the absorptions due to these constituents from the solar spectra. Thus the estimates of the overall accuracy of the determination of the amount of gas in the optical path varies for the various molecules, being $\sim$20% for $CFCl_3$ and CF_2Cl_2 and probably $\sim$30% for the CCl_4. The other source of error, the error of determining the number of molecules in the optical path traversed by the solar radiation, could also be on the order of 20%.

Extrapolating the present values to lower altitudes indicates that the tropospheric mixing ratio for $CFCl_3$ appears higher than the measurements made using in situ techniques (165 ppt compared with 100-140 ppt), while the measurement of CF_2Cl_2 appears lower (185 ppt compared with 200-250 ppt) [7]. Any systematic pointing error would cause both values to be in error in the same direction; therefore, the results appear to be in error due to the determination of the number of molecules in the path. On this basis the values for the $CFCl_3$ and CF_2Cl_2 are probably good to within ±20%. The present values for CCl_4 are accurate to within ±30%. Extrapolating these values to lower altitudes shows agreement with current values within the error limits.

CONCLUSION

This technique for remote sensing of these molecules appears to have given results in reasonably good agreement with the in situ measurements. By adding monitors to the biaxial pointing system, the pointing error can be reduced so that the major uncertainty will lie in the elimination of the effect of absorption due to other constituents. The sensitivity can be increased by increasing the signal to noise in the solar spectra and by increasing the spectral resolution.

TABLE 1

RECENTLY REPORTED OBSERVED FLUOROCARBON MIXING RATIOS
IN THE UPPER TROPOSPHERE AND STRATOSPHERE (ppt v)

Altitude (km)	Heidt et al.[5]		Schmeltekopf et al.[4]		Hester et al.[6]		This work	
	$CFCl_3$	CF_2Cl_2	$CFCl_3$	CF_2Cl_2	$CFCl_3$	CF_2Cl_2	$CFCl_3$	CF_2Cl_2
34	3	35						
31	9	48						
28.6	11							
26.2			<20	75				
24.5	18							
23	45	86					23	120
22.3			30	135				
19.5							49	160
18					57	110		
17.7			80	210				
16.9	95							
16							100	175
13	83	133						
12	94	78			75	140		
11							150	185
8							160	185
6					82	120		

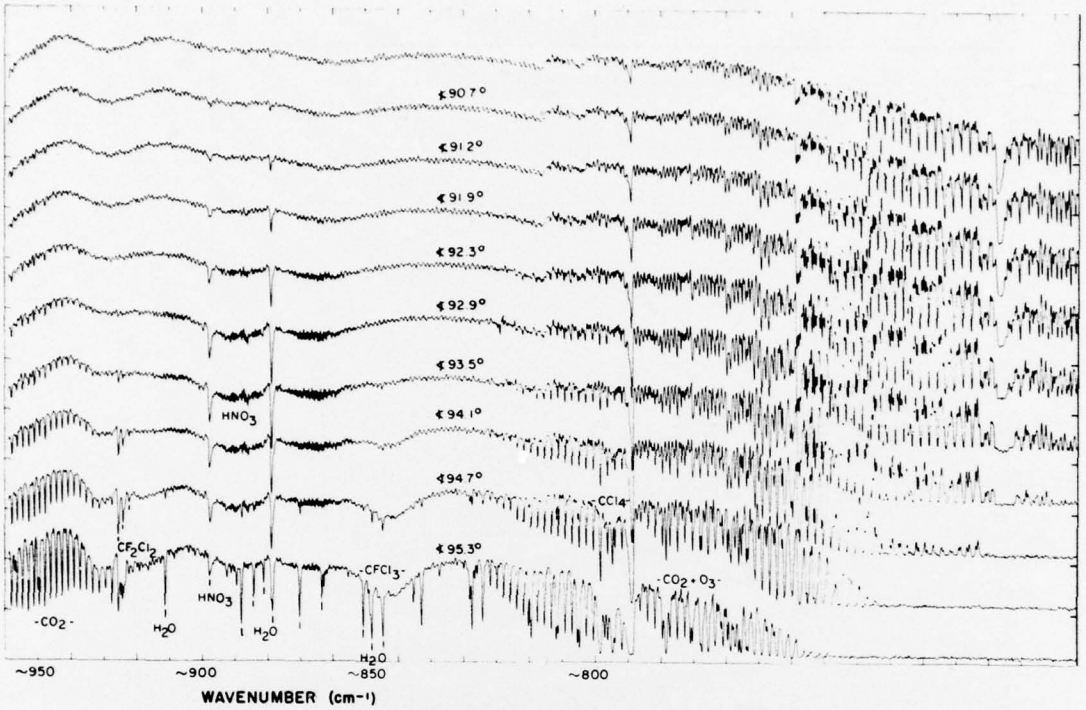

Figure 1. Solar spectra observed at an altitude of 30 km at various angles on September 26, 1975.

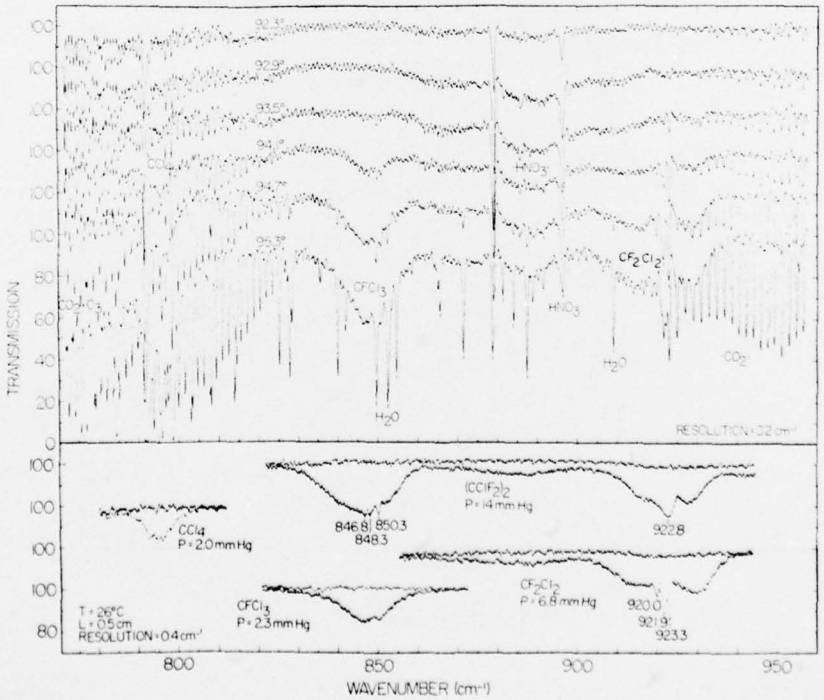

Figure 2. Upper: Atmospheric transmission observed at an altitude of 30 km at various zenith angles. Lower: Laboratory absorption spectra of selected halogenated hydrocarbons.

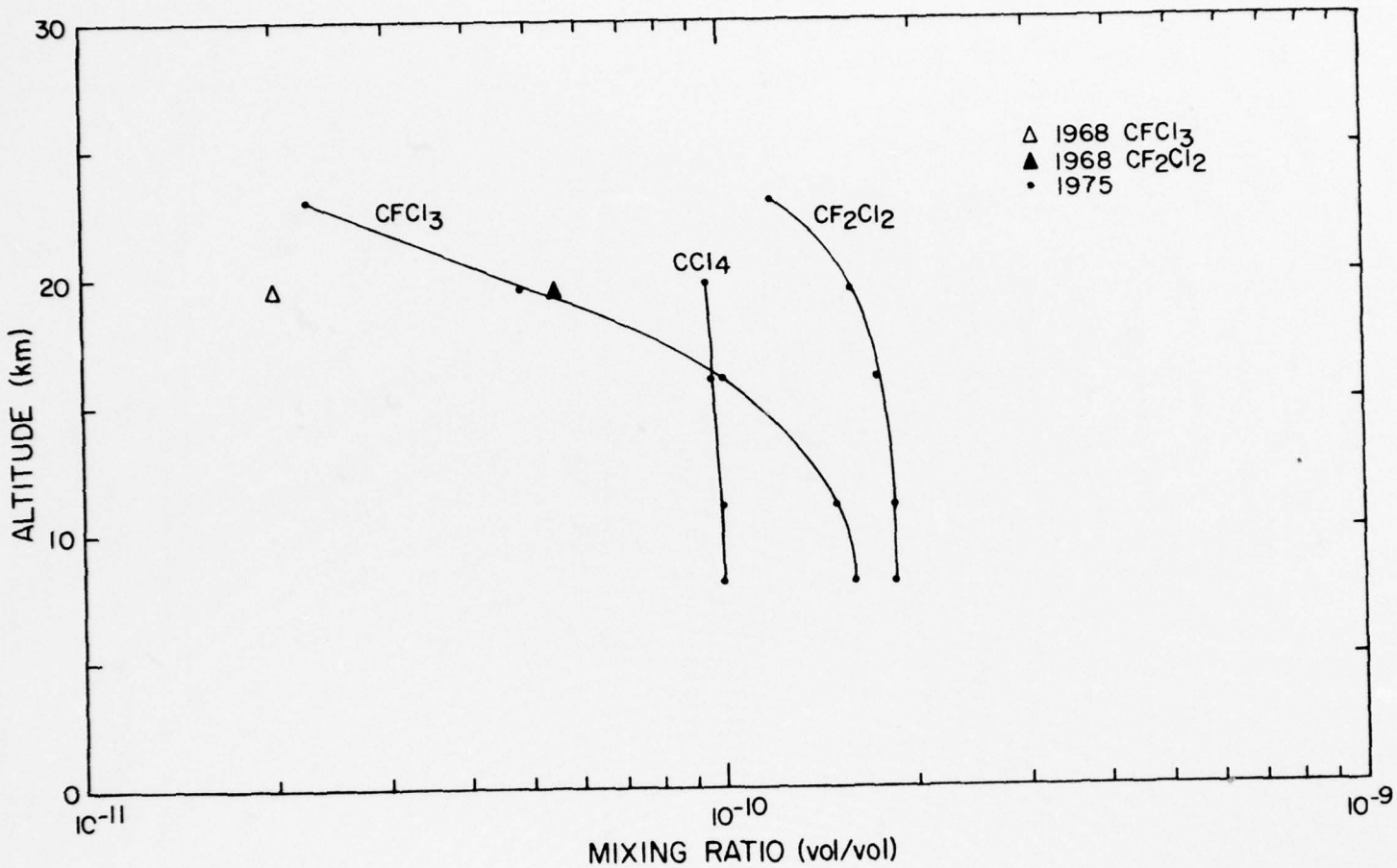

Figure 3. Mixing ratios of $CFCl_3$, CCl_4 and CF_2Cl_2 as a function of altitude.

REFERENCES

1. Goldman, A., F. S. Bonomo, and D. G. Murcray, 1976, "Statistical-Band-Model Analysis and Integrated Intensity for the 10.8μm band of CF_2Cl_2," submitted for publication to Geophys. Res. Lett.

2. Murcray, D. G., F. S. Bonomo, J. N. Brooks, A. Goldman, F. H. Murcray, and W. J. Williams, 1975, "Detection of Fluorocarbons in the Stratosphere," Geophys. Res. Lett. 2: 109-112.

3. Murcray, D. G., F. H. Murcray, W. J. Williams, T. G. Kyle, and A. Goldman, 1969, "Variation of the Infrared Solar Spectrum Between 700 cm^{-1} and 2240 cm^{-1} with Altitude," Appl. Opt. 8: 2519-2536.

4. Schmeltekopf, A. L., P. D. Goldan, W. R. Henderson, W. J. Harrop, T. L. Thompson, F. C. Fehsenfeld, H. I. Schiff, P. J. Crutzen, I. S. A. Isaksen, and E. E. Ferguson, 1975, "Measurements of Stratospheric $CFCl_3$, CF_2Cl_2, and N_2O," Geophys. Res. Lett. 2: 393-396.

5. Heidt, L. E., R. Lueb, W. Pollock, and D. H. Ehhalt, 1975, "Stratospheric Profiles of CCl_3F and CCl_2F_2," Geophys. Res. Lett. 2: 445-447.

6. Hester, N. E., E. R. Stephens, and O. C. Taylor, 1975, "Fluorocarbon Air Pollutants," Environ. Sci. and Technol. 9: 875-876.

7. Manufacturing Chemists Association, Technical Panel on Fluorocarbon Research, 1 March 1976, "The Effect of Fluorocarbons on the Concentration of Atmospheric Ozone," Figures C2 and C3.

DISTRIBUTION LIST

Director
US Army Ballistic Research Laboratory
ATTN: DRDAR-BLB, Dr. G. E. Keller
Aberdeen Proving Ground, MD 21005

Air Force Weapons Laboratory
ATTN: Technical Library (SUL)
Kirtland AFB, NM 87117

Commander
Headquarters, Fort Huachuca
ATTN: Tech Ref Div
Fort Huachuca, AZ 85613

6585 TG/WE
Holloman AFB, NM 88330

Commandant
US Army Field Artillery School
ATTN: Morris Swett Tech Library
Fort Sill, OK 73503

Commandant
USAFAS
ATTN: ATSF-CD-MT (Mr. Farmer)
Fort Sill, OK 73503

Director
US Army Engr Waterways Exper Sta
ATTN: Library Branch
Vicksburg, MS 39180

Commander
US Army Electronics Command
ATTN: DRSEL-CT-S (Dr. Swingle)
Fort Monmouth, NJ 07703
03

CPT Hugh Albers, Exec Sec
Interdept Committee on Atmos Sci
Fed Council for Sci & Tech
National Sci Foundation
Washington, DC 20550

Inge Dirmhirn, Professor
Utah State University, UMC 48
Logan, UT 84322

HQDA (DAEN-RDM/Dr. De Percin)
Forrestal Bldg
Washington, DC 20314

Commander
US Army Aviation Center
ATTN: ATZQ-D-MA
Fort Rucker, AL 36362

CO, USA Foreign Sci & Tech Center
ATTN: DRXST-ISI
220 7th Street, NE
Charlottesville, VA 22901

Director
USAE Waterways Experiment Station
ATTN: Library
PO Box 631
Vicksburg, MS 39180

US Army Research Office
ATTN: DRXRO-IP
PO Box 12211
Research Triangle Park, NC 27709

Mr. William A. Main
USDA Forest Service
1407 S. Harrison Road
East Lansing, MI 48823

Library-R-51-Tech Reports
Environmental Research Labs
NOAA
Boulder, CO 80302

Commander
US Army Dugway Proving Ground
ATTN: MT-S
Dugway, UT 84022

HQ, ESD/DRI/S-22
Hanscom AFB
MA 01731

Head, Atmospheric Rsch Section
National Science Foundation
1800 G. Street, NW
Washington, DC 20550

Office, Asst Sec Army (R&D)
ATTN: Dep for Science & Tech
HQ, Department of the Army
Washington, DC 20310

Commander
US Army Satellite Comm Agc
ATTN: DRCPM-SC-3
Fort Monmouth, NJ 07703

Sylvania Elec Sys Western Div
ATTN: Technical Reports Library
PO Box 205
Mountain View, CA 94040

William Peterson
Research Association
Utah State University, UNC 48
Logan, UT 84322

Defense Communications Agency
Technical Library Center
Code 205
Washington, DC 20305

Dr. A. D. Belmont
Research Division
PO Box 1249
Control Data Corp
Minneapolis, MN 55440

Commander
US Army Electronics Command
ATTN: DRSEL-WL-D1
Fort Monmouth, NJ 07703

Commander
ATTN: DRSEL-VL-D
Fort Monmouth, NJ 07703

Meteorologist in Charge
Kwajalein Missile Range
PO Box 67
APO
San Francisco, CA 96555

The Library of Congress
ATTN: Exchange & Gift Div
Washington, DC 20540
2

US Army Liaison Office
MIT-Lincoln Lab, Library A-082
PO Box 73
Lexington, MA 02173

Dir National Security Agency
ATTN: TDL (C513)
Fort George G. Meade, MD 20755

Director, Systems R&D Service
Federal Aviation Administration
ATTN: ARD-54
2100 Second Street, SW
Washington, DC 20590

Commander
US Army Missile Command
ATTN: DRSMI-RRA, Bldg 7770
Redstone Arsenal, AL 35809

Dir of Dev & Engr
Defense Systems Div
ATTN: SAREA-DE-DDR
H. Tannenbaum
Edgewood Arsenal, APG, MD 21010

Naval Surface Weapons Center
Technical Library & Information
Services Division
White Oak, Silver Spring, MD
20910

Dr. Frank D. Eaton
PO Box 3038
Universtiy Station
Laramie, Wyoming 82071

Rome Air Development Center
ATTN: Documents Library
TILD (Bette Smith)
Griffiss Air Force Base, NY 13441

National Weather Service
National Meteorological Center
World Weather Bldg - 5200 Auth Rd
ATTN: Mr. Quiroz
Washington, DC 20233

USAFETAC/CB (Stop 825)
Scott AFB
IL 62225

Director
Defense Nuclear Agency
ATTN: Tech Library
Washington, DC 20305

Director
Development Center MCDEC
ATTN: Firepower Division
Quantico, VA 22134

Environmental Protection Agency
Meteorology Laboratory
Research Triangle Park, NC
27711

Commander
US Army Electronics Command
ATTN: DRSEL-GG-TD
Fort Monmouth, NJ 07703

Commander
US Army Ballistic Rsch Labs
ATTN: DRXBR-IB
APG, MD 21005

Dir, US Naval Research Lab
Code 5530
Washington, DC 20375

Mil Assistant for
Environmental Sciences
DAD (E & LS), 3D129
The Pentagon
Washington, DC 20301

The Environmental Rsch
Institute of MI
ATTN: IRIA Library
PO Box 618
Ann Arbor, MI 48107

Armament Dev & Test Center
ADTC (DLOSL)
Eglin AFB, Florida 32542

Range Commanders Council
ATTN: Mr. Hixon
PMTC Code 3252
Pacific Missile Test Center
Point Mugu, CA 93042

Commander
Eustis Directorate
US Army Air Mobility R&D Lab
ATTN: Technical Library
Fort Eustis, VA 23604

Commander
Frankford Arsenal
ATTN: SARFA-FCD-O, Bldg 201-2
Bridge & Tarcony Sts
Philadelphia, PA 19137

Director, Naval Oceanography and
Meteorology
National Space Technology Laboratories
Bay St Louis, MS 39529

Commander
US Army Electronics Command
ATTN: DRSEL-CT-S
Fort Monmouth, NJ 07703

Commander
USA Cold Regions Test Center
ATTN: STECR-OP-PM
APO Seattle 98733

Redstone Scientific Information Center
ATTN: DRDMI-TBD
US Army Missile Res & Dev Command
Redstone Arsenal, AL 35809

Commander
AFWL/WE
Kirtland AFB, NM 87117

Naval Surface Weapons Center
Code DT-22 (Ms. Greeley)
Dahlgren, VA 22448

Commander
Naval Ocean Systems Center
ATTN: Research Library
San Diego, CA 92152

Commander
US Army INSCOM
ATTN: IARDA-OS
Arlington Hall Station
Arlington, VA 22212

Commandant
US Army Field Artillery School
ATTN: ATSF-CF-R
Fort Sill, OK 73503

Commander and Director
US Army Engineer Topographic Labs
ETL-GS-AC
Fort Belvoir, VA 22060

Technical Processes Br-D823
NOAA, Lib & Info Serv Div
6009 Executive Blvd
Rockville, MD 20852

Commander
US Army Missile Research
and Development Command
ATTN: DRDMI-CGA, B. W. Fowler
Redstone Arsenal, AL 35809

Commanding Officer
US Army Armament Rsch & Dev Com
ATTN: DRDAR-TSS #59
Dover, NJ 07801

Air Force Cambridge Rsch Labs
ATTN: LCB (A. S. Carten, Jr.)
Hanscom AFB
Bedford, MA 01731

National Center for Atmos Res
NCAR Library
PO Box 3000
Boulder, CO 80307

Air Force Geophysics Laboratory
ATTN: LYD
Hanscom AFB
Bedford, MA 01731

Chief, Atmospheric Sciences Division
Code ES-81
NASA
Marshall Space Flight Center, AL 35812

Department of the Air Force
OL-C, 5WW
Fort Monroe, VA 23651

Commander
US Army Missile Rsch & Dev Com
ATTN: DRDMI-TR
Redstone Arsenal, AL 35809

Meteorology Laboratory
AFGL/LY
Hanscom AFB, MA 01731

Director CFD
US Army Field Artillery School
ATTN: Met Division
Fort Sill, OK 73503

Naval Weapons Center (Code 3173)
ATTN: Dr. A. Shlanta
China Lake, CA 93555

Director
Atmospheric Physics & Chem Lab
Code R31, NOAA
Department of Commerce
Boulder, CO 80302

Department of the Air Force
5 WW/DN
Langley AFB, VA 23665

Commander
US Army Intelligence Center and School
ATTN: ATSI-CD-MD
Fort Huachuca, AZ 85613

Dr. John L. Walsh
Code 4109
Navy Research Lab
Washington, DC 20375

Director
US Army Armament Rsch & Dev Com
Chemical Systems Laboratory
ATTN: DRDAR-CLJ-I
Aberdeen Proving Ground, MD 21010

R. B. Girardo
Bureau of Reclamation
E&R Center, Code 1220
Denver Federal Center, Bldg 67
Denver, CO 80225

Commander
US Army Missile Command
ATTN: DRDMI-TEM
Redstone Arsenal, AL 35809

Commander
US Army Tropic Test Center
ATTN: STETC-MO (Tech Library)
APO New York 09827

Commanding Officer
Naval Research Laboratory
Code 2627
Washington, DC 20375

Defense Documentation Center
ATTN: DDC-TCA
Cameron Station (Bldg 5)
Alexandria, Virginia 22314
12

Commander
US Army Test and Evaluation Command
ATTN: Technical Library
White Sands Missile Range, NM 88002

US Army Nuclear Agency
ATTN: MONA-WE
Fort Belvoir, VA 22060

Commander
US Army Proving Ground
ATTN: Technical Library
Bldg 2100
Yuma, AZ 85364

Office, Asst Sec Army (R&D)
ATTN: Dep for Science & Tech
HQ, Department of the Army
Washington, DC 20310

ATMOSPHERIC SCIENCES RESEARCH PAPERS

1. Lindberg, J.D., "An Improvement to a Method for Measuring the Absorption Coefficient of Atmospheric Dust and other Strongly Absorbing Powders, " ECOM-5565, July 1975.
2. Avara, Elton, P., "Mesoscale Wind Shears Derived from Thermal Winds," ECOM-5566, July 1975.
3. Gomez, Richard B., and Joseph H. Pierluissi, "Incomplete Gamma Function Approximation for King's Strong-Line Transmittance Model," ECOM-5567, July 1975.
4. Blanco, A.J., and B.F. Engebos, "Ballistic Wind Weighting Functions for Tank Projectiles," ECOM-5568, August 1975.
5. Taylor, Fredrick J., Jack Smith, and Thomas H. Pries, "Crosswind Measurements through Pattern Recognition Techniques," ECOM-5569, July 1975.
6. Walters, D.L., "Crosswind Weighting Functions for Direct-Fire Projectiles," ECOM-5570, August 1975.
7. Duncan, Louis D., "An Improved Algorithm for the Iterated Minimal Information Solution for Remote Sounding of Temperature," ECOM-5571, August 1975.
8. Robbiani, Raymond L., "Tactical Field Demonstration of Mobile Weather Radar Set AN/TPS-41 at Fort Rucker, Alabama," ECOM-5572, August 1975.
9. Miers, B., G. Blackman, D. Langer, and N. Lorimier, "Analysis of SMS/GOES Film Data," ECOM-5573, September 1975.
10. Manquero, Carlos, Louis Duncan, and Rufus Bruce, "An Indication from Satellite Measurements of Atmospheric CO2 Variability," ECOM-5574, September 1975.
11. Petracca, Carmine, and James D. Lindberg, "Installation and Operation of an Atmospheric Particulate Collector," ECOM-5575, September 1975.
12. Avara, Elton P., and George Alexander, "Empirical Investigation of Three Iterative Methods for Inverting the Radiative Transfer Equation," ECOM-5576, October 1975.
13. Alexander, George D., "A Digital Data Acquisition Interface for the SMS Direct Readout Ground Station — Concept and Preliminary Design," ECOM-5577, October 1975.
14. Cantor, Israel, "Enhancement of Point Source Thermal Radiation Under Clouds in a Nonattenuating Medium," ECOM-5578, October 1975.
15. Norton, Colburn, and Glenn Hoidale, "The Diurnal Variation of Mixing Height by Month over White Sands Missile Range, N.M," ECOM-5579, November 1975.
16. Avara, Elton P., "On the Spectrum Analysis of Binary Data," ECOM-5580, November 1975.
17. Taylor, Fredrick J., Thomas H. Pries, and Chao-Huan Huang, "Optimal Wind Velocity Estimation," ECOM-5581, December 1975.
18. Avara, Elton P., "Some Effects of Autocorrelated and Cross-Correlated Noise on the Analysis of Variance, " ECOM-5582, December 1975.
19. Gillespie, Patti S., R.L. Armstrong, and Kenneth O. White, "The Spectral Characteristics and Atmospheric CO2 Absorption of the Ho^{+3}:YLF Laser at 2.05μm," ECOM-5583, December 1975.
20. Novlan, David J. "An Empirical Method of Forecasting Thunderstorms for the White Sands Missile Range," ECOM-5584, February 1976.
21. Avara, Elton P., "Randomization Effects in Hypothesis Testing with Autocorrelated Noise," ECOM-5585, February 1976.
22. Watkins, Wendell R., "Improvements in Long Path Absorption Cell Measurement," ECOM-5586, March 1976.
23. Thomas, Joe, George D. Alexander, and Marvin Dubbin, "SATTEL — An Army Dedicated Meteorological Telemetry System," ECOM-5587. March 1976.
24. Kennedy, Bruce W., and Delbert Bynum, "Army User Test Program for the RDT&E-XM-75 Meteorological Rocket," ECOM-5588, April 1976.

25. Barnett, Kenneth M., "A Description of the Artillery Meteorological Comparisons at White Sands Missle Range, October 1974 - December 1974 ('PASS' - Prototype Artillery [Meteorological] Subsystem)," ECOM-5589, April 1976.
26. Miller, Walter B., "Preliminary Analysis of Fall-of-Shot From Project 'PASS'," ECOM-5590, April 1976.
27. Avara, Elton P., "Error Analysis of Minimum Information and Smith's Direct Methods for Inverting the Radiative Transfer Equation," ECOM-5591, April 1976.
28. Yee, Young P., James D. Horn, and George Alexander, "Synoptic Thermal Wind Calculations from Radiosonde Observations Over the Southwestern United States," ECOM-5592, May 1976.
29. Duncan, Louis D., and Mary Ann Seagraves, "Applications of Empirical Corrections to NOAA-4 VTPR Observations," ECOM-5593, May 1976.
30. Miers, Bruce T., and Steve Weaver, "Applications of Meterological Satellite Data to Weather Sensitive Army Operations,"ECOM-5594, May 1976.
31. Sharenow, Moses, "Redesign and Improvement of Balloon ML-566," ECOM-5595, June, 1976.
32. Hansen, Frank V., "The Depth of the Surface Boundary Layer," ECOM-5596, June 1976.
33. Pinnick, R.G., and E.B. Stenmark, "Response Calculations for a Commercial Light-Scattering Aerosol Counter," ECOM-5597, July 1976.
34. Mason, J., and G.B. Hoidale, "Visibility as an Estimator of Infrared Transmittance," ECOM-5598, July 1976.
35. Bruce, Rufus E., Louis D. Duncan, and Joseph H. Pierluissi, "Experimental Study of the Relationship Between Radiosonde Temperatures and Radiometric-Area Temperatures," ECOM-5599, August 1976.
36. Duncan, Louis D., "Stratospheric Wind Shear Computed from Satellite Thermal Sounder Measurements," ECOM-5800, September 1976.
37. Taylor, F., P. Mohan, P. Joseph and T. Pries, "An All Digital Automated Wind Measurement System," ECOM-5801, September 1976.
38. Bruce, Charles, "Development of Spectrophones for CW and Pulsed Radiation Sources," ECOM-5802, September 1976.
39. Duncan, Louis D., and Mary Ann Seagraves,"Another Method for Estimating Clear Column Radiances," ECOM-5803, October 1976.
40. Blanco, Abel J., and Larry E. Taylor, "Artillery Meteorological Analysis of Project Pass," ECOM-5804, October 1976.
41. Miller, Walter, and Bernard Engebos," A Mathematical Structure for Refinement of Sound Ranging Estimates," ECOM-5805, November, 1976.
42. Gillespie, James B., and James D. Lindberg, "A Method to Obtain Diffuse Reflectance Measurements from 1.0 to 3.0 μm Using a Cary 171 Spectrophotometer," ECOM-5806, November 1976.
43. Rubio, Roberto, and Robert O. Olsen,"A Study of the Effects of Temperature Variations on Radio Wave Absorption,"ECOM-5807, November 1976.
44. Ballard, Harold N., "Temperature Measurements in the Stratosphere from Balloon-Borne Instrument Platforms, 1968-1975," ECOM-5808, December 1976.
45. Monahan, H.H., "An Approach to the Short-Range Prediction of Early Morning Radiation Fog," ECOM-5809, January 1977.
46. Engebos, Bernard Francis, "Introduction to Multiple State Multiple Action Decision Theory and Its Relation to Mixing Structures," ECOM-5810, January 1977.
47. Low, Richard D.H.,"Effects of Cloud Particles on Remote Sensing from Space in the 10-Micrometer Infrared Region," ECOM-5811, January 1977.
48. Bonner, Robert S., and R. Newton, "Application of the AN/GVS-5 Laser Rangefinder to Cloud Base Height Measurements," ECOM-5812, February 1977.

49. Rubio, Roberto, "Lidar Detection of Subvisible Reentry Vehicle Erosive Atmospheric Material," ECOM-5813, March 1977.
50. Low, Richard D.H., and J.D. Horn, "Mesoscale Determination of Cloud-Top Height: Problems and Solutions," ECOM-5814, March 1977.
51. Duncan, Louis D., and Mary Ann Seagraves,"Evaluation of the NOAA-4 VTPR Thermal Winds for Nuclear Fallout Predictions," ECOM-5815, March 1977.
52. Randhawa, Jagir S., M. Izquierdo, Carlos McDonald and Zvi Salpeter, "Stratospheric Ozone Density as Measured by a Chemiluminescent Sensor During the Stratcom VI-A Flight," ECOM-5816, April 1977.
53. Rubio, Roberto, and Mike Izquierdo, "Measurements of Net Atmospheric Irradiance in the 0.7- to 2.8-Micrometer Infrared Region," ECOM-5817, May 1977.
54. Ballard, Harold N., Jose M. Serna, and Frank P. Hudson Consultant for Chemical Kinetics, "Calculation of Selected Atmospheric Composition Parameters for the Mid-Latitude, September Stratosphere," ECOM-5818, May 1977.
55. Mitchell, J.D., R.S. Sagar, and R.O. Olsen, "Positive Ions in the Middle Atmosphere During Sunrise Conditions," ECOM-5819, May 1977.
56. White, Kenneth O., Wendell R. Watkins, Stuart A. Schleusener, and Ronald L. Johnson, "Solid-State Laser Wavelength Identification Using a Reference Absorber," ECOM-5820, June 1977.
57. Watkins, Wendell R., and Richard G. Dixon, "Automation of Long-Path Absorption Cell Measurements," ECOM-5821, June 1977.
58. Taylor, S.E., J.M. Davis, and J.B. Mason, "Analysis of Observed Soil Skin Moisture Effects on Reflectance," ECOM-5822, June 1977.
59. Duncan, Louis D. and Mary Ann Seagraves, "Fallout Predictions Computed from Satellite Derived Winds," ECOM-5823, June 1977.
60. Snider, D.E., D.G. Murcray, F.H. Murcray, and W.J. Williams, "Investigation of High-Altitude Enhanced Infrared Backround Emissions" (U), SECRET, ECOM-5824, June 1977.
61. Dubbin, Marvin H. and Dennis Hall, "Synchronous Meteorlogical Satellite Direct Readout Ground System Digital Video Electronics," ECOM-5525, June 1977.
62. Miller, W., and B. Engebos, "A Preliminary Analysis of Two Sound Ranging Algorithms," ECOM-5826, July 1977.
63. Kennedy, Bruce W., and James K. Luers, "Ballistic Sphere Techniques for Measuring Atomspheric Parameters," ECOM-5827, July 1977.
64. Duncan, Louis D., "Zenith Angle Variation of Satellite Thermal Sounder Measurements," ECOM-5828, August 1977.
65. Hansen, Frank V., "The Critical Richardson Number," ECOM-5829, September 1977.
66. Ballard, Harold N., and Frank P. Hudson (Compilers), "Stratospheric Composition Balloon-Borne Experiment," ECOM-5830, October 1977.

☆ U.S. GOVERNMENT PRINTING OFFICE: 1977 777-093/16